TECHNISCHE UNIVERSITÄT MÜNCHEN

Fakultät für Medizin

Klinikum rechts der Isar

Nuklearmedizinische Klinik und Poliklinik

Spatial pattern of beta-amyloid accumulation in Alzheimer's disease as measured with positron emission tomography

Tengfei Guo

Vollständiger Abdruck der von der Fakultät für Medizin der Technischen Universität München zur Erlangung des akademischen Grades eines

Doctor of Philosophy (Ph.D.)

genehmigten Dissertation.

Vorsitzender: Prof. Dr. Arthur Konnerth

Betreuer: Prof. Dr. Markus Schwaiger

Prüfer der Dissertation:

1. Priv.-Doz. Dr. Stephan Nekolla
2. Priv.-Doz. Dr. Timo Grimmer

Die Dissertation wurde am 30.01.2018 bei der Fakultät für Medizin der Technischen Universität München eingereicht und durch die Fakultät für Medizin am 20.04.2018 angenommen.

Abstract

Knowledge about spatial and temporal patterns of beta-amyloid (Aβ) accumulation is essential for understanding Alzheimer's disease (AD) and design of anti-amyloid drug trials. In this thesis, I studied the spatial pattern of Aβ accumulation in subjects with preclinical and manifest sporadic AD (sAD) and autosomal dominant AD (ADAD), as measured with positron emission tomography (PET). Analyzed were baseline and two years' follow-up PET and magnetic resonance imaging data from the Alzheimer's disease Neuroimaging Initiative and Dominantly Inherited Alzheimer Network databases. After pre-processing and partial volume correction of PET images, regional standard uptake values (SUV) were extracted using a probabilistic brain atlas. In the first project, the regional pattern of annual accumulation rate (AAR) of ^{18}F-florbteapir was investigated in 58 Aβ-positive patients with incipient and manifest dementia due to sAD. A pseudo-temporal accumulation rate was estimated from baseline PET only by determining how fast regional SUVR changes relative to the whole gray matter SUVR. The so-called pseudo-temporal measurements explained 87% (p<0.001) of the variance in longitudinal AARs across 62 regions. Thus, this method allows identification of brain regions with a high accumulation rate of Aβ, which are of particular interest for anti-amyloid clinical trials. In the second project, I examined a longitudinal trajectory of AAR in the pre-dementia stage of sAD, using ^{18}F-florbteapir PET data of 246 Aβ-positive cognitively normal subjects and patients with mild cognitive impairment. Subjects with baseline SUVR in whole gray matter ($SUVR_{GM}$) of 0.56 to 0.92 (n=134) appeared to accumulate Aβ approximately 1.5 times faster than remaining subjects. In subjects with $SUVR_{GM}$ above 0.95, most active Aβ accumulating regions were outside the established set of AD-typical regions. When these patterns are taken into account, the sample size in anti-amyloid trials can be substantially reduced. Finally, our data strongly suggested that treated and placebo groups should be matched for baseline $SUVR_{GM}$. Otherwise, a treatment effect can be significantly over- or underestimated. In the third project, I studied the spatial and temporal pattern of Aβ accumulation in ADAD. Analyzed were Pittsburg compound B PET data of 97 mutation carriers (MC) (APP=19, PSEN1=72, PSEN2=6) and 50 Aβ-negative asymptomatic non-mutation carriers (NC). I found that overall the spatial and temporal pattern of Aβ accumulation in MC was very similar to that of sAD except for subcortical nuclei. As compared to sAD, these nuclei

appeared to be fast Aβ accumulating regions. However, due to their relatively small size, these regions did not significantly contribute to the set of AD-typical regions. Thus, the established set of AD-typical regions can be used as target region to detect longitudinal SUVR changes in Aβ-positive MC, too. In summary, the findings of this thesis provide meaningful references for planning and analyses of anti-amyloid clinical trials with PET as biomarker.

Keywords: Alzheimer's disease, amyloid imaging, cognitive normal, mild cognitive impairment, dementia, clinical trial**,** positron emission tomography, florbetapir, PiB, clinical trial, beta-amyloid accumulation.

Zusammenfassung

Kenntnisse über räumliche und zeitliche Muster der Akkumulation von Beta-Amyloid (Aβ) sind essentiell für das Verständnis der Alzheimer-Krankheit (AD) und das Design von Anti-Amyloid-Studien. In dieser Arbeit untersuchte ich daher das räumliche und zeitliche Muster der Aß Akkumulation bei Patienten mit präklinischer und manifester sporadischer AD (sAD) und autosomal dominanter AD (ADAD), gemessen mit der Positronen - Emissions - Tomographie (PET). Analysiert wurden Ausgangs- und zweijährige Verlaufs-PET- und Magnetresonanztomographie -Daten der Alzheimer Disease Neuroimaging Initiative (ADNI) und der Dominantly Inherited Alzheimer Network (DIAN). Nach Vorverarbeitung und partieller Volumenkorrektur von PET-Bildern wurden regionale standard uptake values (SUV) mittels eines probabilistischen Gehirnatlasses extrahiert. Im ersten Projekt wurde das räumliche Muster der jährlichen Akkumulationsrate (AAR) von 18F-Florbteapir bei 58 Aβ-positiven Patienten mit beginnender und manifester Demenz aufgrund von AD von ADNI untersucht. Eine pseudo-temporale Akkumulationsrate wurde auf der Basis der Ausgangs-PET geschätzt. Hierbei wurde bestimmt, wie schnell sich regionales SUVR relativ zu SUVR der gesamten grauen Substanz verändert. Die pseudotemporalen Messungen erklärten 87% ($p < 0{,}001$) der Varianz der longitudinalen AARs in 62 Regionen. Somit können mit dieser Methode Hirnregionen mit einer hohen Akkumulationsrate von Aβ identifiziert werden; diese sind wichtig für Anti-Amyloid-Studien.Im zweiten Projekt untersuchte ich die longitudinale Trajektorie von AAR im prädementiellen Stadium von sAD. Dafür wurden 246 Aβ-positiven kognitiv normalen Probanden und Patienten mit leichter kognitiver Beeinträchtigung von ADNI eingeschlossen. Probanden mit Ausgangs-SUVR in der gesamten grauen Substanz ($SUVR_{GM}$) von 0,56 bis 0,92 (n = 134) erschienen Aβ etwa 1,5-mal schneller Aβ zu akkumulieren als die übrigen Probanden. In Probanden mit $SUVR_{GM}$ über 0,95 lagen die meisten aktiven Aß-Akkumulationsregionen außerhalb des etablierten Sets von AD-typischen Regionen. Durch die Berücksichtigung dieser Befundekönnen Stichproben der Anti-Amyloid-Studien wesentlich reduziert werden. Schließlich sprechen unsere Ergebnisse stark dafür, dass die behandelten und Placebo-Gruppen für Ausgangs-$SUVR_{GM}$ angepasst werden sollten. Ansonsten kann ein Behandlungseffekt signifikant über- oder unterschätzt werden. Im dritten Projekt untersuchte ich das räumliche und

zeitliche Muster der Aß-Akkumulation in ADAD. Analysiert wurden Pittsburg compound B PET-Daten von 97 Mutationsträgern (MC) (APP = 19, PSEN1 = 72, PSEN2 = 6) und 50 Aß-negativen asymptomatischen Nichtmutationsträgern (NC). Ich fand, dass das räumliche und zeitliche Muster der Aß-Akkumulation was sehr ähnlich zu dem der sAD, bis auf subkortikale Nuklei. Im Vergleich zur sAD zeigten sich diese Nuklei als schnell Aß-akkumulierende Regionen. Aufgrund ihrer geringen Größe trugen sie allerdings unwesentlich in das Set der AD-typischen Regionen bei. Somit kann das etablierte Set der AD-typischen Regionen als Targetregion auch bei Anti-Amyloid-Studien in ADAD verwendet werden. Zusammenfassend stellen die Befunde dieser Doktorarbeit eine wertvolle Grundlage für die Planung und Analyse von Anti-Amyloid-Studien mit PET als Biomarker dar.

Stichworte: Alzheimer-Krankheit, Amyloid-Bildgebung, kognitive Normalität, leichte kognitive Beeinträchtigung, Demenz, klinische Studie, Positronen-Emissions-Tomographie, Florbetapir, PiB, klinische Studie, Beta-Amyloid-Akkumulation.

Contents

I. Introduction

1.1. Alzheimer's disease

Nowadays, Alzheimer's disease (AD) is becoming a growing public and financial healthcare problem. There were an estimated 46.8 million people worldwide living with dementia in 2015, and this number, is believed to be close to 50 million people in 2017, reaching around 131.5 million in 2050 [1]. The total estimated worldwide cost of patients with AD and other dementias is US$818 billion in 2015, which represents 1.09% of global GDP. The global cost of dementia will rise above a US$ trillion by 2018, which is predicted to increase beyond a trillion dollar annual cost by 2050 unless disease-modifying treatments are developed. Therefore, specific therapeutic and prevention strategies are urgently needed.

AD is a neurodegenerative disease and the most common cause of dementia [2, 3]. Clinically, it is characterized by a progressive cognitive deterioration, leading to a functional disability and finally to death. Patients with AD may have difficulties with memory, orientation, language, problem-solving that at a certain time point affect a person's ability to perform daily activities. The two key hallmark pathologies of AD are: extracellular beta-amyloid (Aβ) (plaques) and intracellular twisted strands of the protein tau (tangles) [4]. Aβ plaques are believed to contribute to cell death by interfering with neuron-to-neuron communication at synapses. It has been hypothesized that excess amyloid burden initiates a cascade of events that results in neuronal death and cognitive decline [5]. The accumulation of tau tangles blocks the transport of nutrients and other essential molecules inside neurons. Notably, research suggests that accumulation of Aβ and tau tangles start more than 2 decades prior to fist symptoms [6-8]. Here, give a biomarker-based definition of AD (5). Accumulating evidence from the AD research resulted in a conceptual change of disease understanding. Namely, and in contrast to the older diagnostic guidelines [9], the disease can now be diagnosed at the pre-dementia stage, if there is evidence of abnormal biomarkers .

Traditionally, AD is subdivided into two types according to age: 1) early onset AD (EOAD); 2) late onset AD (LOAD). Individuals with EOAD (around 1-5% of AD) tend to develop Alzheimer's symptoms before age 65, sometimes as early as age 30; while the symptoms of LOAD (predominant form of AD) become apparent at age 65 or later

[10]. EOAD develops at an early age due to autosomal dominant mutation in amyloid precursor protein (APP) [11], presenilin 1(PSEN1) [12], or presenilin 2 (PSEN2) [13]. A mutation to the APP or PSEN1 genes will develop AD for sure, and a mutation to the PSEN2 gene will have a 95% chance of developing the disease [14]. Additionally, AD may be classified as three different types according to family history: 1) autosomal dominant AD (ADAD) (<5% of all cases), occurring in at least three individuals in two or more generations, with two of the individuals being first-degree relatives of the third; 2) familial AD (15-25% of all cases), occurring in more than one individual, and at least two of the affected individuals are third-degree relatives or closer; or 3) sporadic AD (sAD) (75% of all cases), isolated case in the family or cases separated by more than three degrees of relationship [14]. Typically, sAD are LOAD, but around 40% EOAD may be classified as sAD, possibly representing hidden familial or autosomal dominant disease.

1.2. Diagnosis

The diagnostic criteria and guidelines published by the National Institute of Neurological and Communicative Disorders and Stroke and the Alzheimer's Association in 1984, then known as the Alzheimer's Disease and Related Disorders Association (ADRDA), have been used for several decades [9]. The ADRNA criteria were based purely on a clinical judgment, including reports from the patient and family members, cognitive tests, the course of symptom progression, and general neurological assessment. These diagnostic criteria largely depend on the exclusion of other causes of cognitive decline. Beside a low to moderate diagnostic accuracy, these criteria supported a diagnosis only at the dementia stage. To overcome this limitation, the National Institute on Aging (NIA) and the Alzheimer's Association proposed new diagnostic guidelines [15-17]. Their novelty consists in incorporation of biomarker tests in the diagnostic algorithm, while keeping the clinical phenotype as the core diagnostic feature. Biomarkers are defined as *in vivo* measurable physiological, biochemical or anatomical variables, indicating specific features of AD-related pathological changes [18]. Five biomarkers have been well established for AD over the past several years. They can be divided into two main categories: 1) biomarkers Aβ deposition, as assessed with measures of $A\beta_{40}$ and $A\beta_{42}$ in the cerebrospinal fluid (CSF) [19-23] and by positron emission tomography (PET) [6, 24-31]; and 2) biomarkers of neurodegeneration,

including increased concentrations of CSF total and phosphorylated tau [20-22, 32-35], hypometabolism on fluorodeoxyglucose (FDG) PET [28, 36-38] and atrophy on structural MRI [39-42]. As shown in Fig.1, a hypothetical model of course of biomarkers findings related to clinical symptoms of AD was proposed by Jack et al. in 2013 [18].

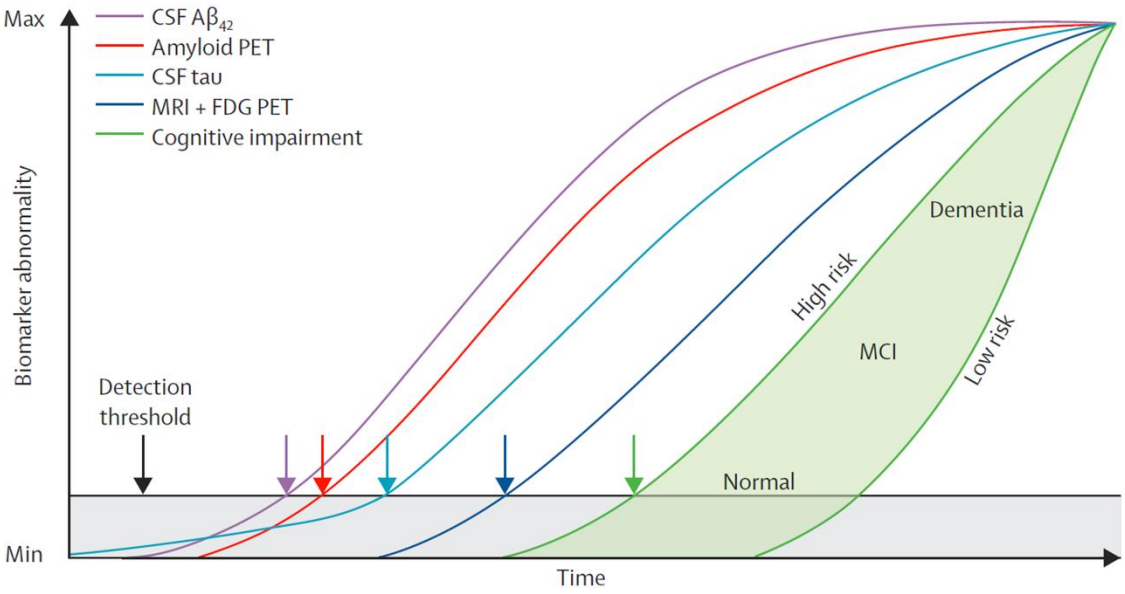

Fig.1. Model integrating Alzheimer's disease immunohistology and biomarkers (taken from Jack et al., Lancet Neurol. 2013) [18]. The threshold for biomarker detection of pathophysiological changes is denoted by the black horizontal line. The grey area denotes the zone in which abnormal pathophysiological changes lie below the biomarker detection threshold.

The revised guidelines identify three different stages of AD: 1) cognitively normal (CN) at preclinical stage of AD that occurs before symptoms develop [15], which was proposed for research. In this stage, individuals may have asymptomatic cerebral amyloidosis, "downstream" neurodegeneration, and neuronal injury and subtle cognitive/behavioral decline that indicate the earliest signs of disease, but they may have not yet developed noticeable symptoms such as memory impairment. This proposed preclinical stage is related to current idea of AD that Alzheimer's-related brain changes may begin 20 years or more before symptoms occur [6, 27, 43-46]. 2) Mild cognitive impairment (MCI) due to AD [16]. In this stage, activities of daily living are basically unimpaired, but individuals show cognitive decline greater than expected for their age and education level. Approximately 15-20% of people age 65 or older have MCI [47]. 3) Dementia due to AD [17]. In this stage, individuals have noticeable memory, thinking and behavioral symptoms that impair a person's ability to function in daily life.

1.3. Anti-amyloid therapies

According to 2017 Alzheimer's disease facts and figures of the Alzheimer's Association [10], 244 drugs for Alzheimer's have been tested in clinical trials registered with clinicaltrials.gov in the decade of 2002-2012, but only one of them successfully completed clinical trials and went on to receive approval from the FDA. So far, none of the pharmacologic treatments (medications) available today for AD slows or stops the damage and destruction of neurons that cause Alzheimer's symptoms. Many factors contribute to the difficulty of developing effective treatments for Alzheimer's, including the high cost of drug development, the relatively long trial duration. According to former investigations [6, 27, 43-46], AD is a slow and gradual process that can extend for more than two decades, which provides a large therapeutic window. In the past decades, most of the clinical trials [48-56] have focused on mild-to-moderate or severe AD symptomatic patients, whose disease may have progressed too far for a successful intervention. Particularly, the phase 3 clinical trials of two high-profile AD antibodies, bapineuzumab [48] and solanezumab [49] against the aggregation-prone peptide Aβ, have failed to improve clinical outcomes in patients with LOAD. Therefore, efforts to develop disease-modifying treatments may require clinical trials to be conducted earlier in the disease process. According to Fig.1, Aβ accumulation emerges early in the disease process, thus *in vivo* imaging of Aβ plays an key role in detecting and identifying individuals who are at high risk of developing AD in the early stages of the disease. Therefore, amyloid PET image has been widely used as the inclusion criteria to identify participants with risk to be AD and a primary or secondary endpoint in clinical trials with anti-amyloid therapeutics over the past years [48, 54, 57-63].

1.4. Amyloid PET in clinical trials

It has been demonstrated that deposition of Aβ starts many years prior to the first clinical symptoms, gradually increasing up to moderate dementia due to AD [6, 15, 26, 64-70]. Amyloid imaging allows studying Aβ deposition in the living human brain. In 2012, Clark and colleagues reported that PET with amyloid tracers is an accurate tool for *in vivo* measurement of neuritic Aβ [31]. Previous investigations proved that Aβ plaques do not affect the brain uniformly but accumulate particularly in the frontal,

parietal, cingulate and temporal cortices [26, 27, 71]. Therefore, the frontal, lateral parietal and temporal cortices as well as the anterior and posterior cingulate regions are regarded as regions with a significant Aβ burden in AD [28]. It should be noted that this regional pattern has been summarized based on cross-sectional studies in patients with dementia due to sAD. Thus, a standardized uptake value ratio (SUVR) in a composite cortical area averaged across these regions (referred to as AD-typical regions thereafter) has been commonly used as a primary or secondary measurement in anti-amyloid trials [48, 54, 57]. Knowledge about regional pattern of Aβ accumulation is essential for understanding AD and Aβ-associated dementing disorders, and for design of anti-amyloid trials.

1.5. Aims

The aim of this thesis was to explore the spatial and temporal pattern of Aβ accumulation in sAD and ADAD in the context of clinical trials. Specifically, I studied whether these patterns can be considered to reduce a sample size and shorten duration of a hypothetical anti-amyloid clinical trial.

1.5.1. Predicting spatial pattern of Aβ accumulation by baseline amyloid PET

Although it always costs numerous human resource and time consuming to acquire longitudinal data, longitudinal analysis is still extremely essential for us to explore the progression of Aβ deposition in brain and conduct anti-plaque drug trial. Regional dynamics of Aβ deposition in sAD has been explored by using longitudinal ^{11}C - Pittsburgh compound B (PiB) PET [26, 27, 72-74]. Some recent longitudinal ^{18}F-Florbetapir studies [29, 75, 76] have been conducted to study Aβ deposition for sAD, but related regional dynamics of Aβ deposition for AD haven't been analyzed. The significant amount of Aβ deposition was also found in patients with Lewy body disease [77], atypical forms of AD, and mixed dementia [78] in addition to the typical AD, but the regional longitudinal studies for non-AD dementia are not as detail as AD due to their uncommon follow-up (FU) data. The ideal way to acquire such longitudinal pattern is to conduct a repeated amyloid PET in the same subject over time. However, large scale PET studies are very expensive and subject to radiation exposure, especially when individuals with mild disease are involved. It could be more difficult to collect such

studies in other Aβ-associated disorders like in Lewy body disease and atypical (as compared to typical AD disorders) forms of AD. No longitudinal PET studies in these Aβ-associated disorders have been published so far. Assumed that the total amyloid burden would be a reasonable approximation of the stage of the pathology, the spatial patterns of the temporal progression of Aβ deposition in older adults has been estimated recently in one cross-sectional PiB PET study [79] , but it is still unclear whether the cross-sectional results correlates related longitudinal measurements. Therefore, I firstly studied if spatial pattern of longitudinal Aβ deposition in sAD could be predicted by baseline amyloid PET data collected from Alzheimer's disease Neuroimaging Initiative (ADNI) database using a pseudo-temporal image analysis. Assuming that there is a spatial spread of amyloid deposition, the pseudo-temporal accumulation rate can be extracted by determining how fast the amyloid amount increases in a given region relative to whole brain GM amyloid load. If effective, such an approach could provide preliminary information for fast accumulating regions (FARs) of Aβ in the beginning of trial. Using those FARs as the target region could reduce the duration and sample size of the trial. This approach may also be used to explore spatiotemporal patterns of Aβ deposition in other Aβ-associated disorders.

1.5.2. Rate of beta-amyloid accumulation varies with baseline amyloid burden: implications for anti-amyloid drug trials

Clinical trials in patients with manifest AD have failed to show clinical efficacy over the past years [48, 49, 51-56, 80]. Therefore, it has been argued that patient with AD may be too late to remedy [48, 81]. In addition to the factors on ability of tested antibodies to adequately engage their targets [82], it was also suggested that therapeutic interventions should be conducted at an earlier disease stages [83-86]. As a result, a few ongoing anti-amyloid trials are testing the efficacy of potential disease-modifying drugs in Aβ-positive CN individuals [58, 60, 62] and subjects with MCI [61, 63].

However, previous longitudinal PET studies of Aβ-positive CN and MCI produced rather inconsistent results. For instance, the anterior cingulate region was reported a fast Aβ accumulating region in one study [87], while none Aβ accumulation of this regions was detected in another study [27]. Although both groups studied CN subjects using PiB-PET. In individuals with MCI, one group observed significant PiB accumulation within the anterior and posterior cingulate, temporal, parietal cortices as well as in the

putamen [88]. However, another group reported a positive PiB rate also within the prefrontal cortex, insula and occipital lobe, but not within the putamen of the same clinical entity [27]. In addition, Villemagne and colleagues did not detect any significant regional PiB accumulation in Aβ-positive CN and MCI subjects within 20 months, but they observed significant Aβ accumulation in the orbitofrontal and dorsolateral prefrontal cortices of Aβ-positive CN subjects within 38 months [89]. Multiple factors such as study duration, proportion of Aβ-positive subjects at baseline or reference region may be related to the inconsistency of these findings. One probable important factor may be that the study subjects may have been at different stages of the Aβ trajectory. As a matter of fact, the trajectory of amyloid accumulation rate may have an inverse U-shape across the whole period of accelerated Aβ deposition [6, 43]. Moreover, a spatial pattern of longitudinal Aβ accumulation may vary nonlinearly over the whole period. To be more specific, some fast accumulating regions at an early stage may become slow accumulating regions at the late stages, while others may become top FARs at a later stage. These factors may be related to the design and analysis of anti-amyloid clinical trials in Aβ-positive CN and MCI.

Considering the discrepancy of previous longitudinal studies above, it is plausible to hypothesize that FARs that affected by Aβ and subjects with high Aβ accumulation rate (fast-accumulators) in Aβ-positive CN and MCI subjects may vary in different stage of CN and MCI. Ideal method to explore FARs and fast-accumulators is to collect a complete data battery at multiple time points in many individuals over the entire course of CN and MCI. However, the more than 20 years' time span makes it extremely difficult to collect such an idealized dataset. Previous results suggested that total amyloid burden may be a valid solution for modeling Aβ trajectory for AD [27, 43, 90]. Therefore, I subsequently adapted the pseudo-temporal analysis approach to model AAR of Aβ in AD-typical regions with baseline total amyloid burden based on Aβ-positive CN and MCI subjects collected from ADNI database in the second project. This established trajectory was applied to explore the pseudo-temporal pattern of AAR in the pre-dementia stage of AD in the context of clinical trials.

1.5.3. Spatial and temporal pattern of Aβ accumulation in autosomal dominant Alzheimer's disease

Currently, several research being conducted through Dominantly Inherited Alzheimer Network (DIAN) are studying families with ADAD. Those ADAD mutation carriers (MCs) provide us the opportunity to investigate the preclinical stage of AD, since their clinical fate is clear due to genetic mutation. Knowledge gained from ADAD MCs may be translated to the asymptomatic, prodromal and clinical symptomatic sAD [91]. A recently launched DIAN Trials Unit (DIAN-TU) aims at testing multiple drugs for slowing or preventing the progression of ADAD [92]. Herewith, amyloid PET is used as a surrogate biomarker to track target engagement [92]. However, optimal brain regions to be targeted in longitudinal analyses of amyloid PiB PET have not yet been established for ADAD. A lot of studies have demonstrated Aβ deposition in subcortical regions in ADAD MCs, and the regional distribution of Aβ plaques in ADAD may different from that in sAD [93-96]. The difference of longitudinal amyloid accumulation may be even larger. Thus, the set of AD-typical regions that has been established in symptomatic sAD may not be necessarily optimal to track Aβ accumulation over time in presymptomatic ADAD. However, only few longitudinal studies have examined a (mean cortical) Aβ accumulation in ADAD so far [97], while knowledge on a regional pattern of Aβ accumulation over time is still missing. Such a pattern may provide a set of regions that accumulate Aβ significantly faster than the composite cortical region. As a result, the trial duration and drug costs can be reduced. In addition, Bateman et al. reported that Aβ deposition in MCs could be detected 15 years before estimated years to symptom onset (EYO) [44], therefore, DIAN-TU has recruited those MCs with EYO > -15 as the target of the anti-amyloid drug trial. However, it is still unclear whether the cutoff EYO -15 can identify suitable target with significant highly amyloid accumulation or amyloid deposition for anti-amyloid drug trial. Therefore, I investigated the regional pattern of longitudinal Aβ accumulation in ADAD and suitability of EYO cutoff -15 of identifying target for DIAN-TU in the end of the thesis.

II. Predicting spatial pattern of Aβ accumulation by baseline amyloid PET

The advancing of in-vivo amyloid imaging allows us to study Aβ deposition in the living human brain. The spatial and temporal patterns of Aβ accumulation is relevant for understanding AD and designing anti-amyloid trials. The aim of the first project is to investigate whether it is possible to use baseline amyloid PET to predict the spatial pattern of longitudinal Aβ accumulation. This approach may be also useful in exploring spatial patterns of Aβ accumulation in other amyloid-associated disorders such as Lewy body disease and atypical forms of AD.

2.1. Materials and Methods

2.1.1. Participants

The ^{18}F-florbetapir PET data of patients with AD were collected from the ADNI database (ida.loni.usc.edu). The ADNI study was approved by institutional review boards of all participating centres, and written informed consent was obtained from all participants or authorized representatives. All patients with incipient and mild dementia due to AD with structural magnetic resonance imaging (MRI), baseline and 2 years' follow up (FU) ^{18}F-florbetapir PET scans available from ADNI database by August, 2015 were considered. Subjects with incipient AD were those diagnosed with late mild cognitive impairment at the time of baseline florbetapir scan, but who converted to dementia due to AD at FU. In addition, the present of AD pathology was confirmed by including only individuals with an Aβ-positive scan at baseline [17]. Inclusion of clinically manifest patients with AD resulted in a homogenous data set in respect to both clinical phenotype and underlying pathology. Aβ-positivity was determined according to the SUVR in AD-typical regions with a threshold of >1.11 as described elsewhere [28]. Particularly, SUVR in the AD-typical regions was calculated by averaging SUVR across the frontal, anterior/posterior cingulate, lateral parietal, lateral temporal regions, and dividing by the value in the whole cerebellum. Thus, out of 69 initially selected patients, 59 were Aβ-positive. After exclusion of one significant outlier (Grubbs' test

[98]; Graph-Pad Software, La Jolla, CA, USA), 58 patients remained for further analyses (Fig. 2). The outlier was a subject with a 40% reduction in SUVR at FU as compared to baseline PET. To explore potential influence of the apolipoprotein E (APOE) ε4 gene carrier [99], age and gender onto results, subgroup analyses were performed.

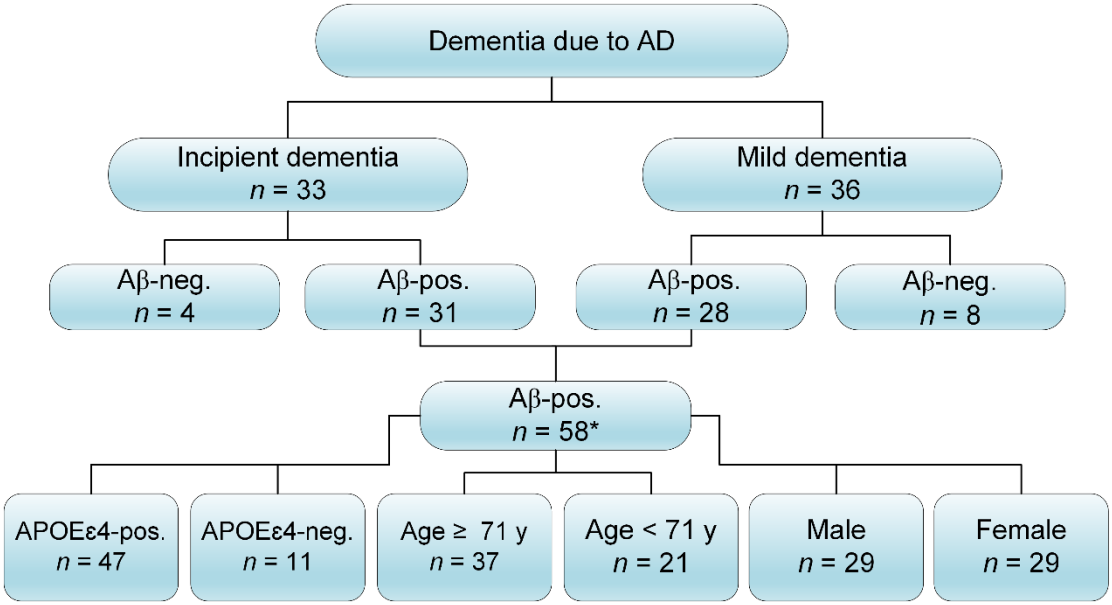

Fig.2.*The process of collecting image data from ADNI. Aβ-pos and Aβ-neg denote Aβ-positivity and Aβ-negativity individually. The cutoff age between Age-N and Age-P was set as 71, by referring to previous literature (Fleisher et al., 2013).*

2.1.2. Image acquisition and analysis

Details on image acquisition are given elsewhere (http://adni-info.org). Briefly, PET data were acquired at 50–70 min p.i. as 4×5 min frames. Images were realigned, averaged, resliced to a common voxel size (1.5 mm^3), and smoothed to a common resolution of 8 mm^3 in full width at half maximum.

The PMOD PNEURO tool (V. 3.5 PMOD Technologies, Zürich) was applied to conduct the image analysis. First of all, PET images were rigidly co-registered to the corresponding MRI to calculate a linear transformation (PET-2-MRI). Then, individual MRI images were nonlinearly co-registered to the standard MRI template in the Montreal Neurological Institute (MNI) space (MRI-2-MNI), while PET-2-MRI and MRI-2-MNI transformations were used to transform PET images into the MNI space. Individual T1-weighted MRI images were segmented into gray matter (GM), white matter (WM) and cerebrospinal fluid [100] to generate a total of 83 volumes of interests for each subject in the MNI space [101]. Out of 83 volumes of interests, 62 cortical

regions with a volume above 1 cm^3 (i.e. 2 x full width at half maximum) were included in the final analyses.

A volumes of interest based partial volume correction (PVC) was performed in the original PET space [102]. Regional SUVR was calculated as ratio of florbetapir uptake in each region to that in WM [75]. SUVR in whole brain GM (whole-GM) was calculated as a volume-weighted mean value of 62 GM regions, likewise intensity normalized to WM.

2.1.3. Pseudo-temporal image analysis

Sixty two regional SUVR values from the baseline ^{18}F-florbetapir PET were used for the pseudo-temporal analysis. Specifically, subjects were ranked according to their SUVR in whole-GM ($SUVR_{GM}$), resulting in an across-subject waveform for each region [79]. For a given region r, the SUVRs for n subjects can be expressed as:

$$SUVR_r(i), i = 1 \dots n \qquad \text{(Eq.1)}$$

where $SUVR_r(i)$ denotes the SUVR of the ith subject for region r.

Then, $SUVR_r$ may be organized by ranking corresponding individual $SUVR_{GM}$ from minimal to maximal value, forming a pseudo-temporal waveform W_r

$$W_r(j) = \left[SUVR^{(1)}_{SUVR_{GM}(min)}, \dots, SUVR^{(n)}_{SUVR_{GM}(max)}\right], j = 1 \dots n. \qquad \text{(Eq.2)}$$

where $W_r(j)$ denotes the jth element of W_r.

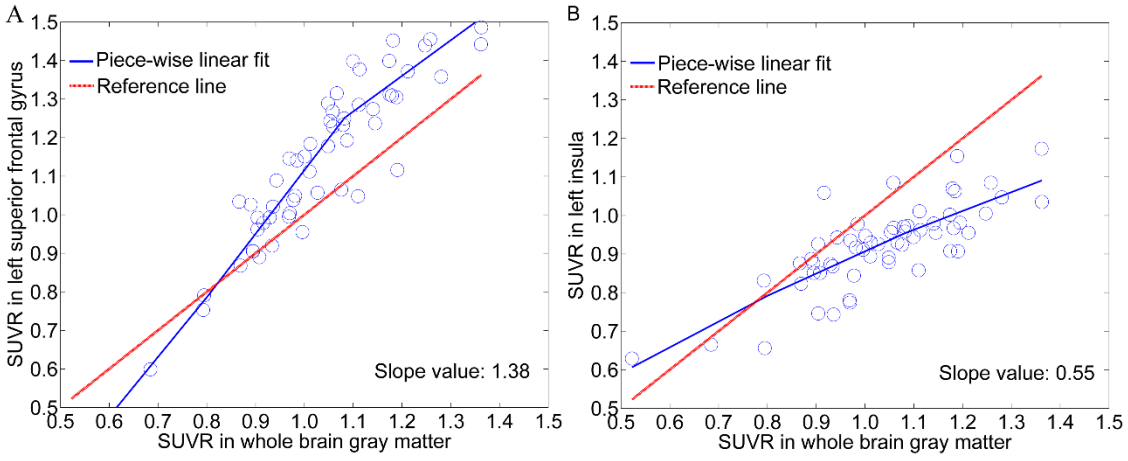

Fig. 3. *Piecewise linear fit of pseudo-temporal waveforms for a fast (A: left superior frontal gyrus) and slow (B: left insula) accumulating region. Reference line corresponds to SUVR in whole brain gray matter with a slope value of 1.0.*

Assuming that there is a spatial spread of amyloid deposition with disease progression, the pseudo-temporal accumulating rate can be extracted by determining how fast amyloid deposits in a given region relative to whole-GM. To be more specific, each region's waveform was fitted using a piecewise linear fit. Each fit was modeled with a restricted linear spline with 4 knots to allow the fitted line varying nonlinearly with total amyloid burden. As shown in Fig. 3, examples of piecewise linear fit of a fast and slow accumulating region are illustrated. Subsequently, a derivative function of the fitted line was obtained for each region. Finally, a mean slope value (pseudo-temporal accumulating rate) across 58 subjects was calculated for each region according to the derivative function.

2.1.4. Regression analyses between baseline and follow-up measurements

The annual accumulation rate (AAR) of Aβ was calculated as following:

$$\mathrm{AAR} = \frac{\mathrm{SUVR_{FU}} - \mathrm{SUVR_{BL}}}{\text{FU time}} \quad \text{(Eq.3)}$$

where, $\mathrm{SUVR_{FU}}$ is the SUVR of the FU PET data, $\mathrm{SUVR_{BL}}$ is baseline, and FU time (years) is the time between two PET scans. The mean AAR across subjects was calculated for each region.

A linear regression analysis was performed to predict the AAR (as dependent variable) by slope values (as independent variable) across 62 regions. The same analysis was performed in subgroups of subjects stratified according to age, gender and APOE ε4 status. For the former, the age of 71 years was used as cut-off [103].

The linear regression analysis was performed using baseline SUVR and the ratio of baseline SUVR to $\mathrm{SUVR_{GM}}$ as independent variables for a reference, respectively.

Additionally, the same analysis was conducted for 417 subjects (including 148 CN, 231 MCI, 38 AD), in order to explore how such a pseudo-temporal analysis approach performs without considering amyloid status or the presence of AD pathology,

2.1.5. Fast and slow accumulating regions

To explore utility of these analyses in the context of clinical trials, FARs and slow accumulating regions (SARs) were determined according to ranks of both longitudinal (AARs) and baseline (slope values) measurements. Top 10 FARs were combined into

one single composited FAR according to the Eq.4 and used as a putative target in clinical trials. Then, AAR in this composited FAR was compared with that in AD-typical regions. The set of AD-typical regions consisted of 18 regions, covering the frontal (8 regions), parietal (3 regions including precuneal/posterior cingulate), temporal (6 regions) lobes plus anterior cingulate region [104].

$$SUVR_{\text{Composited}} = \frac{(\text{SUVR}_{\text{region(1)}} * \text{Volume}_{\text{region(1)}} + \cdots + \text{SUVR}_{\text{region(K)}} * \text{Volume}_{\text{region(K)}} \ldots + \text{SUVR}_{\text{region(N)}} * \text{Volume}_{\text{region(N)}})}{(\text{Volume}_{\text{region(1)}} + \cdots + \text{Volume}_{\text{region(K)}} \cdots + \text{Volume}_{\text{region(N)}})} \quad \text{(Eq.4)}$$

where $\text{SUVR}_{\text{region(K)}}$ is the SUVR of K^{th} region, $\text{Volume}_{\text{region(K)}}$ is the volume of K^{th} region, and $SUVR_{\text{Composited}}$ is SUVR of composited FAR, AD-typical regions or whole-GM.

2.1.6. Statistics

Normality of distribution was tested using the D'Agostino-Pearson test (Graph-Pad Software, La Jolla, CA, USA) and visual inspection of variable histograms. Data were presented as mean ± SD. Mean AAR of the composited FAR across 58 subjects was compared with those of whole-GM and AD-typical regions using a two-tailed paired-sample *t*-test. Statistical significance was defined as $p<0.05$. Regression and statistical analyses were performed using SPSS for Windows (version 22.0).

2.2. Results

2.2.1. Demographics

Demographic data of patients at baseline are summarized in Table 1.

Table 1. *Demographics of patients at baseline*

Group	N	FU (years)	Age (years)	Gender (f/m)	Education (years)	APOE ε4-pos. (%)	MMSE	ADAS-cog
Incipient dementia	30	1.97± 0.12	70.67± 7.91	16/14	16.33± 2.70	73%	24.87 ±2.79	19.77± 6.80
Mild dementia	28	2.00± 0.10	75.25± 7.37	13/15	14.96± 2.83	89%	21.57 ±2.17	31.71± 10.64
All patients	58	1.99± 0.11	72.88± 7.93	29/29	15.67± 2.82	81%	23.28 ±3.00	25.53± 10.65

2.2.2. Regression analysis between baseline and follow-up measurements

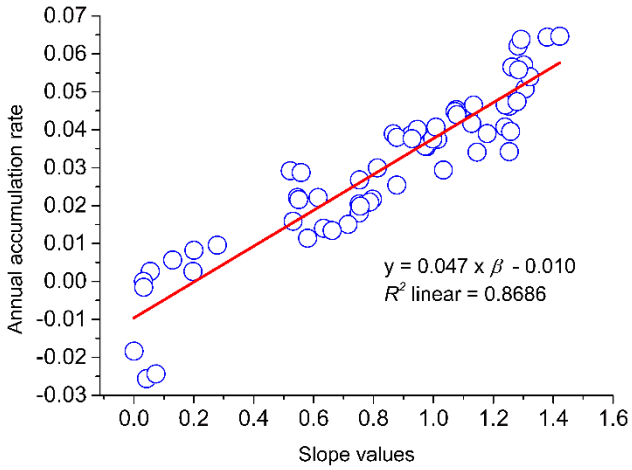

Fig. 4. *Linear regression across 62 regions*

As illustrated in Fig. 4, pseudo-temporal accumulating rates (slope values) could predict AARs across 62 regions (R^2 =0.87, p<0.001) accurately following the function as follow:

$$y = 0.047 \times \beta - 0.010 \quad \text{(Eq.7)}$$

where y indicates AAR, and β means slope value of each region.

The correlation between pseudo-temporal accumulating rate and AAR was still very strong for incipient (n=30, R^2 =0.77, p<0.001) and mild (n=28, R^2=0.58, p<0.001) dementia due to AD, respectively. The regression remained highly significant after stratification according to age, gender, and the APOE ε4 status (p<0.001 for all, Table 2).

Table 2. *Linear regression coefficient (Pearson) between pseudo-temporal and longitudinal measurements in subgroups of patients*

Sub-group	APOE ε4-pos.	APOE ε4-neg.	Age ≥ 71 y	Age < 71 y	Male	Female
N	47	11	37	21	29	29
R^2	0.82	0.32	0.72	0.58	0.79	0.70

APOE ε4-pos. and APOE ε4-neg. indicate APOE ε4 status is positive and negative, respectively.

For the reference, baseline SUVR and the ratio of baseline SUVR/$SUVR_{GM}$ predicted AARs across 62 regions with a similar accuracy (R^2 =0.53 and =0.49, respectively, p<0.001 for both). As compared to baseline SUVR, pseudo-temporal

accumulating rates explained an additional significant amount of variance (R^2 change = 0.35, p<0.001) in the linear regression analysis.

Without considering amyloid status or the presence of AD pathology, pseudo-temporal accumulating rates still accurately (Fig.5) predicted AARs across 62 regions (R2 =0.84, p<0.001) following the function:

$$y1 = 0.020 \times \beta1 - 0.001 \quad \text{(Eq.8)}$$

Where y1 indicates AAR of Aβ, and β1 means slope value of each region.

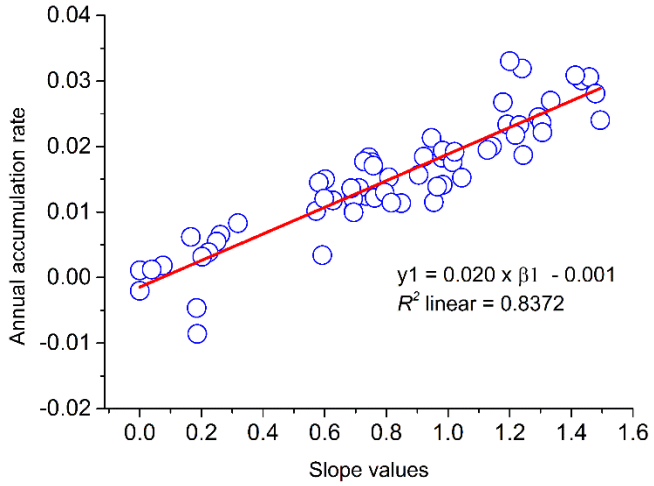

Fig. 5. *Linear regression across 62 regions for 417 subjects.*

2.2.3. Fast and slow accumulating regions

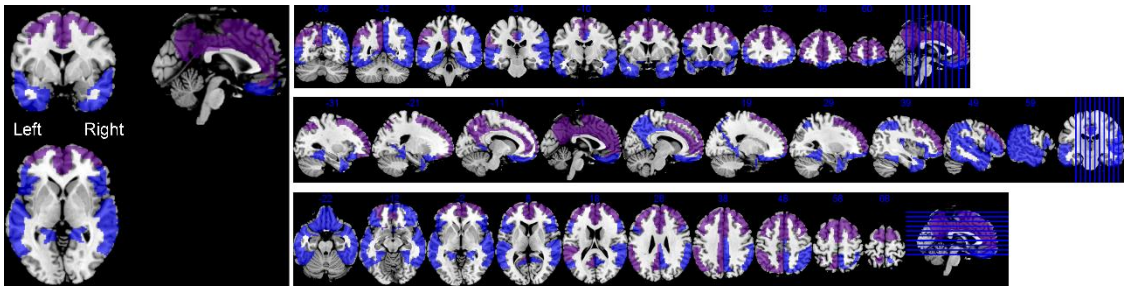

Fig. 6*: Composited FAR (purple) and AD-typical regions (blue) as overlaid onto a standard T1 MRI template in the MNI space. Note that the composited FAR region fully overlaps with the AD-typical regions.*

Bilateral anterior cingulate, superior and middle frontal gyri, left superior parietal, anterior orbital, posterior cingulate regions, and inferiolateral remainder of the parietal lobe were found to be top 10 FARs (table 3). These 10 regions (Fig. 6) were combined

into one composited FAR according to the equation 4. Bilateral hippocampus, caudate nucleus, thalamus, amygdala, and parahippocampal gyrus appeared to be top 10 slow accumulating regions (table 4). Notably, 10 regions with the highest AAR were the same 10 regions with the largest fitted line' slope. The same was true for 10 regions with the lowest AAR.

Table 3. *Fast accumulating regions of Aβ-positive patient due to sAD*

Regions	Rank of slope	Slope	Rank of AAR	AAR (mean±SD)	Volume (mm^3)
Anterior cingulate gyrus_L	1	1.42	1	0.0646±0.0621	7747
Superior frontal gyrus_L	2	1.38	2	0.0644±0.0565	46866
Superior parietal gyrus_L	3	1.32	8	0.0540±0.0505	38141
Anterior orbital gyrus_L	4	1.31	9	0.0508±0.0636	5164
Superior frontal gyrus_R	5	1.30	5	0.0571±0.0614	46158
Anterior cingulate gyrus_R	6	1.29	3	0.0638±0.0515	7441
Posterior cingulate gyrus _L	7	1.28	7	0.0558±0.0598	7159
Middle frontal gyrus_R	8	1.28	4	0.0621±0.0534	42929
Inferiolateral remainder of parietal lobe_L	9	1.28	10	0.0474±0.0479	37662
Middle frontal gyrus_L	10	1.26	6	0.0566±0.0500	44690
Posterior superior temporal gyrus_L	11	1.26	22	0.0396±0.0633	12220
Lateral remainder of occipital lobe_L	12	1.25	13	0.0462±0.0547	38030
Cuneus_L	13	1.25	33	0.0342±0.0560	9438
Superior parietal gyrus_R	14	1.24	11	0.0465±0.0492	37509
Anterior orbital gyrus_R	15	1.24	19	0.0407±0.0686	4807
Lateral remainder of occipital lobe_R	16	1.18	23	0.0390±0.0424	38789
Lingual gyrus_L	17	1.15	34	0.0341±0.0529	12333
Postcentral gyrus_L	18	1.13	12	0.0465±0.0550	23201
Inferiolateral remainder of parietal lobe_R	19	1.13	18	0.0417±0.0450	38214
Inferior frontal gyrus_R	20	1.12	17	0.0439±0.0526	15294
Posterior superior temporal gyrus_R	21	1.08	16	0.0440±0.0665	12468
Inferior frontal gyrus_L	22	1.08	14	0.0453±0.0597	14448
Postcentral gyrus_R	23	1.07	15	0.0448±0.0550	25731
Cuneus_R	24	1.03	36	0.0294±0.0548	9224
Posterior cingulate gyrus_R	25	1.01	30	0.0375±0.0487	7557
Posterior temporal lobe_L	26	1.01	20	0.0407±0.0393	44469
Whole-GM	27	1	26	0.0386±0.0321	851002

Note: '_L' and '_R' indicate left and right, respectively. Abbreviations: AAR = annual accumulation rate; whole-GM = whole brain gray matter.

Table 4. *Slow accumulating regions of Aβ-positive patient due to sAD*

Regions	Rank of slope	slope	Rank of AAR	AAR (mean±SD)	Volume (mm^3)
Hippocampus_L	1	0	3	-0.0184±0.0400	1626
Thalamus_R	2	0.03	5	-0.0004±0.0383	5676
Thalamus_L	3	0.03	4	-0.0015±0.0352	5452
Caudate nucleus_R	4	0.04	1	-0.0256±0.0515	3411
Hippocampus_R	5	0.05	7	0.0027±0.0454	1825
Caudate nucleus_L	6	0.07	2	-0.0244±0.0600	3456
Parahippocampal and ambient gyri_R	7	0.13	8	0.0057±0.0510	3583
Amygdala_R	8	0.20	6	0.0026±0.0500	1057
Amygdala_L	9	0.20	9	0.0082±0.0535	1120
Parahippocampal and ambient gyri_L	10	0.28	10	0.0096±0.0566	3595
Putamen_R	11	0.52	27	0.0292±0.0367	4063
Anterior superior temporal gyrus_R	12	0.53	15	0.0159±0.0541	4205
Insula_R	13	0.55	23	0.0222±0.0335	12323
Insula_L	14	0.55	20	0.0216±0.0381	12275
Putamen_L	15	0.56	26	0.0287±0.0397	3957
Medial anterior temporal lobe_L	16	0.58	11	0.0114±0.0461	4975
Posterior orbital gyrus_R	17	0.61	22	0.0221±0.0452	4476
Lateral orbital gyrus_L	18	0.63	13	0.0141±0.0690	3328
Anterior superior temporal gyrus_L	19	0.66	12	0.0134±0.0558	4033
Medial anterior temporal lobe_R	20	0.71	14	0.0151±0.0458	5107
Lateral anterior temporal lobe _R	21	0.75	18	0.0204±0.0766	2842
Lateral orbital gyrus_R	22	0.75	16	0.0181±0.0662	2967
Straight gyrus_L	23	0.75	25	0.0268±0.0630	3142
Fusiform gyrus_L	24	0.76	17	0.0199±0.050	3486
Fusiform gyrus_R	25	0.79	19	0.0210±0.0520	3479
Posterior orbital gyrus_L	26	0.80	21	0.0217±0.0530	4594
Straight gyrus_R	27	0.81	29	0.0300±0.0552	2856
Medial orbital gyrus_R	28	0.87	40	0.0389±0.0590	4962
Lateral anterior temporal lobe _L	29	0.88	24	0.0254±0.0716	2856
Precentral gyrus_R	30	0.88	37	0.0380±0.0452	27438
Medial orbital gyrus_L	31	0.93	39	0.0386±0.0594	4780
Middle and inferior temporal gyrus_L	32	0.93	36	0.0377±0.0418	13115
Precentral gyrus_L	33	0.95	43	0.0401±0.0420	28237

Middle and inferior temporal gyrus_R	34	0.97	33	0.0357±0.0401	13452
Lingual gyrus_R	35	0.98	32	0.0355±0.0481	11970
Posterior temporal lobe_R	36	1	35	0.0376±0.0395	43594
Whole-GM	37	1	38	0.0386±0.0321	851002

Note: '_L' and '_R' indicate left and right, respectively. Abbreviations: AAR = annual accumulation rate; whole-GM = whole brain gray matter.

FARs and SARs were also determined according to ranks of both longitudinal (AARs) and baseline (pseudo-temporal accumulating rate) measurements for 417 subjects without considering amyloid status or the presence of AD pathology. As shown in Table 5, top 21 FARs were within the top 26 FARs in Table 3, although the ranks were not exactly same. The difference may be due to the fact that regions may have different AAR of Aβ in different stage of AD. Interestingly, top 10 SARs in Table 6 were also within the top 10 SARs in Table 4, implying that FARs may vary for different group, but SARs tend to be those same regions.

Table 5. Fast accumulating regions for 417 CN, MCI and AD subjects

Regions	Rank of slope	Slope	Rank of AAR	AAR (mean±SD)	Volume (mm^3)
Superior parietal gyrus_R	1	1.49	10	0.0240±0.0510	37509
Superior parietal gyrus_L	2	1.48	6	0.0281±0.0524	38141
Superior frontal gyrus_L	3	1.46	4	0.0306±0.0561	46866
Superior frontal gyrus_R	4	1.43	5	0.0301±0.0556	46158
Posterior cingulate gyrus _L	5	1.41	3	0.0308±0.0565	7159
Middle frontal gyrus_R	6	1.33	7	0.0270±0.516	42929
Inferiolateral remainder of parietal lobe_L	7	1.31	14	0.0221±0.0490	37662
Inferior frontal gyrus_L	8	1.30	11	0.0237±0.0499	14448
Middle frontal gyrus_L	9	1.29	9	0.0245±0.0516	44690
Inferiolateral remainder of parietal lobe_R	10	1.24	21	0.0187±0.0462	38214
Anterior cingulate gyrus_R	11	1.24	2	0.0319±0.0559	7441
Inferior frontal gyrus_R	12	1.23	13	0.0233±0.0521	15294
Posterior cingulate gyrus_R	13	1.22	15	0.0217±0.0486	7557
Anterior cingulate gyrus_L	14	1.20	1	0.0330±0.0595	7747
Anterior orbital gyrus_R	15	1.19	12	0.0234±0.0718	4807
Anterior orbital gyrus_L	16	1.18	8	0.0268±0.0669	5164
Posterior superior temporal gyrus_R	17	1.14	17	0.0200±0.0606	12468
Posterior superior temporal gyrus_L	18	1.13	18	0.0195±0.0561	12220
Posterior temporal lobe_R	19	1.04	32	0.0153±0.0373	43594
Posterior temporal lobe_L	20	1.02	20	0.0192±0.0368	4469

Lateral remainder of occipital lobe_L	21	1.02	28	0.0176±0.0517	38030
Whole-GM	22	1	25	0.0182±0.0341	851002

Note: '_L' and '_R' indicate left and right, respectively. Abbreviations: AAR = annual accumulation rate; whole-GM = whole brain gray matter.

Table 6. slow accumulating regions for 417 CN, MCI and AD subjects

Regions	Rank of slope	Slope	Rank of AAR	AAR (mean±SD)	Volume (mm^3)
Hippocampus_R	1	0	4	0.0011±0.0418	1825
Hippocampus_L	2	0	3	-0.0020±0.0416	1626
Thalamus_L	3	0.04	5	0.0012±0.0408	5452
Thalamus_R	4	0.08	6	0.0018±0.0396	5676
Parahippocampal and ambient gyri_R	5	0.17	11	0.0062±0.0510	3583
Caudate nucleus_R	6	0.18	2	-0.0046±0.0461	3411
Caudate nucleus_L	7	0.19	1	-0.0086±0.0472	3456
Parahippocampal and ambient gyri_L	8	0.20	7	0.0032±0.0490	3595
Amygdala_L	9	0.22	9	0.0039±0.0530	1120
Amygdala_R	10	0.25	10	0.0055±0.0519	1057
Medial part of anterior temporal lobe_L	11	0.26	12	0.0065±0.0456	4975
Medial part of anterior temporal lobe_R	12	0.32	13	0.0083±0.0538	5107
Anterior superior temporal gyrus_R	13	0.57	16	0.0102±0.0486	4205
Putamen_L	14	0.58	30	0.0145±0.0398	3957
Anterior superior temporal gyrus_L	15	0.59	8	0.0034±0.0508	4033
Insula_L	16	0.60	22	0.0121±0.0355	12275
Putamen_R	17	0.60	31	0.0150±0.0392	4063
Insula_R	18	0.63	20	0.0118±0.0352	12323
Fusiform gyrus_L	19	0.69	26	0.0136±0.0475	3486
Lateral part of anterior temporal lobe _R	20	0.69	21	0.0121±0.0701	2842
Straight gyrus_L	21	0.69	15	0.0100±0.0581	3142
Fusiform gyrus_R	22	0.69	14	0.0100±0.0511	3479
Lingual gyrus_R	23	0.71	27	0.0137±0.0475	11970
Lingual gyrus_L	24	0.73	38	0.0177±0.0479	12333
Posterior orbital gyrus_R	25	0.74	24	0.0124±0.0502	4476
Straight gyrus_R	26	0.74	41	0.0184±0.0559	2856
Cuneus_R	27	0.75	37	0.0176±0.0590	9224
Cuneus_L	28	0.76	35	0.0171±0.0602	9438
Posterior orbital gyrus_L	29	0.76	23	0.0122±0.0550	4594
Precentral gyrus_L	30	0.79	25	0.0130±0.0494	28237
Precentral gyrus_R	31	0.81	33	0.0153±0.0529	27438

Lateral anterior temporal lobe _L	32	0.82	18	0.0114±0.0630	2856
Lateral orbital gyrus_L	33	0.85	17	0.0114±0.0779	3328
Middle and inferior temporal gyrus_L	34	0.90	34	0.0157±0.0415	13115
Medial orbital gyrus_L	35	0.92	42	0.0184±0.0618	4780
Medial orbital gyrus_R	36	0.95	48	0.0213±0.0615	4962
Lateral remainder of occipital lobe_R	37	0.95	19	0.0115±0.0495	38789
Middle and inferior temporal gyrus_R	38	0.97	28	0.0139±0.0424	13452
Postcentral gyrus_R	39	0.98	40	0.0183±0.0542	25731
Postcentral gyrus_L	40	0.98	45	0.0194±0.0538	23201
Lateral orbital gyrus_R	41	0.98	29	0.0141±0.0754	2967
Whole-GM	42	1	39	0.0182±0.0341	851002

Note: '_L' and '_R' indicate left and right, respectively. Abbreviations: AAR = annual accumulation rate; whole-GM = whole brain gray matter.

2.2.4. Implications for anti-amyloid drug trials

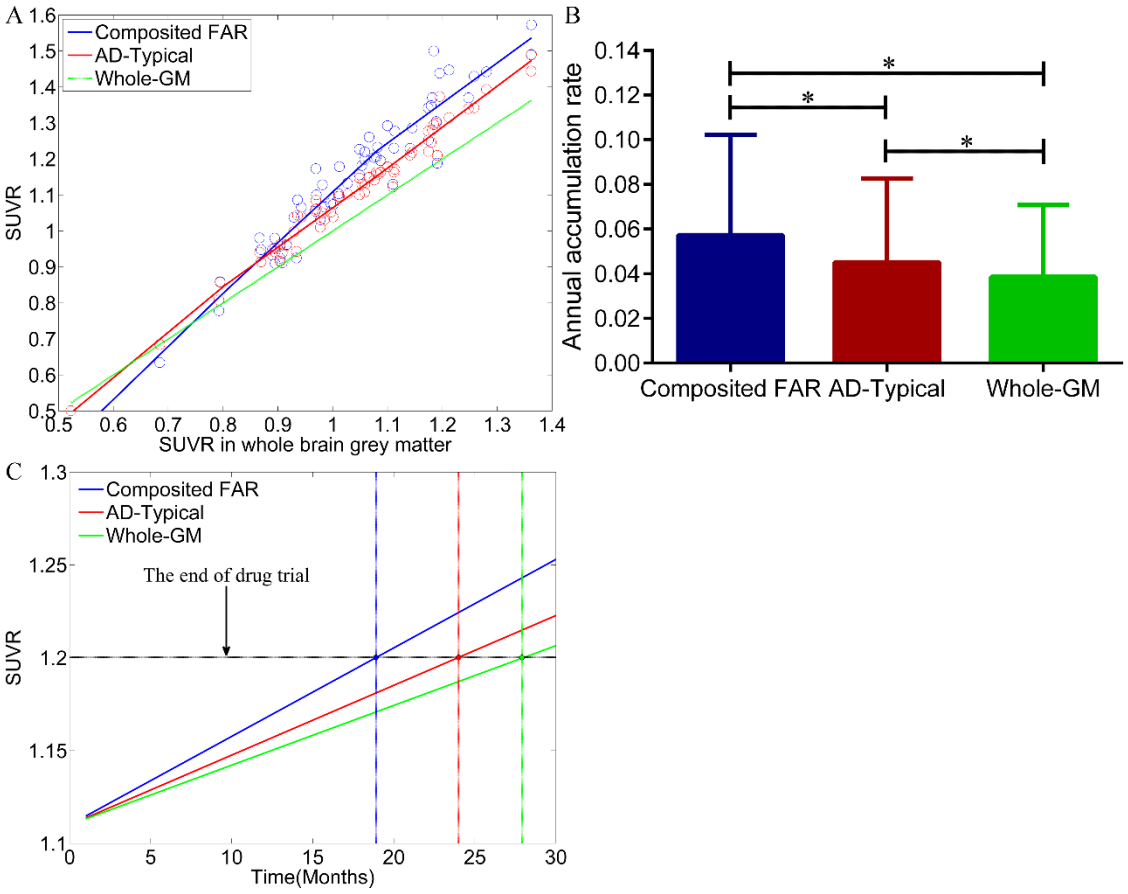

Fig. 7. *(A) Pseudo-temporal analysis of three sets of regions. Note that the green line is a reference fit with a slope value of 1.0. (B) Annual accumulation rates (Mean±SD) for composited FAR, AD-typical regions and whole-GM. * p <0.001 in a two tailed paired t-test. (C) Three sets of regions as putative targets in a hypothetical drug trial of 24 months.*

The mean slope of the composited FAR (1.31±0.15) was higher than those of the composited AD-typical regions (1.15±0.12) and whole-GM (1.00) (Fig. 7A). The mean AAR of the composited FAR (0.057±0.045) was significantly higher than the mean AARs of whole-GM (0.039±0.032, $p<0.001$, paired-sample t-test) and AD-typical regions (0.046±0.038, $p<0.001$) respectively (Fig.7B). Assuming a roughly linear relationship between Aβ and time in Aβ-positive subjects [6, 43], SUVR of the composited FAR increased 1.48 and 1.24 times faster than that of the whole-GM and AD-typical regions, respectively (Fig. 7C). Thus, using the composited FAR as the target region can reduce duration of a 2 years' drug trial by approximately 32 and 19 %, respectively. The sample size (n=246) per arm needed to detect 20% atteunation of further SUVR increase Aβ-modifying treatment effect in clinical trial with 80% power and two-tailed ($\alpha=0.05$) using FAR as the target region could be reduced as compared to the set of AD-typical regions (n=269) and whole-GM (n=266).

III. Rate of beta-amyloid accumulation varies with baseline amyloid burden: implications for anti-amyloid drug trials

It has been suggested that therapeutic interventions should be conducted at an earlier disease stages [83-86]. However, previous longitudinal PET studies of Aβ-positive CN and MCI produced rather inconsistent results over the past several years. As a result, I hypothesize that FARs that affected by Aβ and subjects with high Aβ accumulation rate (fast-accumulators) may vary in different stage of Aβ-positive CN and MCI. These factors may be of relevance for design and analysis of anti-amyloid clinical trials. Therefore, the aim of the second project is to investigate the spatial and temporal pattern of Aβ accumulation by adapting the pseudo-temporal analysis approach to model AAR of Aβ with baseline total amyloid burden.

3.1. Materials and Methods

3.1.1. Participants

The ^{18}F-florbetapir PET data of CN and MCI were also obtained from the ADNI database. Considered were CN and MCI subjects with structural MRI and at least one FU ^{18}F-florbetapir PET scan were available, and only Aβ-positive subject at baseline were included. Aβ-positivity was defined the same as in 2.1.1.

3.1.2. Image data acquisition and analysis

Image analysis was performed using SPM8 (Welcome Department of Imaging Neuroscience, London, UK). Specifically, PET images were rigidly co-registered to concurrently acquired T1 MRI images to calculate a linear transformation (PET-2-MRI). Individual MRI images were nonlinearly co-registered to the MNI space MRI template, and those deformations were used to transform the co-registered PET images into the MNI space. T1 MRI images were segmented into GM, WM and cerebrospinal fluid [100]. Then, a region-based voxel-wise PVC of PET images was performed using the PETPVC toolbox [105]. A total of 83 individual brain VOIs [101] were transferred to individual PET space using the inverse of the above transformations. Sixty two regions

with a volume above 1 cm^3 were included in the final analysis [104]. SUVR was calculated as a ratio of regional SUV to SUV in WM that was recommended as reference region for longitudinal ^{18}F-florbetapir PET studies [29, 75, 76, 106, 107]. WM mask was defined the same as in 2.1.2 and described elsewhere [75]. $SUVR_{GM}$ was calculated as mean value of all 62 GM regions [104]. The set of AD-typical regions were defined the same as in 2.1.5.

3.1.3. Spatial pattern of Aβ accumulation

AAR of ^{18}F-florbetapir was also calculated according to Eq.3 in 2.1.4. An average AAR across all subjects was calculated for each region, the set of AD-typical regions as well as for the whole-GM.

3.1.4. Trajectory of Aβ accumulation as a function of total amyloid burden

In order to explore the variability in regional AAR as a function of total amyloid burden, an across-subject waveform for a given set of region was calculated [104]. Specifically, AAR in AD-typical regions from the baseline ^{18}F-florbetapir PET were modeled with a restricted cubic spline with 4 knots to allow AAR to vary nonlinearly with baseline $SUVR_{GM}$ [43, 104].

As shown in Fig. 8, starting from low baseline SUVR, AAR increased until baseline $SUVR_{GM}$ of 0.70. Afterwards, AAR decreased reaching a plateau at 0.95. Consequently, three phases were defined: baseline $SUVR_{GM} \leq 0.70$ as phase 1, $0.70 < SUVR_{GM} \leq 0.95$ as phase 2, and > 0.95 as phase 3.

In phase 3, all regions including whole-GM were ranked according to their AARs. The hierarchical clustering analysis (HCA) was applied to assess potential clustering of regions based on minimum variance within clusters and relatively equal cluster sizes [108]. The sequence of mergers in the dendrogram suggested a cluster solution for given regions. As a result, regions within the first cluster were subsequently composed into a single region according to Eq. 4. They are referred to as FARs thereafter. Random sampling without replacement was applied using in-house Matlab codes (Matlab R2014b, The Mathworks, Natick, USA) to evaluate consistency of the ranking of top 7 FARs in Table 13. Herewith, individuals were selected randomly not more than once to

calculate an estimate of the error due to sampling [109]. Specifically, 75 subjects were randomly selected from the original sample (n= 77) to create a new one.

3.1.5. Two-fold cross-validation

Two-fold cross-validation was conducted using in-house Matlab codes (Matlab R2014b, The Mathworks, Natick, USA) to evaluate the robustness of the cutoffs for different phases and fast/slow accumulators (more details were in 3.2.3), and consistency of FARs in phase 3.

The cutoff of $SUVR_{GM}$ between phase 1 and phase 2 was defined as the maximal AAR point, and the cutoff between phase 2 and phase 3 was defined as the first derivative function of the fitted plot reaching 0. The mean AAR of whole-GM was used on the fitted plot to find out the corresponding cutoffs of $SUVR_{GM}$ for fast accumulators and slow accumulators. The Cohen's d [110] was calculated as a measure of effect size of AAR between fast accumulators and slow accumulators. Absolute effect sizes of approximately ± 0.1 are considered small, approximately ± 0.3 medium and approximately ± 0.5 large. Effect size d was calculated using

$$d = \frac{M_1 - M_2}{\sigma_{pooled}} \quad \text{(Eq. 5)}$$

Where, σ_{pooled} is calculated[111] according to

$$\sigma_{pooled} = \sqrt{({\sigma_1}^2 + {\sigma_2}^2)/2} \quad \text{(Eq. 6)}$$

Where, M_1, M_2 and σ_1, σ_2 are mean value and standard deviation of either group.

Two-fold cross-validation was conducted to explore the cutoffs for different phases, fast accumulators and slow accumulators. For each fold, the whole cohort was randomly assigned to two equal sets data1 and data2. AAR was modeled as a function of baseline $SUVR_{GM}$, and cutoffs were defined for different phases, fast accumulators and slow accumulators on data1, and then the effect size d2 was calculated for data2, followed by modeling AAR as a function of baseline $SUVR_{GM}$ and defining cutoffs for different phases, fast accumulators and slow accumulators on data2, then the effect size d1 was calculated for data1. In the end, the model with the larger effect size was selected

for each iteration. The distributions of effect size d were obtained after implementing the two-fold cross-validation test 30000 times.

The effect size Cohen's d of AAR between the proposed set of FAR in phase 3 (more details in 3.2.3) and AD-typical regions was calculated as 0.39. Two-fold cross-validation was conducted to testify whether this effect size was statistically significant. For each fold, subjects in phase 3 were randomly assigned to two sub sets data3 and data4. FARs were defined according to AARs in 62 regions of data3, and then the effect size Cohen's d4 of AAR between FAR and AD-typical regions was calculated for data4, followed by defining FAR according to data4, and then calculating the effect size Cohen's d3 for data3. In the end, the FAR with larger d among d3 and d4 was selected to validate the whole cohort. The distribution of effect size Cohen's d was obtained after implementing the two-fold cross-validation test 30000 times.

3.1.6. Statistics

Normality of distributions was tested using the D'Agostino-Pearson test and visual inspection of data histograms. Given a normal data distribution, a parametric (two-tailed) t-test at the significance level of $p<0.05$ was applied. Data are presented as mean ± SD. Statistical analyses were performed using Graph-Pad Prism 6 for Windows (La Jolla, CA, USA), if not otherwise noted. The number of subjects per arm to detect a treatment effect in a hypothetical 24-month placebo-controlled anti-amyloid clinical trial with 80% power was computed in G Power 3.1 [112].

3.2. Results

3.2.1. Demographics

Demographic data of each group are summarized in table 7. There was no significant difference in AAR between subgroups.

Table 7. *Demographic characteristics of CN and MCI*

Group	N	Age (years)	Gender (f/m)	Education (years)	APOE ε4-pos. (%)	MMSE	CDR-SB	ADAS-13
CN	83	76.77± 5.72	49/34	16.06± 2.89	48.19%	28.86± 1.33	0.19± 0.48	10.47± 4.93
Early MCI	82	*73.10± 7.27	30/52	15.90± 2.84	†67.07%	§27.79± 1.81	§1.34 ±0.79	§14.34± 5.10
Late MCI	81	*72.56± 7.51	38/43	16.15± 2.80	†66.67%	§27.32± 1.92	§1.85 ±0.94	§18.39± 7.75
All	246	74.16± 7.10	117/129	16.04± 2.84	60.57%	28.00± 1.81	1.12± 1.02	14.35± 6.84

	$SUVR_{baseline}$ in AD-typical regions	$SUVR_{baseline}$ in whole gray matter	AAR in AD-typical regions	AAR in whole gray matter
CN	0.83±0.18	0.81±0.17	0.033±0.034	0.032±0.033
Early MCI	ǂ0.90± 0.20	ǂ0.87±0.18	0.029±0.030	0.028±0.028
Late MCI	ǂ0.97± 0.22	ǂ0.93±0.21	0.034±0.034	0.032±0.032
All	ǂ0.90± 0.21	ǂ0.87±0.19	0.032±0.032	0.031±0.031

All significant differences refer to a comparison with CN: * p<0.001, two-sample t-test; † p<0.05, Fisher's exact test; § p<0.001, Mann-Whitney test (MMSE, CDR-SB and ADAS-13 were not normally distributed). ǂ *p<0.05*, two-sample *t*-test.

3.2.2. Spatial pattern of AAR

In CN group, only bilateral amygdala, thalamus and hippocampus, and right caudate nucleus had no significant increase in SUVR from baseline to FU. As shown in Table 8, thirty two had a higher AAR than whole-GM. Out of these 32 regions, bilateral anterior orbital and medial orbital, left superior parietal and posterior cingulate, and right middle frontal had significantly higher AAR than whole-GM (0.032±0.033). Out of these 7 regions, bilateral medial orbital had significantly higher AAR than AD-Typical regions (0.034±0.034).

Table 8*. Rank of annual accumulation rates in sub-regions, AD-typical regions and the whole gray matter of CN group*

Region	Mean	SD	Volume(mm3)
Anterior orbital gyrus_R*,ǂ	0.044	0.072	4807
Anterior orbital gyrus_L*,ǂ	0.043	0.069	5164
Medial orbital gyrus_L*, †,ǂ	0.042	0.048	4780
Straight gyrus_Lǂ	0.041	0.050	3142
Medial orbital gyrus_R*, †,ǂ	0.040	0.043	4962
Lateral orbital gyrus_Lǂ	0.039	0.078	3328
Superior parietal gyrus_L*,ǂ	0.038	0.037	38141

Middle frontal gyrus_R‡	0.038	0.045	42929
Posterior part of cingulate gyrus _L*‡	0.037	0.040	7159
Middle frontal gyrus_L*‡	0.037	0.039	44690
Superior frontal gyrus_L‡	0.037	0.041	46866
Inferiolateral remainder of parietal lobe_R‡	0.036	0.038	38214
Lateral orbital gyrus_R‡	0.036	0.060	2967
Lateral remainder of occipital lobe_R‡	0.036	0.037	38789
Inferiolateral remainder of parietal lobe_L‡	0.036	0.034	37662
Superior parietal gyrus_R‡	0.035	0.038	37509
Straight gyrus_R‡	0.035	0.041	2856
Lateral part of anterior temporal lobe _L‡	0.035	0.043	2856
Middle and inferior temporal gyrus_R‡	0.035	0.044	13452
Inferior frontal gyrus_R‡	0.034	0.041	15294
AD-typical regions‡	0.034	0.034	530664
Postcentral gyrus_L‡	0.034	0.034	23201
Posterior part of cingulate gyrus_R‡	0.034	0.047	7557
Cuneus_R‡	0.034	0.037	9224
Middle and inferior temporal gyrus_L‡	0.033	0.047	13115
Precentral gyrus_L‡	0.033	0.035	28237
Posterior part of superior temporal gyrus_R‡	0.033	0.039	12468
Superior frontal gyrus_R‡	0.033	0.038	46158
Inferior frontal gyrus_L‡	0.033	0.043	14448
Lateral remainder of occipital lobe_L‡	0.033	0.036	38030
Cuneus_L‡	0.032	0.037	9438
Precentral gyrus_R‡	0.032	0.038	27438
Postcentral gyrus_R‡	0.032	0.036	25731
Whole gray matter‡	0.032	0.033	851002
Anterior part of cingulate gyrus_L‡	0.032	0.042	7747
Posterior temporal lobe_R‡	0.032	0.036	47598
Lateral part of anterior temporal lobe _R‡	0.031	0.044	2842
Posterior orbital gyrus_L‡	0.030	0.055	4594
Posterior temporal lobe_L‡	0.030	0.041	48665
Posterior orbital gyrus_R‡	0.030	0.051	4476
Posterior part of superior temporal gyrus_L‡	0.030	0.051	12220
Anterior part of superior temporal gyrus_L‡	0.029	0.049	4033
Fusiform gyrus_L‡	0.027	0.045	3486
Lingual gyrus_L‡	0.026	0.041	12333
Lingual gyrus_R‡	0.026	0.048	11970
Insula_R‡	0.025	0.053	12323
Anterior part of cingulate gyrus_R‡	0.025	0.053	7441
Anterior part of superior temporal gyrus_R‡	0.025	0.048	4205
Medial part of anterior temporal lobe_L‡	0.024	0.042	4975
Fusiform gyrus_R‡	0.024	0.048	3479
Putamen_R‡	0.022	0.053	4063
Insula_L‡	0.022	0.064	12275
Putamen_L‡	0.021	0.056	3957
Medial part of anterior temporal lobe_R‡	0.020	0.041	5107
Caudate nucleus_L‡	0.018	0.045	3456

Parahippocampal and ambient gyri_L‡	0.017	0.050	3595
Parahippocampal and ambient gyri_R‡	0.017	0.046	3583
Amygdala_L	0.013	0.063	1120
Thalamus_L	0.011	0.074	5452
Amygdala_R	0.011	0.056	1057
Hippocampus_R	0.008	0.069	1825
Hippocampus_L	0.008	0.064	1626
Thalamus_R	0.008	0.075	5676
Caudate nucleus_R	0.007	0.070	3411

Regions within the set of AD-typical regions were highlighted as red. SD: Standard deviation. '_L' and '_R' indicate the left and right hemisphere, respectively. *and † *denote AAR was significantly different from (p <0.05, two-tailed paired-sample t-test) that of whole gray matter and AD-typical regions respectively.* ‡ *denotes AAR was significant different from zero (two-tailed one-sample t-test).*

In MCI group, all the 62 regions had significant increase in SUVR from baseline to FU. As shown in table 9, twenty six regions had a higher AAR than whole-GM. Out of these 26 regions, bilateral anterior orbital, posterior cingulate and middle frontal, and left medial orbital, lateral orbital, superior frontal, superior parietal, middle and inferior temporal and inferior frontal had significantly higher AAR than whole-GM (0.030±0.030). Out of these 12 regions, left anterior orbital, medial orbital and right posterior cingulate and bilateral middle frontal had significantly higher AAR than AD-Typical regions (0.032±0.032).

Table 9. *. Rank of annual accumulation rates in sub-regions, AD-typical regions and the whole gray matter of MCI group*

Region	Mean	SD	Volume(mm3)
Anterior orbital gyrus_L*,†	0.037	0.044	5164
Medial orbital gyrus_L*,†	0.037	0.043	4780
Posterior part of cingulate gyrus_R*,†	0.035	0.035	7557
Anterior orbital gyrus_R*	0.035	0.045	4807
Lateral orbital gyrus_L*	0.035	0.044	3328
Middle frontal gyrus_L*,†	0.034	0.037	44690
Superior frontal gyrus_L	0.034	0.040	46866
Middle frontal gyrus_R*,†	0.034	0.038	42929
Superior parietal gyrus_L*	0.034	0.035	38141
Posterior part of cingulate gyrus _L*	0.034	0.035	7159
Middle and inferior temporal gyrus_L*	0.033	0.037	13115
Lateral orbital gyrus_R	0.033	0.045	2967
Inferior frontal gyrus_L*	0.033	0.038	14448
Medial orbital gyrus_R	0.033	0.042	4962

Lateral part of anterior temporal lobe _L	0.032	0.041	2856
Middle and inferior temporal gyrus_R	0.032	0.037	13452
Posterior orbital gyrus_L	0.032	0.040	4594
Superior frontal gyrus_R	0.032	0.037	46158
Superior parietal gyrus_R	0.032	0.033	37509
Inferiolateral remainder of parietal lobe_L	0.032	0.034	37662
Straight gyrus_L	0.032	0.045	3142
Postcentral gyrus_L	0.032	0.030	23201
Anterior part of cingulate gyrus_L	0.032	0.040	7747
AD-typical regions	0.032	0.032	530664
Inferior frontal gyrus_R	0.031	0.038	15294
Lateral part of anterior temporal lobe _R	0.031	0.042	2842
Lateral remainder of occipital lobe_L	0.031	0.031	38030
Whole gray matter	0.030	0.030	851002
Inferiolateral remainder of parietal lobe_R	0.030	0.033	38214
Postcentral gyrus_R	0.030	0.031	25731
Posterior temporal lobe_L	0.030	0.031	48665
Precentral gyrus_L	0.029	0.031	28237
Lateral remainder of occipital lobe_R	0.029	0.031	38789
Posterior part of superior temporal gyrus_L	0.029	0.037	12220
Posterior orbital gyrus_R	0.029	0.040	4476
Anterior part of cingulate gyrus_R	0.029	0.039	7441
Straight gyrus_R	0.029	0.045	2856
Lingual gyrus_L	0.029	0.033	12333
Lingual gyrus_R	0.029	0.032	11970
Posterior part of superior temporal gyrus_R	0.029	0.036	12468
Precentral gyrus_R	0.029	0.032	27438
Cuneus_R	0.028	0.033	9224
Fusiform gyrus_R	0.028	0.041	3479
Posterior temporal lobe_R	0.027	0.030	47598
Putamen_R	0.027	0.032	4063
Putamen_L	0.027	0.033	3957
Fusiform gyrus_L	0.026	0.038	3486
Anterior part of superior temporal gyrus_L	0.026	0.041	4033
Cuneus_L	0.026	0.033	9438
Insula_L	0.025	0.034	12275
Medial part of anterior temporal lobe_L	0.025	0.034	4975
Insula_R	0.025	0.032	12323
Anterior part of superior temporal gyrus_R	0.024	0.043	4205
Medial part of anterior temporal lobe_R	0.022	0.036	5107
Parahippocampal and ambient gyri_R	0.019	0.032	3583
Parahippocampal and ambient gyri_L	0.019	0.031	3595
Amygdala_L	0.017	0.034	1120
Amygdala_R	0.017	0.037	1057
Caudate nucleus_L	0.016	0.039	3456
Thalamus_L	0.015	0.035	5452
Hippocampus_R	0.014	0.031	1825
Thalamus_R	0.013	0.035	5676

Caudate nucleus_R	0.013	0.041	3411
Hippocampus_L	0.012	0.030	1626

*'_L' and '_R' indicate the left and right hemisphere, respectively. *and † denote AAR of the region was significantly higher (p <0.05, two-tailed paired-sample t-test) than that of whole gray matter and AD-Typical regions respectively.*

In the whole cohort, all 62 regions showed a significant (p<0.05, one sample t-test) Aβ accumulation over 2 years (table 10) and AARs were normally distributed. Bilateral anterior orbital, medial orbital, middle frontal, superior parietal and posterior cingulate, and left lateral orbital, superior frontal and inferiolateral remainder of parietal lobe, and right middle and inferior temporal had significantly higher AARs than whole-GM (0.031±0.031). Out of these 14 regions, bilateral anterior orbital and middle frontal, and left medial orbital, superior parietal and posterior cingulate had significantly higher AARs than AD-typical regions (0.033±0.032).

Table 10. *Rank of annual accumulation rates in sub-regions, AD-typical regions and the whole gray matter of the whole cohort*

Region	Mean	SD	Volume(mm^3)
Anterior orbital gyrus_L*,†	0.039	0.054	5164
Medial orbital gyrus_L*,†	0.039	0.045	4780
Anterior orbital gyrus_R*,†	0.038	0.055	4807
Lateral orbital gyrus_L*	0.036	0.058	3328
Middle frontal gyrus_R*,†	0.035	0.040	42929
Superior parietal gyrus_L*,†	0.035	0.036	38141
Medial orbital gyrus_R*	0.035	0.042	4962
Middle frontal gyrus_L*,†	0.035	0.038	44690
Posterior cingulate gyrus _L*,†	0.035	0.037	7159
Superior frontal gyrus_L*	0.035	0.040	46866
Straight gyrus_L	0.035	0.047	3142
Posterior cingulate gyrus_R*	0.035	0.039	7557
Lateral orbital gyrus_R	0.034	0.051	2967
Lateral anterior temporal lobe _L	0.033	0.042	2856
Middle and inferior temporal gyrus_R*	0.033	0.040	13452
Middle and inferior temporal gyrus_L	0.033	0.041	13115
Inferiolateral remainder of parietal lobe_L*	0.033	0.034	37662

Superior parietal gyrus_R*	0.033	0.035	37509
Inferior frontal gyrus_L	0.033	0.040	14448
Inferior frontal gyrus_R	0.033	0.039	15294
AD-typical regions	0.033	0.032	530644
Postcentral gyrus_L	0.033	0.032	23201
Superior frontal gyrus_R	0.032	0.038	46158
Inferiolateral remainder of parietal lobe_R	0.032	0.035	38214
Anterior cingulate gyrus_L	0.032	0.041	7747
Lateral remainder of occipital lobe_R	0.032	0.033	38789
Posterior orbital gyrus_L	0.032	0.046	4594
Lateral remainder of occipital lobe_L	0.031	0.033	38030
Straight gyrus_R	0.031	0.044	2856
Lateral anterior temporal lobe _R	0.031	0.043	2842
Precentral gyrus_L	0.031	0.032	28237
Whole gray matter	0.031	0.031	851002
Postcentral gyrus_R	0.031	0.033	25731
Posterior superior temporal gyrus_R	0.030	0.037	12468
Cuneus_R	0.030	0.034	9224
Posterior temporal lobe_L†	0.030	0.035	48665
Precentral gyrus_R†	0.030	0.034	27438
Posterior orbital gyrus_R	0.030	0.044	4476
Posterior superior temporal gyrus_L†	0.029	0.042	12220
Posterior temporal lobe_R*,†	0.029	0.032	47598
Cuneus_L†	0.028	0.035	9438
Lingual gyrus_L†	0.028	0.036	12333
Lingual gyrus_R†	0.028	0.038	11970
Anterior cingulate gyrus_R†	0.028	0.044	7441
Anterior superior temporal gyrus_L*,†	0.027	0.044	4033
Fusiform gyrus_L*,†	0.027	0.041	3486
Fusiform gyrus_R*,†	0.026	0.043	3479
Putamen_R*,†	0.025	0.040	4063
Putamen_L*,†	0.025	0.042	3957
Insula_R*,†	0.025	0.040	12323
Medial anterior temporal lobe_L*,†	0.025	0.037	4975
Anterior superior temporal gyrus_R*,†	0.025	0.045	4205

Insula_L[*,†]	0.024	0.046	12275
Medial anterior temporal lobe_R[*,†]	0.021	0.038	5107
Parahippocampal and ambient gyri_R[*,†]	0.018	0.037	3583
Parahippocampal and ambient gyri_L[*,†]	0.018	0.039	3595
Caudate nucleus_L[*,†]	0.017	0.041	3456
Amygdala_L[*,†]	0.016	0.046	1120
Amygdala_R[*,†]	0.015	0.044	1057
Thalamus_L[*,†]	0.014	0.052	5452
Hippocampus_R[*,†]	0.012	0.047	1825
Thalamus_R[*,†]	0.011	0.052	5676
Caudate nucleus_R[*,†]	0.011	0.052	3411
Hippocampus_L[*,†]	0.010	0.044	1626

Regions within the set of AD-typical regions were highlighted as red. '_L' and '_R' indicate the left and right hemisphere, respectively. [*] *and* [†] *denote AAR of the region was significantly different from ($p < 0.05$, two-tailed paired-sample t-test) that of whole gray matter and AD-typical regions respectively.*

3.2.3. Trajectory of Aβ accumulation as a function of baseline amyloid deposition

Fig. 8 shows AAR in AD-typical regions as a function of baseline $SUVR_{GM}$. According to the criteria in 2.2.4, three different phases were defined. Out of 246 subjects, 52, 117, and 77 subjects fall within the phases 1, 2, and 3, respectively. Subjects with $SUVR_{GM}$ between 0.56 and 0.92 had higher AARs in AD-typical regions than the mean AAR of whole-GM (0.031±0.031) (Fig. 8). They are further referred to as fast accumulators (n=134); subjects with SUVR below 0.56 and above 0.92 are referred to as slow accumulators (n=112). In fast accumulators, the mean AAR in AD-typical regions (0.038±0.033) was significantly higher (p=0.045, one-sample *t*-test) than the mean AAR of the whole cohort (0.033±0.032). In slow accumulators, AAR in AD-typical regions (0.026±0.030) was significantly lower (p=0.016). AAR in AD-typical regions was 1.50 (p=0.002, two-sample *t*-test) times higher in fast accumulators than in slow accumulators (Fig. 9A).

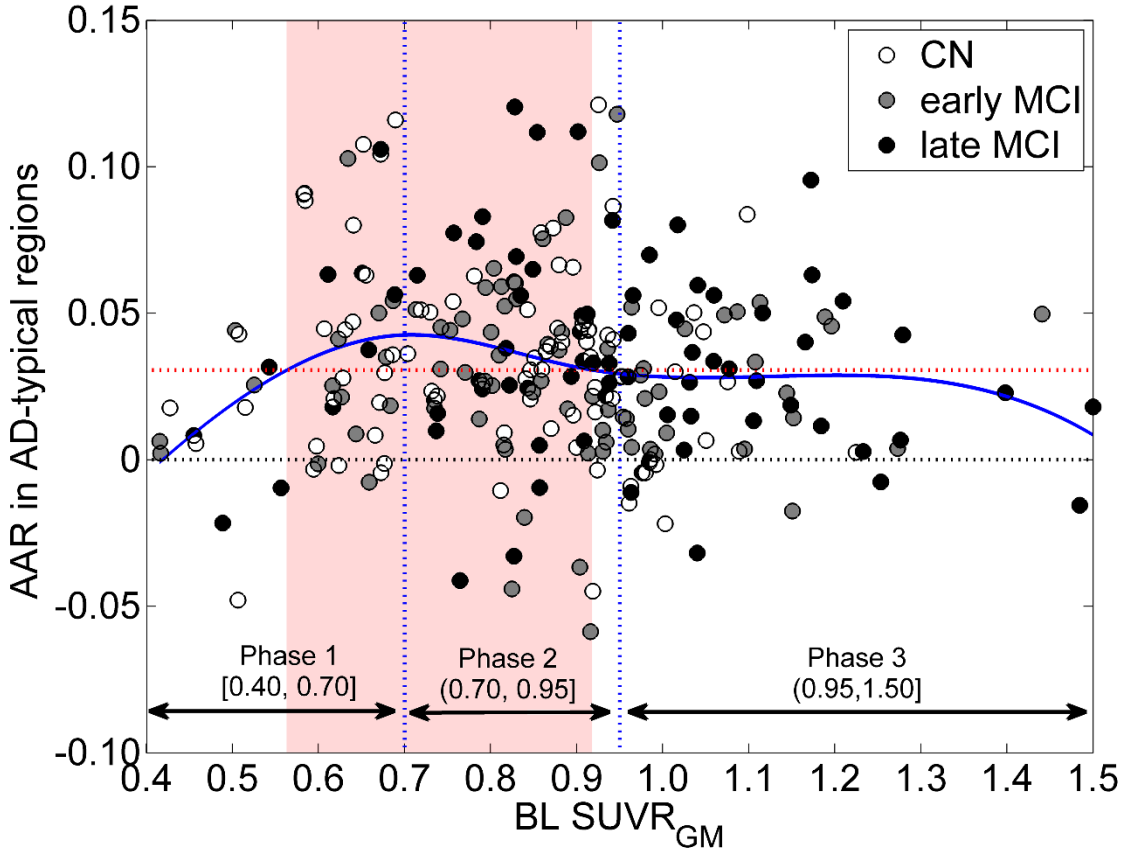

Fig. 8. *Annual accumulation rate (AAR) in AD-typical regions as a function of baseline (baseline) $SUVR_{GM}$. Horizontal red line is the mean AAR in whole gray matter of the whole cohort. Horizontal black line is zero. From left to right, blue lines are cutoffs 0.70 and 0.95 for phase 1 and phase 2, and phase 2 and phase 3, respectively. A background red area indicates fast accumulators with the cutoffs 0.56 and 0.92.*

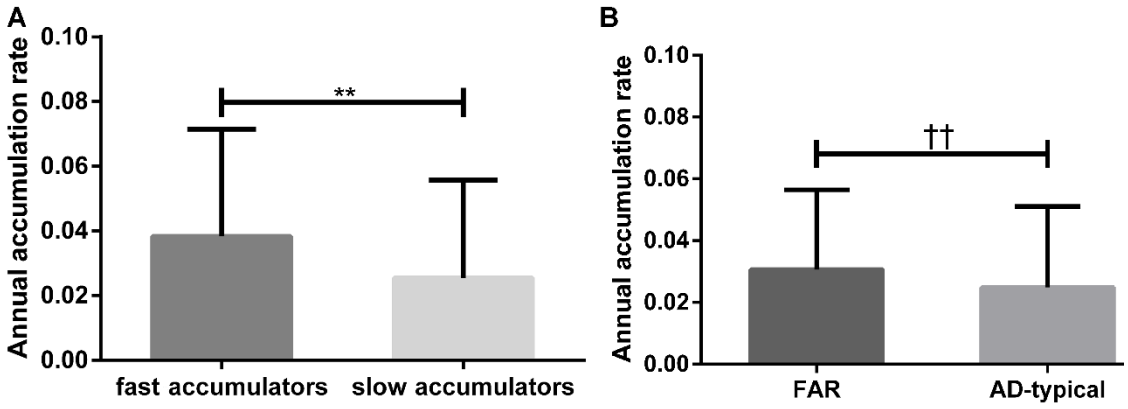

Fig. 9. *Annual accumulation rates (A) of fast accumulators and slow accumulators in AD-typical regions; ** $p<0.01$ in a two-tailed two-sample t-test (B) in fast accumulating regions (FAR) and AD-typical regions in phase 3; †† $p<0.01$ in a two-tailed paired-sample t-test.*

3.2.4. Spatial pattern of AAR at different phases

In phase 1, out of 31 regions with a higher AAR than whole-GM, right anterior orbital, lateral orbital, straight, posterior orbital, middle frontal and superior frontal, and bilateral medial orbital, inferior frontal and posterior cingulate, and left middle and inferior temporal and inferiolateral remainder of parietal lobe had significantly higher AARs than whole-GM (table 11). Among of these 14 regions, right anterior orbital, medial orbital, lateral orbital and inferior frontal had significantly higher AARs than AD-typical regions (0.035±0.037).

Table 11. *Rank of annual accumulation rates in sub-regions, AD-typical regions and the whole gray matter of subjects in phase 1*

Sub regions	Mean	SD	Volume (mm^3)
Anterior orbital gyrus_R*,†	0.047	0.060	4807
Lateral orbital gyrus_L	0.045	0.067	3328
Medial orbital gyrus_R*,†	0.044	0.041	4962
Anterior orbital gyrus_L	0.043	0.064	5164
Lateral orbital gyrus_R*,†	0.040	0.043	2967
Medial orbital gyrus_L*	0.039	0.049	4780
Straight gyrus_R*	0.039	0.041	2856
Inferior frontal gyrus_R*,†	0.038	0.038	15294
Posterior cingulate gyrus_R*	0.038	0.040	7557
Inferior frontal gyrus_L*	0.038	0.038	14448
Posterior orbital gyrus_R*	0.038	0.045	4476
Middle frontal gyrus_R*	0.038	0.041	42929
Anterior cingulate gyrus_R	0.038	0.039	7441
Posterior orbital gyrus_L	0.038	0.045	4594
Posterior cingulate gyrus _L*	0.037	0.040	7159
Middle and inferior temporal gyrus_L*	0.037	0.039	13115
Superior parietal gyrus_L	0.037	0.040	38141
Superior frontal gyrus_R*	0.036	0.037	46158
Anterior cingulate gyrus_L	0.036	0.041	7747
Lateral anterior temporal lobe _L	0.036	0.042	2856

Inferiolateral remainder of parietal lobe_R	0.036	0.037	38214
Middle and inferior temporal gyrus_R	0.035	0.040	13452
Inferiolateral remainder of parietal lobe_L*	0.035	0.037	37662
Straight gyrus_L	0.035	0.044	3142
Middle frontal gyrus_L	0.035	0.042	44690
AD-typical regions	0.035	0.037	530644
Superior parietal gyrus_R	0.035	0.037	37509
Posterior superior temporal gyrus_R	0.035	0.038	12468
Superior frontal gyrus_L	0.034	0.040	46866
Insula_R	0.034	0.037	12323
Lateral anterior temporal lobe _R	0.033	0.044	2842
Posterior temporal lobe_R	0.033	0.036	47598
Whole gray matter	0.033	0.036	851002
Posterior temporal lobe_L†	0.032	0.036	48665
Insula_L	0.031	0.038	12275
Fusiform gyrus_R	0.031	0.039	3479
Putamen_R†	0.031	0.035	4063
Postcentral gyrus_R†	0.030	0.034	25731
Posterior superior temporal gyrus_L†	0.030	0.041	12220
Anterior superior temporal gyrus_L	0.030	0.039	4033
Anterior superior temporal gyrus_R†	0.030	0.038	4205
Fusiform gyrus_L†	0.030	0.040	3486
Lateral remainder of occipital lobe_R†	0.029	0.037	38789
Lateral remainder of occipital lobe_L†	0.029	0.038	38030
Putamen_L†	0.029	0.038	3957
Postcentral gyrus_L*,†	0.029	0.036	23201
Precentral gyrus_R*,†	0.028	0.035	27438
Precentral gyrus_L*,†	0.028	0.036	28237
Cuneus_L*,†	0.027	0.038	9438
Medial anterior temporal lobe_R*,†	0.027	0.033	5107
Lingual gyrus_L*,†	0.027	0.036	12333
Cuneus_R*,†	0.027	0.036	9224
Medial anterior temporal lobe_L*,†	0.026	0.033	4975
Lingual gyrus_R*,†	0.025	0.033	11970
Caudate nucleus_R*,†	0.023	0.035	3411

Parahippocampal and ambient gyri_L[*,†]	0.022	0.034	3595
Thalamus_R[*,†]	0.021	0.037	5676
Thalamus_L[*,†]	0.021	0.038	5452
Parahippocampal and ambient gyri_R[*,†]	0.021	0.032	3583
Amygdala_R[*,†]	0.021	0.034	1057
Hippocampus_R[*,†]	0.021	0.031	1825
Caudate nucleus_L[*,†]	0.019	0.037	3456
Amygdala_L[*,†]	0.018	0.035	1120
Hippocampus_L[*,†]	0.018	0.031	1626

Regions within the set of AD-typical regions were highlighted as red. SD: Standard deviation. '_L' and '_R' indicate the left and right hemisphere, respectively. [*]*and* [†] *denote AAR was significantly different from (p <0.05, two-tailed paired-sample t-test) that of whole gray matter and AD-typical regions respectively.*

In phase 2, out of 28 regions with a higher AAR than whole-GM, bilateral anterior orbital, medial orbital, posterior cingulate, lateral orbital, middle frontal and middle and inferior temporal, and left superior parietal, superior frontal, posterior superior temporal and inferiolateral remainder of parietal lobe had significantly higher AARs than whole-GM (table 12). Among of these 16 regions, bilateral anterior orbital and posterior cingulate, and left medial orbital had significantly higher AARs than AD-typical regions (0.036±0.033).

Table 12*. Rank of annual accumulation rates in sub-regions, AD-typical regions and the whole gray matter of subjects in phase 2*

Region	Mean	SD	Volume(mm3)
Anterior orbital gyrus_L[*,†]	0.045	0.051	5164
Medial orbital gyrus_L[*,†]	0.045	0.046	4780
Anterior orbital gyrus_R[*,†]	0.044	0.052	4807
Medial orbital gyrus_R[*]	0.041	0.044	4962
Posterior cingulate gyrus_R[*,†]	0.040	0.034	7557
Straight gyrus_L	0.040	0.050	3142
Lateral orbital gyrus_R[*]	0.040	0.045	2967
Lateral orbital gyrus_L[*]	0.040	0.045	3328
Posterior cingulate gyrus _L[*,†]	0.039	0.036	7159

Superior parietal gyrus_L*	0.039	0.036	38141
Middle frontal gyrus_R*	0.038	0.040	42929
Superior frontal gyrus_L*	0.038	0.041	46866
Middle frontal gyrus_L*	0.038	0.038	44690
Middle and inferior temporal gyrus_R*	0.038	0.039	13452
Posterior superior temporal gyrus_L*	0.038	0.038	12220
Middle and inferior temporal gyrus_L*	0.038	0.038	13115
Inferiolateral remainder of parietal lobe_L*	0.037	0.035	37662
Superior parietal gyrus_R	0.037	0.035	37509
Straight gyrus_R	0.037	0.045	2856
Inferior frontal gyrus_L	0.036	0.039	14448
AD-typical regions	0.036	0.033	530644
Posterior superior temporal gyrus_R	0.036	0.036	12468
Inferior frontal gyrus_R	0.036	0.040	15294
Postcentral gyrus_L	0.036	0.031	23201
Superior frontal gyrus_R	0.036	0.041	46158
Posterior temporal lobe_L	0.035	0.032	48665
Anterior cingulate gyrus_L	0.035	0.042	7747
Lateral anterior temporal lobe _L	0.035	0.044	2856
Posterior orbital gyrus_L	0.034	0.041	4594
Whole gray matter	0.034	0.031	851002
Posterior orbital gyrus_R	0.034	0.039	4476
Lateral remainder of occipital lobe_R	0.034	0.033	38789
Inferiolateral remainder of parietal lobe_R	0.034	0.035	38214
Precentral gyrus_L†	0.033	0.032	28237
Lateral remainder of occipital lobe_L	0.033	0.032	38030
Postcentral gyrus_R†	0.033	0.032	25731
Anterior cingulate gyrus_R†	0.032	0.039	7441
Posterior temporal lobe_R†	0.032	0.032	47598
Precentral gyrus_R†	0.032	0.033	27438
Lateral anterior temporal lobe _R	0.032	0.043	2842
Anterior superior temporal gyrus_L†	0.032	0.043	4033
Anterior superior temporal gyrus_R†	0.032	0.043	4205
Cuneus_R†	0.031	0.034	9224
Lingual gyrus_R†	0.031	0.033	11970

Insula_L[*,†]	0.030	0.036	12275
Insula_R[*,†]	0.030	0.034	12323
Putamen_L[†]	0.030	0.037	3957
Lingual gyrus_L[*,†]	0.030	0.032	12333
Putamen_R[†]	0.030	0.036	4063
Fusiform gyrus_R[*,†]	0.029	0.038	3479
Fusiform gyrus_L[*,†]	0.028	0.037	3486
Cuneus_L[*,†]	0.028	0.033	9438
Medial anterior temporal lobe_L[*,†]	0.027	0.041	4975
Medial anterior temporal lobe_R[*,†]	0.024	0.039	5107
Parahippocampal and ambient gyri_R[*,†]	0.022	0.033	3583
Caudate nucleus_L[*,†]	0.021	0.043	3456
Amygdala_L[*,†]	0.020	0.039	1120
Parahippocampal and ambient gyri_L[*,†]	0.020	0.034	3595
Amygdala_R[*,†]	0.018	0.040	1057
Hippocampus_R[*,†]	0.017	0.033	1825
Caudate nucleus_R[*,†]	0.017	0.039	3411
Thalamus_L[*,†]	0.016	0.039	5452
Hippocampus_L[*,†]	0.015	0.032	1626
Thalamus_R[*,†]	0.014	0.043	5676

*Regions within the set of AD-typical regions were highlighted as red. SD: Standard deviation. '_L' and '_R' indicate the left and right hemisphere, respectively. *and † denote AAR was significantly different from (p <0.05, two-tailed paired-sample t-test) that of whole gray matter and AD-typical regions respectively.*

In the phases 1 and 2, all regions with AAR above that of the AD-typical region set (n=36) were part of the latter set (phase 1: n=25, phase 2: n=20). Specifically, anterior, medial, and lateral orbital, posterior cingulate, superior parietal, middle, superior, inferior frontal and middle, inferior temporal regions showed the fastest AARs both in the phase 1 (table 11) and 2 (table 12). Thus, the set of AD-typical regions adequately captured the most active Aβ accumulating regions in these two phases.

In the phase 3, 9 regions showed no significant increase in SUVR (table 13). However, among 25 regions with a higher AAR than the AD-typical region, 10 were not part of that set. Moreover, among the top 10 fastest Aβ accumulating regions only 4 were part of the AD-typical region set. In contrast to the phases 1 and 2, bilateral lateral

remainder of occipital lobe, postcentral, precentral, cuneus, and lingual gyrus showed a higher AAR than the set of AD-typical regions. The HCA analysis revealed that the left middle frontal, superior frontal, postcentral, lateral anterior temporal lobe, bilateral lateral remainder of occipital lobe, and the right cuneus were within the same cluster as the top fast Aβ accumulating regions. The random sampling test proved that 93.40% fell into the same top 7 regions within 5852 trials, although they did not have completely the same ranks across 5852 trials. Thus, these 7 regions (Fig. 10) were composed into a set of the phase 3' FARs. The pseudo-temporal analysis for this composited FARs revealed an additional acceleration in the phase 3 (Fig. 11).

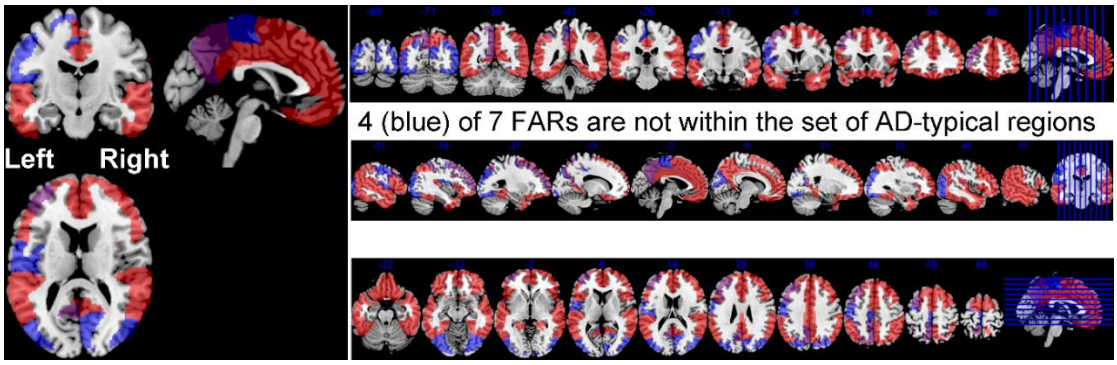

Fig. 10. *Seven fast accumulating regions (FARs) in phase 3 (purple plus blue) and AD-typical regions (red) are overlaid on a standard MRI template in MNI space. Purple and blue denote that FAR is within (3 regions) and outside (4 regions) the set of AD-typical regions, respectively.*

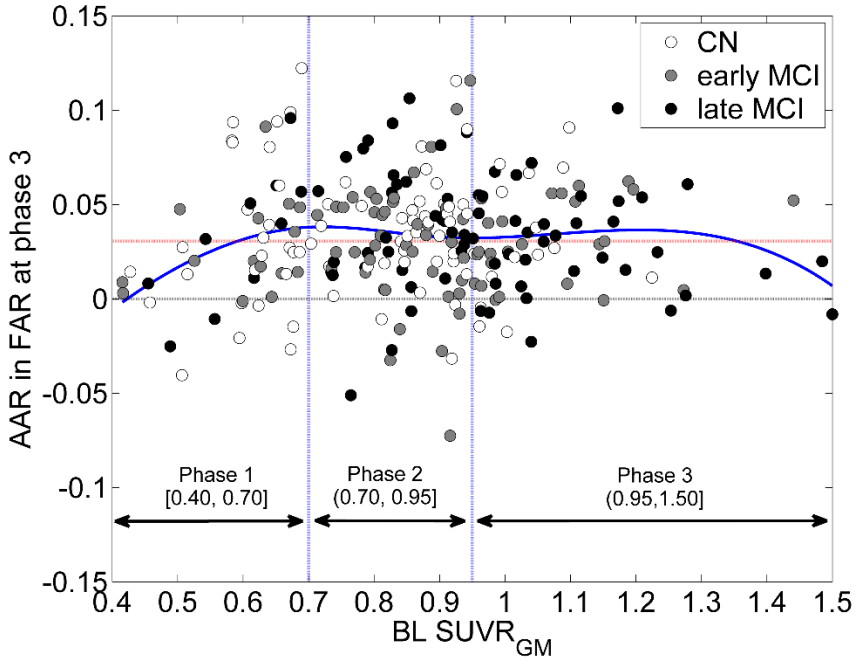

Fig. 11. *Annual accumulation rates (AAR) in composited fast accumulating regions (FARs) of phase 3 as a function of baseline (baseline) SUVR$_{GM}$.*

Table 13. *Rank of annual accumulation rates in sub-regions, AD-typical regions and the whole gray matter in phase 3*

Region	Mean	SD	Volume(mm^3)
Middle frontal gyrus_L *,†,‡	0.031	0.035	44690
Superior frontal gyrus_L‡	0.031	0.039	46866
Cuneus_R*,‡	0.031	0.034	9224
Lateral remainder of occipital lobe_L *,†,‡	0.031	0.030	38030
Postcentral gyrus_L *,†,‡	0.030	0.029	23201
Lateral anterior temporal lobe _L‡	0.030	0.038	2856
Lateral remainder of occipital lobe_R *,†,‡	0.030	0.031	38789
Middle frontal gyrus_R‡	0.029	0.040	42929
Cuneus_L‡	0.029	0.035	9438
Precentral gyrus_L*,‡	0.029	0.030	28237
Superior parietal gyrus_L‡	0.029	0.032	38141
Lateral anterior temporal lobe _R‡	0.028	0.041	2842
Medial orbital gyrus_L‡	0.028	0.039	4780
Precentral gyrus_R‡	0.028	0.035	27438
Postcentral gyrus_R‡	0.027	0.034	25731
Inferiolateral remainder of parietal lobe_R‡	0.027	0.034	38214
Posterior cingulate gyrus _L‡	0.027	0.036	7159
Lingual gyrus_L‡	0.027	0.042	12333
Straight gyrus_L‡	0.027	0.045	3142
Anterior orbital gyrus_L‡	0.027	0.047	5164
Lingual gyrus_R‡	0.026	0.048	11970
Superior parietal gyrus_R‡	0.026	0.032	37509
Lateral orbital gyrus_L‡	0.025	0.066	3328
Inferiolateral remainder of parietal lobe_L‡	0.025	0.029	37662
Middle and inferior temporal gyrus_R‡	0.025	0.040	13452
AD-typical regions‡	0.025	0.026	530644
Superior frontal gyrus_R‡	0.025	0.032	46158
Middle and inferior temporal gyrus_L‡	0.024	0.045	13115
Whole gray matter‡	0.024	0.026	851002
Posterior cingulate gyrus_R‡	0.024	0.044	7557
Anterior cingulate gyrus_L‡	0.024	0.037	7747
Inferior frontal gyrus_L‡	0.024	0.040	14448
Anterior orbital gyrus_R‡	0.024	0.055	4807
Posterior orbital gyrus_L‡	0.023	0.052	4594
Inferior frontal gyrus_R‡	0.023	0.035	15294

Fusiform gyrus_L‡	0.022	0.046	3486
Lateral orbital gyrus_R‡	0.022	0.061	2967
Medial orbital gyrus_R‡	0.022	0.039	4962
Posterior temporal lobe_L‡	0.021	0.037	48665
Posterior temporal lobe_R *,†,‡	0.021	0.030	47598
Medial anterior temporal lobe_L‡	0.021	0.034	4975
Fusiform gyrus_R‡	0.020	0.053	3479
Posterior superior temporal gyrus_R†,‡	0.019	0.037	12468
Anterior superior temporal gyrus_L‡	0.018	0.048	4033
Straight gyrus_R†,‡	0.017	0.041	2856
Posterior orbital gyrus_R‡	0.017	0.048	4476
Posterior superior temporal gyrus_L‡	0.017	0.048	12220
Putamen_R*,†,‡	0.015	0.048	4063
Putamen_L*,†,‡	0.015	0.050	3957
Anterior cingulate gyrus_R*,†,‡	0.014	0.052	7441
Medial anterior temporal lobe_R*,†,‡	0.013	0.039	5107
Parahippocampal and ambient gyri_L*,†,‡	0.012	0.047	3595
Parahippocampal and ambient gyri_R*,†,‡	0.011	0.046	3583
Insula_R*,‡	0.011	0.047	12323
Anterior superior temporal gyrus_R*,†,‡	0.010	0.049	4205
Insula_L*,†	0.010	0.059	12275
Caudate nucleus_L*,†,‡	0.009	0.041	3456
Amygdala_L*,†	0.008	0.059	1120
Thalamus_L*,†	0.007	0.072	5452
Amygdala_R*,†	0.005	0.054	1057
Thalamus_R*,†	-0.000	0.069	5676
Hippocampus_L*,†	-0.001	0.063	1626
Hippocampus_R*,†	-0.002	0.068	1825
Caudate nucleus_R*,†	-0.007	0.072	3411

Regions within the set of AD-typical regions were highlighted as red. SD: Standard deviation. '_L' and '_R' indicate the left and right hemisphere, respectively. *and † *denote AAR was significantly different from (p <0.05, two-tailed paired-sample t-test) that of Whole-GM and AD-typical regions respectively.* ‡ *denotes AAR was significant different from zero (two-tailed one-sample t-test).*

AAR in FARs (0.031 ± 0.026) was 1.23 (Fig. 9B) and 1.27 times higher than that in AD-typical regions (0.025±0.026, p=0.001) and whole-GM (0.024±0.026, p=0.001), respectively. AAR in AD-typical regions was not significantly higher than AAR in whole-GM (p=0.209). The mean baseline SUVR in FARs (1.07±0.15) was lower (p<0.001, two-tailed paired-sample t-test) than that in AD-typical regions (1.12±0.13).

3.2.5. Two-fold cross-validation

The mean effect size d of the 30000 iterations was 0.35±0.12, implying that using the mean AAR of whole-GM to classify fast accumulators and slow accumulators was statistically robust. Mean cutoffs of $SUVR_{GM}$ for phase 1 and phase 2, phase 2 and phase3 were 0.70±0.05 and 0.95±0.07 for 30000 iterations, respectively. Moreover, mean cutoffs of $SUVR_{GM}$ for fast accumulators and slow accumulators were 0.56±0.04 and 0.92±0.05 for 30000 iterations, respectively. The effect size between fast accumulator and slow accumulator using the cut-offs of 0.56 and 0.92 was 0.40 (Fig. 12).

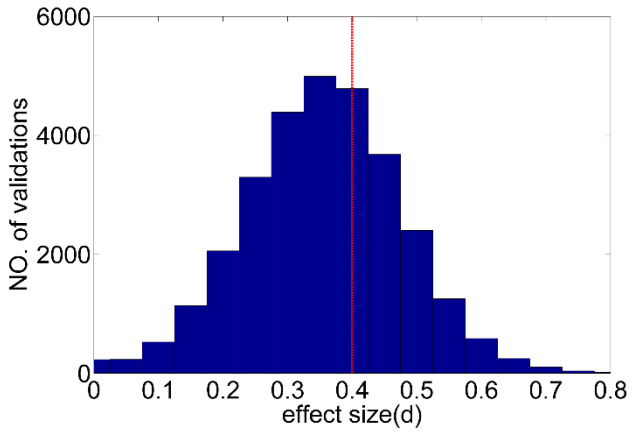

Fig. 12. Two-fold cross-validation test for the selection of mean AAR of whole-GM to define fast accumulators and slow accumulators, the effect size 0.40 between fast accumulator and slow accumulator using the cut-offs of 0.56 and 0.92 was illustrated as red line.

The effect size of 0.39 between AAR in FARs and AD-typical regions was not significantly lower (p=0.299) than the mean value of 30000 iterations in a two-fold cross-validation test (Fig. 13).

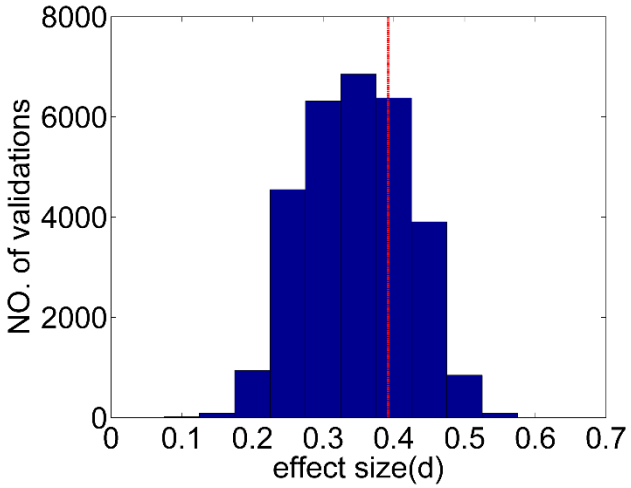

Fig. 13. *Two-fold cross-validation test for effect size (Cohen's d) in AAR between FAR and AD-typical regions in phase 3. The effect size Cohen's d of AAR between the proposed set of FAR and AD-typical regions was illustrated as red line.*

3.2.6. Implications for hypothetical anti-amyloid drug trials at pre-dementia stage of sporadic Alzheimer's disease

Two mechanisms of actions of an anti-amyloid drug were considered: 1) the drug attenuates a (further) Aβ accumulation, and 2) the drug reduces baseline Aβ burden. Assuming a linear relationship between Aβ accumulation and time [6, 53], inclusion of fast accumulators instead of the whole (unselected) cohort would reduce the sample size to treat by around 24 % in the first scenario (table 14). In the second scenario, inclusion of fast accumulators would reduce the sample size to treat by 61 to 70% (table 14). As compared to AD-typical regions, utilization of FARs as target region in subjects with $SUVR_{GM}$ > 0.95 (phase 3) would reduce the sample size to treat by 36 % in the first scenario (table 14). In the second scenario, the sample size would be marginally larger.

Assuming that an anti-amyloid drug attenuates a further SUVR increase by 20% within 24 months, inclusion of fast accumulators only would shorten the trial duration by 3.7 and 10.2 months, as compared to the whole cohort and slow accumulators, respectively (Fig. 14A). Assuming that an anti-amyloid drug reduces baseline SUVR in the treated group by 20% within 24 months, inclusion of fast accumulators only would shorten the trial duration by 4.0 and 9.4 months, respectively (Fig. 14C). As compared to AD-typical regions, utilization of FARs as target region in subjects with $SUVR_{GM}$ >0.95 (phase 3) would shorten the trial duration by 4.5 (Fig. 14B) and 2.2 (Fig. 14D) months for the attenuation and reduction scenarios, respectively.

Table 14. *Number of subjects per arm needed to detect Aβ-modifying treatment effect in clinical trial with 80% power and two-tailed (α=0.05) in the whole cohort, fast accumulators, slow accumulators and the phase 3.*

	whole cohort	**fast accumulators**	**slow accumulators**	**phase 3**	
	AD-typical	AD-typical	AD-typical	AD-typical	FAR
20% attenuation in further SUVR	391	296	552	433	279
50% attenuation in further SUVR	64	49	90	70	46
10% decrease in SUVR from baseline	30	9	37	12	14
20% decrease in SUVR from baseline	13	5	14	5	6

Furthermore, it was examined how differences in baseline $SUVR_{GM}$ between hypothetical treated and placebo groups can impact a clinical trial. Assuming that a drug attenuates Aβ accumulation by 20 % in the end of trial, it would observe 20% attenuation in the end (Fig. 15B) if treated and placebo groups were matched at BL $SUVR_{GM}$ (Fig. 15 A). Figures 15 and 16 (C-F) depict how imbalances in BL $SUVR_{GM}$ between treated and placebo groups can impact PET-based endpoints of a hypothetical clinical trial. Considering an extreme case, where an average baseline $SUVR_{GM}$ of a treated and placebo correspond to the maximal difference in AAR over the trajectory (Fig. 8), i.e. the values of 0.95 and 0.70 or vice versa (Fig. 15). As shown in Fig. 15C, a false 31% ((0.0294-0.0426)/0.0426) attenuation (Fig. 15C) would be detected even without drug. With drug, one would observe a 125 % ((-45%-(-20%)) / (-20%)) overestimation of treatment effect (observed treatment effect= (0.0294*0.8-0.0426)/0.0426= -0.0191/0.0426 = -45%) in the end (Fig. 15D). Conversely, a false 45% ((0.0426-0.0294)/0.0294) enhancement (Fig. 15E) would be detected even without drug. With drug, one would observe a 180 % ((16%-(-20%)) / (-20%)) underestimation of treatment effect (observed treatment effect = (0.0426*0.8-0.0294) /0.0294 = 0.0047/0.0294 = 16%) in the end (Fig. 15F). Assuming that a drug attenuates Aβ accumulation by 20 %, one would observe an overestimation of 125 % in the former case (Fig. 15D). In the latter case, an underestimation of 180 % would appear (Fig. 15F).

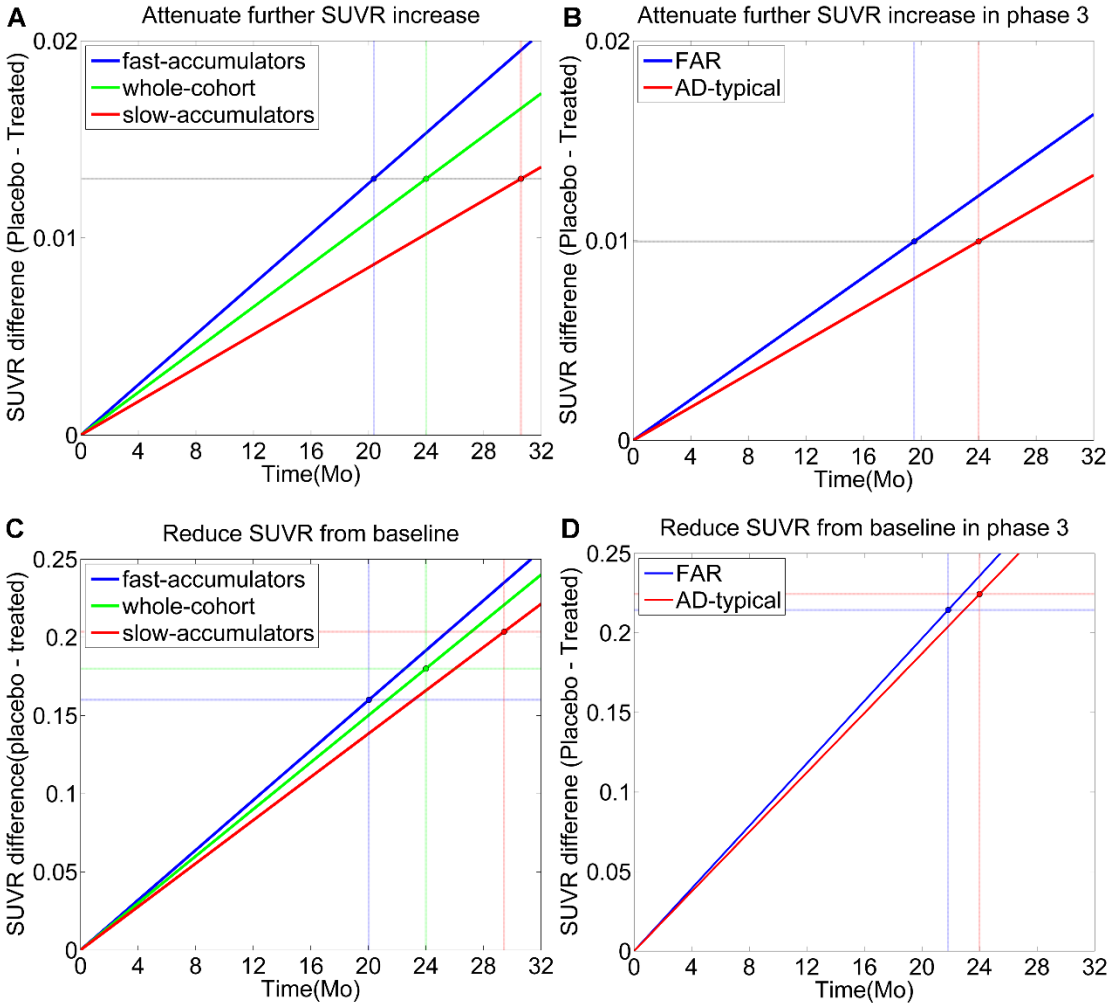

Fig. 14*. Simulation of trial duration using fast accumulators (blue line) and slow accumulators (red line) to detect the same Aβ-modifying treatment effect (20%) as using whole cohort (green line) within 24 months on (A) attenuating further SUVR increase and (C) reducing baseline SUVR in AD-typical regions as compared to placebo group. Simulation of trial duration using fast accumulating regions (FARs) (blue line) to detect the same Aβ-modifying treatment effect (20%) as AD-typical regions (green line) within 24 months on (B) attenuating further SUVR increase and (D) reducing baseline SUVR as compared to placebo group in phase 3.*

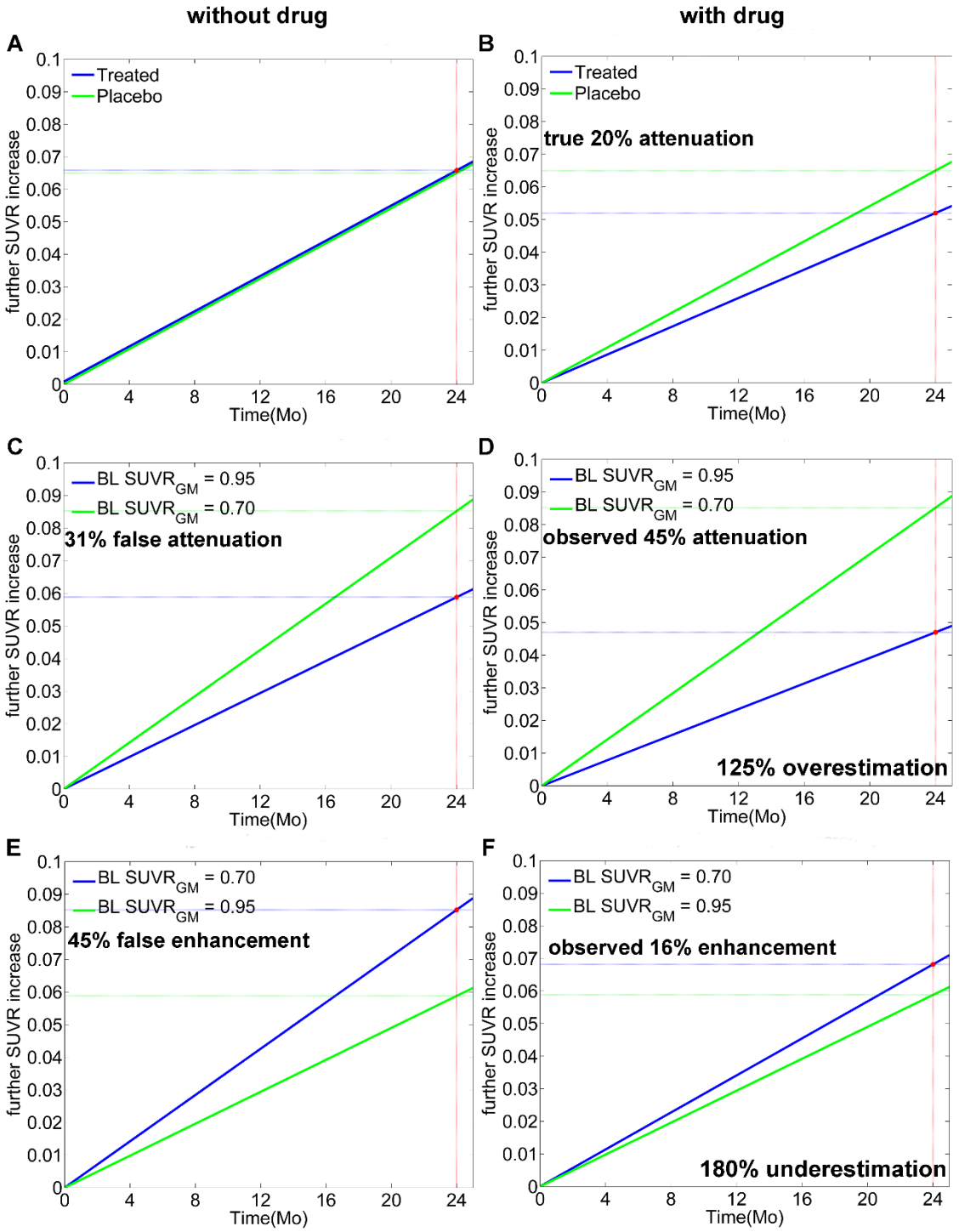

Fig. 15*. Simulation of a drug trial based on the mean annual accumulation rate (AAR) of the whole cohort (A) and a true drug effect of 20% attenuation of a further SUVR increase in AD-typical regions within 24 months (B).*

In reality, the difference in baseline $SUVR_{GM}$ between two groups, which are translated into a distinct natural AAR will be lower. Still, simulations with a difference in baseline $SUVR_{GM}$ of just 0.10 produce a significant bias. Simulations with baseline $SUVR_{GM}$ of 0.60 vs. 0.70 and 0.80 vs. 0.90 are presented in figures 16 and 17,

respectively. In the latter case, an overestimation of 75 % and underestimation of 90 % is evident.

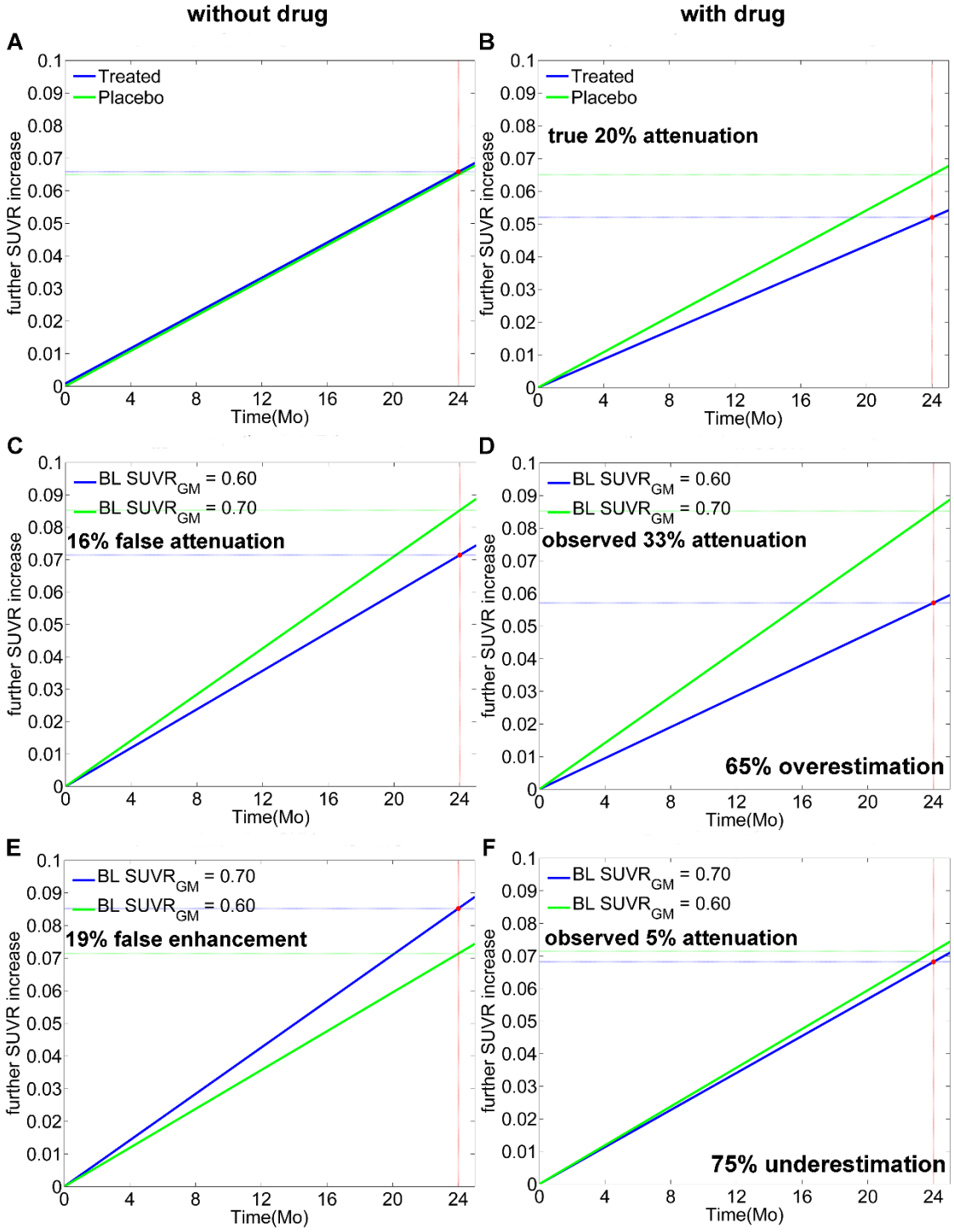

Fig. 16*. Simulation of drug trial using mean annual accumulation rates (AARs) of whole cohort (A), and two example AARs corresponding to baseline SUVR 0.60 and 0.70 to detect 20% attenuation of further SUVR increase in treated group within 24 months. Green and blue line denote treated and placebo groups respectively. Note: "underestimation" and "overestimation" denote the drug is underestimated and overestimated respectively. Baseline SUVR$_{GM}$=0.60 and*

0.70 denote the placebo group having an AAR corresponding to baseline $SUVR_{GM}$ 0.60 and 0.70 respectively.

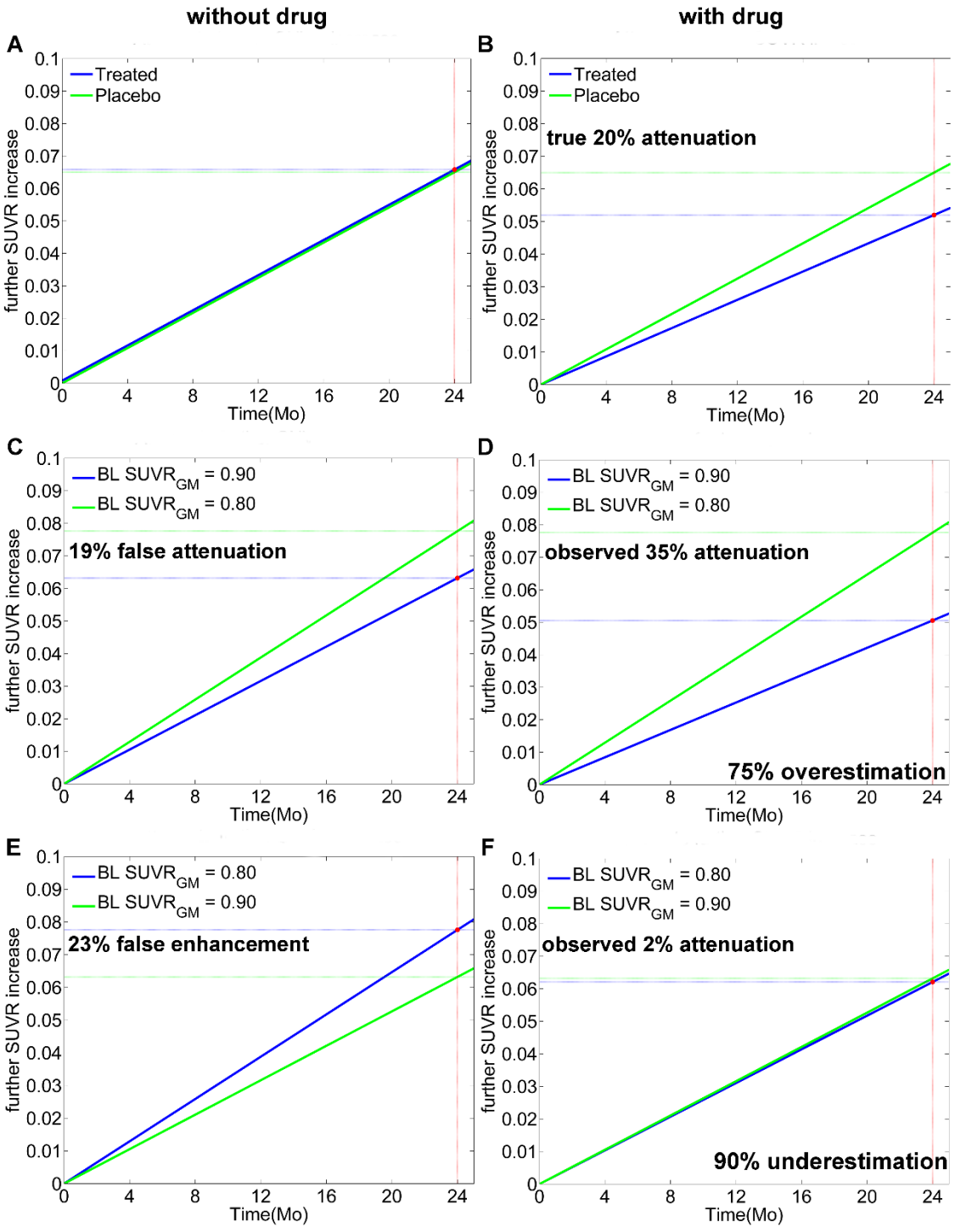

Fig. 17*. Simulation of drug trial using mean annual accumulation rates (AARs) of whole cohort (A), and two example AARs corresponding to baseline SUVR 0.80 and 0.90 to detect 20% attenuation of further SUVR increase in treated group within 24 months. Baseline $SUVR_{GM}$=0.80 and 0.90 denote the placebo group having an AAR corresponding to baseline $SUVR_{GM}$ 0.80 and 0.90 respectively.*

As shown in Fig. 18, the bias also appears if average AARs of two groups correspond to different phases.

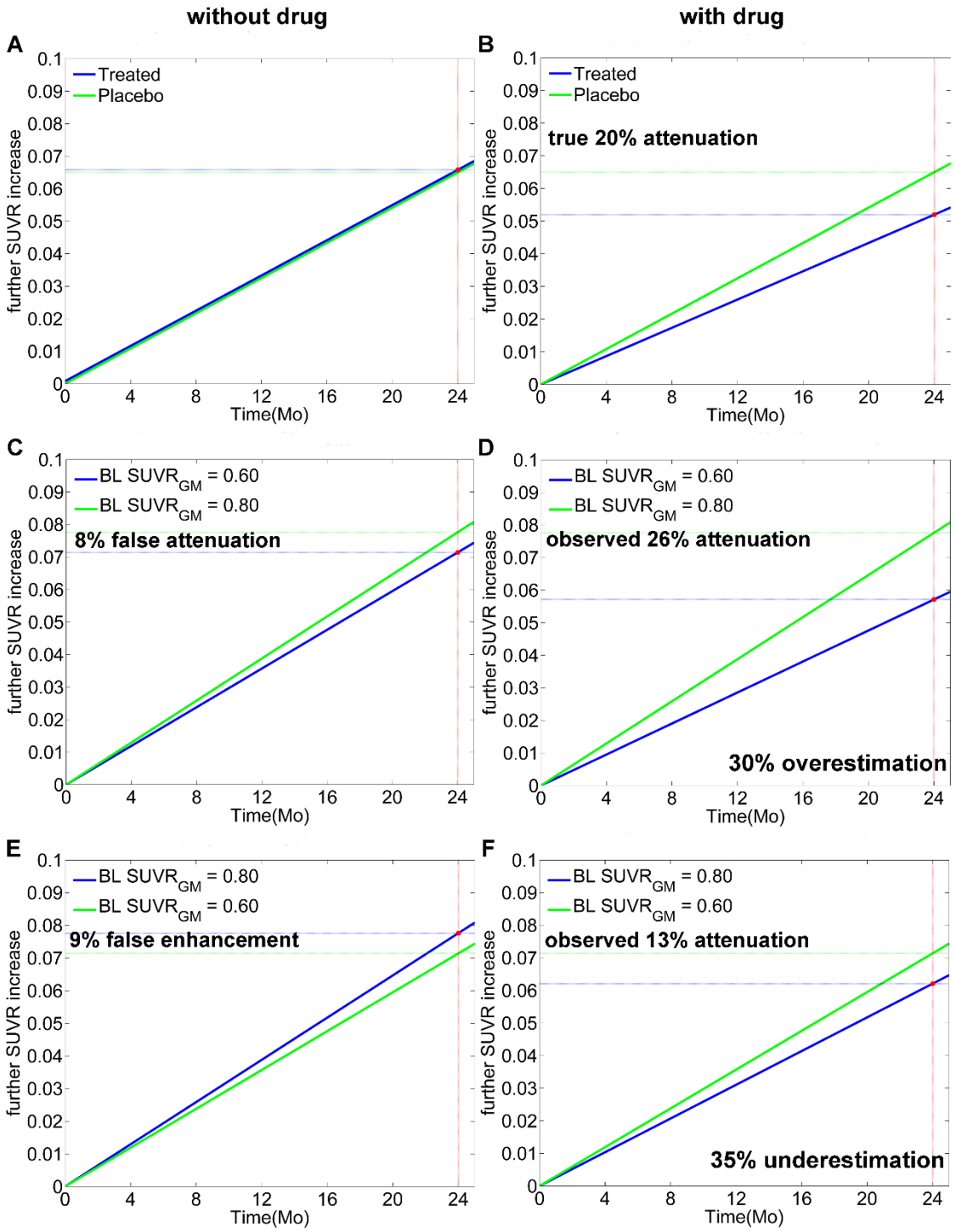

***Fig. 18**. Simulation of drug trial using mean annual accumulation rates (AARs) of whole cohort (A), and two example AARs corresponding to baseline SUVR 0.60 and 0.80 to detect 20% attenuation of further SUVR increase in treated group within 24 months. Baseline $SUVR_{GM}$=0.60 and 0.80 denote the placebo group having an AAR corresponding to baseline $SUVR_{GM}$ 0.60 and 0.80 respectively.*

IV. Spatial and temporal pattern of Aβ accumulation in autosomal dominant Alzheimer's disease

So far, optimal brain regions to be targeted in clinical trials have not been established in ADAD. Such a pattern is useful for design of anti-amyloid drug trials for ADAD. Indeed, DIAN-TU project has included amyloid PET as the secondary outcome measures. The aim of the third project is to explore the spatial pattern of Aβ accumulation in MC in the context of clinical anti-amyloid drug trial.

4.1. Materials and Methods

4.1.1. Participants

The PiB PET data were obtained from DIAN database [113]. The DIAN includes individuals from families with known autosomal dominant mutation in APP [11], PSEN1 [12], or PSEN2 [13]. Considered for the present study were individuals, for whom structural MRI and at least one FU PiB PET scan were available. The current study was based on the eleventh semiannual data cutoff with a total of 151 participants, who had usable PiB scans for at least two visits on the same scanner. Out of them, 1 MC and 1 non-mutation carrier (NC) were detected as significant outlier in respect to AAR (22.3% increase in SUVR from baseline) and baseline SUVR respectively. For those with more than two PiB scans among the final 149 participants, the first two usable visits with an interval as close as to 2 years as possible (median: 2.26, mean: 2.33±0.90) were included. Among 149 participants, 97 were MCs (APP=19, PSEN1=72, PSEN2=6) and 52 were NCs. Following recommendations of the DIAN, Aβ-positivity was defined as SUVR in a composite cortical region (PVC, cerebellum as reference region) [114] of >1.42 downloaded from DIAN database.

4.1.2. PET data acquisition and analysis

Details on image acquisition and preprocessing can be found in [93]. Image analysis was performed using SPM8 (Welcome Department of Imaging Neuroscience, London, UK). The regional analysis was identical to 3.2.2. The set of AD-typical regions was defined as described in 2.1.5. SUVR was calculated as a ratio of regional SUV to SUV in brainstem, which was recommended as reference region for PiB PET data by the DIAN [97]. Corresponding cutoff SUVR referring to brainstem after PVC was identified as 0.81 by performing HCA on Aβ-positive MC and Aβ- NC defined by the cutoff SUVR 1.42 referring to cerebellum cortex provided by DIAN database.

4.1.3. Spatial pattern of Aβ accumulation

AAR of PiB was calculated according to Eq.3 in 2.2.4. An average baseline SUVR and AAR across all subjects were calculated for each region, the set of AD-typical regions as well as for the whole-GM. Mean baseline SUVR and AAR were ranked in a descending order across 62 regions.

4.1.4 Estimated Years to Symptom Onset

Estimated Years to Symptom Onset (EYO) is defined as the estimated time of individual becoming symptomatic in ADAD. The EYO was calculated as follows: 1) the visit age minus the mean mutation age of symptom onset (EYO=Visit age - Mean mutation age of symptom onset) if the individual's mutation was known and the mean mutation age of symptom onset for this individual's mutation was available in the master genetic database. 2) If any given individual's mutation was not available in the master genetic database (e.g. the mutation has not been previously reported or other member age of onset not available), then at any visit, EYO equals to the visit age minus the parental age of symptom onset (EYO=Visit age – parental age of symptom onset).

4.1.5. Fast accumulating regions of Aβ-negative asymptomatic mutation carriers

Aβ-negative asymptomatic MC with EYO >= -15 were included in DIAN-TU trial because it has been reported that significant difference in SUVR between MC and NC appears since EYO -15 [44]. Those Aβ-negative asymptomatic MC don't have substantial amyloid deposition yet, so it may be more suitable to attenuate further SUVR

increase on them. Consequently, spatial pattern of AAR in those individuals are of interest for DIAN-TU trial. Top FARs were investigated if there were any regions having higher AAR than AD-typical regions. To be more specific, all regions including whole-GM were ranked according to their AARs. A HCA analysis was applied to assess potential clustering of regions based on minimum variance within clusters and relatively equal cluster sizes [108]. The sequence of mergers in the dendrogram suggested a cluster solution for regions with AAR above AAR of whole-GM. As a result, regions within the first cluster were subsequently composed into a single region according to equation (4). They are referred to as FARs thereafter.

4.1.6. Statistics

Normality of distributions was tested using the D'Agostino-Pearson test and visual inspection of data histograms. Given a normal data distribution, a parametric (two-tailed) t-test at the significance level of $p<0.05$ was applied, if not otherwise notified. Spearman correlation test was used to check the association between SUVR/AAR and CDR-SB, MMSE, cognitive-composite score. The cognitive-composite represents the average of the z scores from tests including episodic memory, complex attention and processing speed and a general cognitive screen (MMSE) [92]. Data are presented as mean ± SD. Statistical analyses were performed using Graph-Pad Prism 6 for Windows (La Jolla, CA, USA). The number of subjects per arm to detect a treatment effect in a hypothetical 24-month placebo-controlled anti-amyloid clinical trial with 80% power was computed in G Power 3.1 [112].

4.2. Results

4.2.1. Demographics

Table 15. Demographic data of each group of ADAD at baseline

	FU	Age	EYO	APOE ε4	MMSE	CDR-SB	Cog-composite
MC (n=97)	2.16± 0.92	*41.20± 10.02	‡-4.69± 9.57	29.89%	†26.98± 4.71	†1.34± 2.59	†† -0.77±1.06

Aβ-positive MC (n=65)	1.87± 0.73	*43.52± 9.63	ǂ-1.01± 7.02	§35.38%	†26.02± 5.44	†1.93± 2.97	†† -1.17±1.01
Aβ-positive asymptomatic MC (n=31)	2.30± 0.72	39.31± 7.99	ǂ-5.97± 6.80	§45.16%	28.97± 0.95	0.05± 0.15	†† -0.42±0.58
Aβ-positive symptomatic MC (n=34)	1.48± 0.51	*47.37± 9.47	†3.52± 3.03	26.47%	†23.32± 6.39	†3.65± 3.28	††,ǂǂ -1.85±0.83
¶Aβ-negative asymptomatic MC (n=29)	2.82± 0.92	36.22± 9.35	-13.29± 9.57	13.79%	28.86± 1.41	0	0.06±0.60
**Aβ-negative asymptomatic NC (n=50)	2.66± 0.77	39.16± 10.12	-9.26± 9.65	24.00%	29.08± 1.21	0	0.16±0.57

* *denotes significantly different from Aβ-negative and Aβ-positive asymptomatic MC, p<0.05, two-sample t-test.*
† *denotes significantly different from Aβ-negative and Aβ-positive asymptomatic MC, p<0.05, Mann Whitney test.*
ǂ *denotes significantly different from Aβ-negative asymptomatic MC, p<0.05, Mann Whitney test.*
§ *denotes significantly different from Aβ-negative asymptomatic MC, p<0.05, Fisher's exact test.*
¶ *denotes three Aβ-negative symptomatic MC were excluded from 32 Aβ-negative MCs.*
** *denotes two symptomatic NC were excluded from 52 NCs.*
†† *denotes significantly different from Aβ-negative asymptomatic MC and NC, p<0.01, two-sample t-test.*
ǂǂ *denotes significantly different from Aβ-positive asymptomatic MC, p<0.0001, two-sample t-test.*
FU: follow up duration; Cog-composite: The DIAN-TU cognitive composite.

Table 15 shows the demographics of ADAD subjects at baseline. As expected, Aβ-positive symptomatic MC had significantly higher age and EYO than Aβ-positive/negative asymptomatic MC/NC. Aβ-negative asymptomatic MC had significantly lower percentage of APOE ε4 than Aβ-positive asymptomatic MC. Aβ-positive symptomatic MC showed significantly stronger cognitive decline as measured with MMSE, CDR-SB and cog-composite, than asymptomatic MC. Interestingly, Aβ-positive asymptomatic MC had significantly lower cog-composite score than Aβ-negative asymptomatic MC/NC, but had no significant difference in MMSE and CDR-SB.

Baseline SUVR was significantly correlated with EYO (R = 0.61, p<0.0001), Age (R = 0.39, p=0.0001), CDR-SB (R = 0.52, p<0.0001), MMSE (R= -0.32, p=0.0016) and cognitive-composite (R= -0.58, p<0.0001), while AAR was only significantly correlated to baseline SUVR (R= 0.37, p=0.0002) in MC group. There was no correlation between

any parameter in Aβ-negative MC. In Aβ-positive MC, baseline SUVR had correlation with EYO (R = 0.38, p=0.0017), age (R = 0.31, p=0.0112), CDR-SB (R = 0.33, p=0.0076) and cognitive-composite (R = -0.30, p=0.0143) but not in AAR and MMSE. In Aβ-positive asymptomatic MC, baseline SUVR only had significant correlation (R = 0.42, p=0.0198) with EYO, however, there was significant correlation (R = 0.37, p=0.0433) between AAR and cognitive-composite. In Aβ-positive symptomatic MC, the correlation between baseline SUVR and age, CDR-SB, MMSE and cognitive-composite didn't retain, but there was significantly correlation (R=0.39, p=0.023) between baseline SUVR and AAR.

As shown in table 16, SUVR and AAR of each group were summarized. All MC groups had significantly higher SUVR than NC group at baseline. Aβ-negative MC and NC had no significantly positive AAR. Particularly, Aβ-negative asymptomatic MC with EYO >= -15 had no significant increase in SUVR from baseline to FU. The effect size of baseline SUVR of Aβ-negative asymptomatic MC with EYO >= -15 was 22~26% of Aβ-positive MCs. Concerning AAR, the effect size of Aβ-negative asymptomatic MCs was only 41~45% of Aβ-positive MCs. The cutoff EYO -15 identified 65 Aβ-positive MCs out of 78 MCs. However, AAR in AD-typical regions of 13 Aβ-negative asymptomatic MCs was 4.4 and 4.9 times lower ($p<0.0001$) than those of 31 Aβ-positive asymptomatic MCs and 34 symptomatic MCs, respectively. These results suggest that using cutoff EYO -15 may have included Aβ-negative MCs without significantly amyloid accumulation or deposition into the DIAN-TU, thus we may need to exclude them from the drug trial or find out new target regions with more higher AAR to track longitudinal SUVR change.

Table 16. *AARs and baseline SUVRs in AD-typical regions*

All subjects		**SUVR**	**Cohen's d in SUVR**	**AAR**	**Cohen's d in AAR**
MC (n=97)		[*, †]0.99±0.34	1.63	[§,‡]0.029±0.046	0.86
MC with EYO>=-15 (n=78)		[*, †]1.07±0.33	2.00	[§,‡]0.033±0.049	0.92
Aβ-positive MC	all (n=65)	[*, †]1.15±0.30	2.62	[§,‡]0.039±0.051	1.05
	asymptomatic (n=31)	[*, †]1.06±0.28	2.30	[§,‡]0.035±0.051	0.95
	symptomatic (n=34)	[*, †]1.24±0.30	3.05	[§,‡]0.043±0.051	1.16
[¶]Aβ-negative asymptomatic MC	all (n=29)	[†]0.64±0.08	0.67	0.008±0.022	0.43
	EYO< -15 (n=16)	[†]0.64±0.08	0.67	0.009±0.026	0.43
	EYO>= -15 (n=13)	[†]0.65±0.09	0.57	0.008±0.019	0.47
Aβ-negative asymptomatic NC (n=50)		0.60±0.04	---------	[-]0.001±0.019	---------

[*] *denotes significantly higher than Aβ-negative asymptomatic MC, p<0.0001, Mann Whitney test.*
[†] *denotes significantly higher than Aβ- asymptomatic NC, p<0.05, Mann Whitney test.*
[§] *denotes significantly higher than Aβ- asymptomatic MC and NC, p<0.0001, two-sample t-test.*
[‡] *denotes significantly higher than zero, p<0.05, one-sample t-test.*
[¶] *denotes three Aβ-negative symptomatic MC were excluded*
Cohen's d was calculated by comparing to Aβ-negative asymptomatic NC

4.2.2. Spatial pattern of Aβ accumulation

Aβ-negative asymptomatic MC with EYO < -15 and EYO >= -15 had significantly higher SUVR than Aβ-negative asymptomatic NC at both baseline and FU. At baseline, 26 regions of Aβ-negative asymptomatic MC with EYO< -15 and EYO>= -15 have significantly higher SUVR than corresponding subregion of Aβ-negative asymptomatic NC, while the number of regions increased to 51 at FU. There were no significant difference in SUVR of AD-typical regions and 62 sub regions between Aβ-negative asymptomatic MC with EYO<-15 and EYO>=-15 either at baseline or FU. None of 62 regions has significant increase from baseline to FU in Aβ-negative asymptomatic NC and MC with EYO < -15. In contrast, seven regions had significant SUVR increase from baseline to FU in Aβ-negative asymptomatic MC with EYO >= -15, including bilateral superior parietal gyrus, postcentral gyrus and precentral gyrus, and right posterior cingulate gyrus (table 17).

***Table 17**. Annual accumulation rates in sub regions, AD-typical regions and the whole gray matter of Aβ-negative asymptomatic MC with EYO >= -15*

Region	Mean	SD	Volume(mm^3)
Superior parietal gyrus_R[*,†,‡]	0.016	0.016	37509
Superior parietal gyrus_L[†,‡]	0.015	0.024	38141
Middle frontal gyrus_L	0.015	0.025	44690
Inferiolateral remainder of parietal lobe_L	0.013	0.025	37662
Postcentral gyrus_R[‡]	0.013	0.019	25731
Precentral gyrus_L[‡]	0.012	0.017	28237
Precentral gyrus_R[‡]	0.012	0.012	27438
Postcentral gyrus_L[‡]	0.012	0.020	23201
Inferiolateral remainder of parietal lobe_R	0.012	0.022	38214
Posterior part of cingulate gyrus _L	0.011	0.024	7159
Posterior part of cingulate gyrus_R[‡]	0.011	0.014	7557
Lateral remainder of occipital lobe_R	0.011	0.020	38789
Superior frontal gyrus_L	0.011	0.018	46866
Lateral remainder of occipital lobe_L	0.010	0.027	38030
Cuneus_L	0.009	0.025	9438
Anterior part of superior temporal gyrus_L	0.009	0.023	4033
Lateral orbital gyrus_L	0.009	0.047	3328

Lateral part of anterior temporal lobe _R	0.009	0.026	2842
Thalamus_L	0.008	0.020	5452
Anterior orbital gyrus_L	0.008	0.038	5164
Whole gray matter	0.008	0.018	851002
AD-typical regions	0.008	0.019	530664
Superior frontal gyrus_R	0.008	0.018	46158
Anterior part of cingulate gyrus_R	0.008	0.023	7441
Lateral part of anterior temporal lobe _L	0.007	0.034	2856
Middle frontal gyrus_R	0.007	0.024	42929
Middle and inferior temporal gyrus_R	0.007	0.019	13452
Fusiform gyrus_L	0.007	0.028	3486
Inferior frontal gyrus_L	0.007	0.029	14448
Lingual gyrus_R	0.006	0.026	11970
Insula_L	0.006	0.023	12275
Medial orbital gyrus_R	0.006	0.036	4962
Posterior part of superior temporal gyrus_L	0.005	0.027	12220
Posterior temporal lobe_L	0.005	0.023	48665
Posterior temporal lobe_R	0.005	0.019	47598
Cuneus_R	0.004	0.026	9224
Posterior orbital gyrus_L	0.004	0.023	4594
Middle and inferior temporal gyrus_L	0.004	0.026	13115
Fusiform gyrus_R	0.004	0.032	3479
Medial part of anterior temporal lobe_L	0.004	0.028	4975
Posterior orbital gyrus_R	0.003	0.030	4476
Straight gyrus_R	0.003	0.027	2856
Putamen_R	0.003	0.019	4063
Parahippocampal and ambient gyri_L	0.002	0.021	3595
Hippocampus_R	0.002	0.026	1825
Insula_R	0.002	0.024	12323
Parahippocampal and ambient gyri_R	0.002	0.021	3583
Posterior part of superior temporal gyrus_R	0.001	0.021	12468
Lingual gyrus_L	0.001	0.031	12333
Straight gyrus_L	0.001	0.021	3142
Inferior frontal gyrus_R	0.000	0.026	15294
Amygdala_R	0.000	0.028	1057
Anterior part of superior temporal gyrus_R	-0.001	0.014	4205
Medial part of anterior temporal lobe_R	-0.001	0.027	5107
Anterior part of cingulate gyrus_L	-0.001	0.024	7747
Anterior orbital gyrus_R	-0.001	0.046	4807
Putamen_L	-0.001	0.027	3957
Caudate nucleus_L	-0.002	0.020	3456
Medial orbital gyrus_L	-0.002	0.025	4780
Lateral orbital gyrus_R	-0.003	0.035	2967
Thalamus_R	-0.003	0.026	5676
Amygdala_L	-0.005	0.023	1120
Hippocampus_L	-0.006	0.023	1626
Caudate nucleus_R	-0.011	0.022	3411

*Regions within the set of AD-typical regions were highlighted as red. SD: Standard deviation. '_L' and '_R' indicate the left and right hemisphere, respectively. *and † denote AAR was significantly different from ($p < 0.05$, two-tailed paired-sample t-test) that of Whole-GM and AD-typical regions respectively. ‡ denotes AAR was significant different from zero (two-tailed one-sample t-test).*

As shown in table 18, most of top regions with high SUVR at baseline of Aβ-positive MC were within the set of AD-typical regions except for subcortical regions putamen and caudate nucleus. Considering those subcortical regions have small volumes, therefore adding them into the set of AD-typical regions or not may not change SUVR a lot.

***Table 18**. Top regions with a higher baseline SUVR than AD-typical region and whole gray matter of Aβ-positive MC*

Region	Mean	SD	Volume(mm^3)
Putamen_R	1.45	0.39	4063
Putamen_L	1.44	0.38	3957
Posterior part of cingulate gyrus_R	1.29	0.31	7557
Posterior part of cingulate gyrus _L	1.28	0.31	7159
Caudate nucleus_R	1.28	0.33	3411
Caudate nucleus_L	1.27	0.34	3456
Anterior part of cingulate gyrus_R	1.27	0.32	7441
Medial orbital gyrus_R	1.27	0.35	4962
Anterior part of cingulate gyrus_L	1.26	0.31	7747
Anterior orbital gyrus_R	1.26	0.38	4807
Medial orbital gyrus_L	1.25	0.35	4780
Anterior orbital gyrus_L	1.25	0.38	5164
Straight gyrus_R	1.25	0.34	2856
Superior parietal gyrus_R	1.25	0.31	37509
Superior parietal gyrus_L	1.24	0.31	38141
Middle frontal gyrus_R	1.24	0.37	42929
Superior frontal gyrus_R	1.24	0.34	46158
Straight gyrus_L	1.24	0.33	3142
Superior frontal gyrus_L	1.22	0.35	46866
Middle frontal gyrus_L	1.21	0.36	44690
Lateral orbital gyrus_R	1.16	0.35	2967
Inferior frontal gyrus_R	1.16	0.32	15294
Lateral orbital gyrus_L	1.15	0.33	3328
AD-typical regions	1.15	0.30	530664
Inferior frontal gyrus_L	1.14	0.33	14448
Posterior part of superior temporal gyrus_L	1.11	0.31	12220
Posterior orbital gyrus_L	1.11	0.28	4594
Posterior orbital gyrus_R	1.11	0.28	4476
Whole gray matter	1.11	0.27	851002

Regions within the set of AD-typical regions were highlighted as red. SD: Standard deviation. '_L' and '_R' indicate the left and right hemisphere, respectively.

Concerning symptomatic status, top regions with higher baseline SUVR than AD-typical regions of Aβ-positive asymptomatic and symptomatic MC were illustrated in table 19 and 20. Those top regions were still within the set of AD-typical regions except for subcortical regions putamen and caudate nucleus. All those top regions of Aβ-positive asymptomatic MC had significantly lower baseline SUVR than corresponding region of symptomatic individuals.

***Table 19**. Top regions with a higher baseline SUVR than AD-typical regions of Aβ-positive asymptomatic MC*

Region	Mean	SD	Volume(mm^3)
Putamen_R	1.23	0.34	4063
Putamen_L	1.23	0.33	3957
Posterior part of cingulate gyrus_R	1.19	0.29	7557
Posterior part of cingulate gyrus _L	1.19	0.29	7159
Anterior part of cingulate gyrus_R	1.16	0.31	7441
Superior parietal gyrus_R	1.16	0.31	37509
Superior parietal gyrus_L	1.16	0.31	38141
Anterior part of cingulate gyrus_L	1.16	0.29	7747
Straight gyrus_R	1.13	0.29	2856
Straight gyrus_L	1.13	0.30	3142
Superior frontal gyrus_R	1.13	0.33	46158
Medial orbital gyrus_R	1.13	0.30	4962
Medial orbital gyrus_L	1.12	0.30	4780
Middle frontal gyrus_R	1.12	0.34	42929
Caudate nucleus_R	1.12	0.31	3411
Superior frontal gyrus_L	1.11	0.33	46866
Caudate nucleus_L	1.11	0.32	3456
Anterior orbital gyrus_R	1.10	0.32	4807
Anterior orbital gyrus_L	1.09	0.34	5164
Middle frontal gyrus_L	1.07	0.33	44690
AD-typical regions	1.06	0.28	530664

Regions within the set of AD-typical regions were highlighted as red. SD: Standard deviation. '_L' and '_R' indicate the left and right hemisphere, respectively.

***Table 20**. Top regions with a higher baseline SUVR than AD-typical regions of Aβ-positive symptomatic MC*

Region	Mean	SD	Volume(mm^3)
Putamen_R	1.64	0.34	4063
Putamen_L	1.62	0.32	3957
Caudate nucleus_L	1.42	0.29	3456
Caudate nucleus_R	1.42	0.27	3411
Anterior orbital gyrus_R	1.41	0.37	4807

Anterior orbital gyrus_L	1.39	0.36	5164
Medial orbital gyrus_R	1.39	0.36	4962
Posterior part of cingulate gyrus_R	1.38	0.30	7557
Anterior part of cingulate gyrus_R	1.37	0.31	7441
Medial orbital gyrus_L	1.37	0.35	4780
Posterior part of cingulate gyrus _L	1.37	0.31	7159
Anterior part of cingulate gyrus_L	1.36	0.30	7747
Middle frontal gyrus_R	1.36	0.35	42929
Straight gyrus_R	1.36	0.35	2856
Superior frontal gyrus_R	1.33	0.33	46158
Straight gyrus_L	1.33	0.33	3142
Middle frontal gyrus_L	1.33	0.35	44690
Superior parietal gyrus_R	1.32	0.28	37509
Superior parietal gyrus_L	1.32	0.29	38141
Superior frontal gyrus_L	1.32	0.34	46866
Lateral orbital gyrus_R	1.29	0.33	2967
Lateral orbital gyrus_L	1.27	0.32	3328
Inferior frontal gyrus_R	1.26	0.33	15294
Inferior frontal gyrus_L	1.24	0.34	14448
AD-typical regions	1.24	0.30	530664

Regions within the set of AD-typical regions were highlighted as red. SD: Standard deviation. '_L' and '_R' indicate the left and right hemisphere, respectively.

As shown in table 21, 56 regions had significant increase in SUVR from baseline to FU in Aβ-positive MC. Out of 27 regions with a higher AAR than whole-GM in Aβ-positive MC, only bilateral putamen, left caudate nucleus, and right lateral remainder of occipital lobe were not within the set of AD-typical regions, and note that they were not top high regions.

Table 21. *Annual accumulation rates in sub regions, AD-typical regions and the whole gray matter of Aβ-positive MC*

Region	Mean	SD	Volume(mm^3)
Lateral orbital gyrus_R[*,‡]	0.058	0.097	2967
Anterior orbital gyrus_R[*,‡]	0.054	0.089	4807
Lateral orbital gyrus_L[*,‡]	0.053	0.086	3328
Inferiolateral remainder of parietal lobe_R[*,‡]	0.046	0.064	38214
Superior parietal gyrus_R[*,‡]	0.045	0.062	37509
Middle frontal gyrus_L[*,‡]	0.044	0.063	44690
Anterior orbital gyrus_L[‡]	0.044	0.085	5164
Superior parietal gyrus_L[‡]	0.044	0.074	38141
Inferiolateral remainder of parietal lobe_L[‡]	0.043	0.074	37662
Middle and inferior temporal gyrus_L[‡]	0.043	0.055	13115
Superior frontal gyrus_L[‡]	0.042	0.061	46866
Lateral part of anterior temporal lobe _L[‡]	0.042	0.060	2856
Middle frontal gyrus_R[‡]	0.041	0.074	42929
Putamen_L[‡]	0.040	0.060	3957

Caudate nucleus_L‡	0.040	0.086	3456
AD-typical regions‡	0.039	0.051	**530664**
Medial orbital gyrus_L‡	0.039	0.077	4780
Medial orbital gyrus_R‡	0.038	0.075	4962
Inferior frontal gyrus_R‡	0.038	0.076	15294
Inferior frontal gyrus_L‡	0.038	0.057	14448
Putamen_R‡	0.038	0.064	4063
Middle and inferior temporal gyrus_R‡	0.037	0.053	13452
Lateral remainder of occipital lobe_R‡	0.037	0.059	38789
Superior frontal gyrus_R‡	0.037	0.067	46158
Posterior temporal lobe_R‡	0.037	0.045	47598
Posterior part of superior temporal gyrus_R‡	0.036	0.056	12468
Posterior part of superior temporal gyrus_L‡	0.036	0.060	12220
Posterior part of cingulate gyrus_R‡	0.036	0.053	7557
Whole gray matter‡	0.036	0.048	**851002**
Cuneus_L‡	0.035	0.064	9438
Lateral part of anterior temporal lobe _R‡	0.035	0.068	2842
Straight gyrus_R‡	0.035	0.077	2856
Posterior orbital gyrus_R‡	0.034	0.070	4476
Postcentral gyrus_R‡	0.034	0.064	25731
Anterior part of superior temporal gyrus_L‡	0.034	0.061	4033
Lateral remainder of occipital lobe_L‡	0.034	0.065	38030
Straight gyrus_L‡	0.034	0.074	3142
Posterior part of cingulate gyrus _L‡	0.034	0.051	7159
Posterior temporal lobe_L‡	0.033	0.051	48665
Anterior part of cingulate gyrus_L‡	0.032	0.064	7747
Postcentral gyrus_L‡	0.032	0.061	23201
Posterior orbital gyrus_L‡	0.032	0.068	4594
Insula_R‡	0.031	0.049	12323
Cuneus_R‡	0.030	0.061	9224
Precentral gyrus_L‡	0.028	0.058	28237
Precentral gyrus_R‡	0.028	0.059	27438
Anterior part of superior temporal gyrus_R‡	0.027	0.058	4205
Anterior part of cingulate gyrus_R‡	0.025	0.059	7441
Insula_L‡	0.025	0.044	12275
Fusiform gyrus_L‡	0.023	0.048	3486
Fusiform gyrus_R‡	0.020	0.056	3479
Medial part of anterior temporal lobe_L‡	0.020	0.039	4975
Medial part of anterior temporal lobe_R‡	0.020	0.045	5107
Lingual gyrus_R‡	0.019	0.048	11970
Caudate nucleus_R	0.018	0.102	3411
Thalamus_L‡	0.016	0.051	5452
Lingual gyrus_L‡	0.015	0.055	12333
Amygdala_L	0.010	0.044	1120
Parahippocampal and ambient gyri_R‡	0.010	0.039	3583
Parahippocampal and ambient gyri_L‡	0.009	0.033	3595
Hippocampus_R	0.007	0.034	1825
Amygdala_R	0.007	0.047	1057

Hippocampus_L	0.004	0.046	1626
Thalamus_R	0.001	0.064	5676

Regions within the set of AD-typical regions were highlighted as red. SD: Standard deviation. '_L' and '_R' indicate the left and right hemisphere, respectively. **and* † *denote AAR was significantly different from ($p < 0.05$, two-tailed paired-sample t-test) that of Whole-GM and AD-typical regions respectively.* ‡ *denotes AAR was significant different from zero (two-tailed one-sample t-test).*

In Aβ-positive asymptomatic MC, 33 regions had higher AAR than whole-GM (table 22). Out of those 33 FARs, only bilateral putamen were not within the set of AD-typical regions. In contrast, only 23 regions had higher AAR than whole-GM in Aβ-positive symptomatic MC (table 23), out of top 10 FARs, left caudate nucleus and cuneus, and bilateral lateral remainder of occipital lobe were not within the set of AD-typical regions. Particularly, cuneus and lateral remainder of occipital lobe were also within top FARs of phase3 of pre-dementia stage of sAD (table 13).

Table 22*. Top 33 FARs with a higher AAR than the whole gray matter of Aβ-positive asymptomatic MC*

Region	Mean	SD	Volume(mm^3)
Lateral orbital gyrus_R^{x}	0.061	0.099	2967
Anterior orbital gyrus_R*,‡	0.060	0.097	4807
Lateral orbital gyrus_L*,†,‡	0.059	0.088	3328
Anterior orbital gyrus_L‡	0.058	0.093	5164
Medial orbital gyrus_L‡	0.048	0.079	4780
Middle frontal gyrus_L*,†,‡	0.046	0.061	44690
Medial orbital gyrus_R‡	0.046	0.078	4962
Lateral part of anterior temporal lobe _L‡	0.044	0.057	2856
Superior frontal gyrus_L‡	0.039	0.062	46866
Straight gyrus_R‡	0.039	0.066	2856
Middle frontal gyrus_R*,‡	0.039	0.063	42929
Putamen_L‡	0.039	0.053	3957
Inferior frontal gyrus_L‡	0.038	0.059	14448
Superior frontal gyrus_R‡	0.037	0.065	46158
Middle and inferior temporal gyrus_L‡	0.037	0.051	13115
Middle and inferior temporal gyrus_R‡	0.036	0.053	13452
Superior parietal gyrus_R‡	0.036	0.057	37509
Posterior part of cingulate gyrus _L‡	0.036	0.049	7159
Superior parietal gyrus_L‡	0.036	0.061	38141
AD-typical regions‡	0.035	0.051	**530664**
Anterior part of cingulate gyrus_R‡	0.035	0.062	7441
Posterior orbital gyrus_R‡	0.035	0.070	4476
Posterior part of cingulate gyrus_R‡	0.035	0.055	7557
Inferiolateral remainder of parietal lobe_R‡	0.034	0.051	38214
Posterior orbital gyrus_L‡	0.034	0.062	4594

Inferiolateral remainder of parietal lobe_L‡	0.033	0.062	37662
Posterior part of superior temporal gyrus_R‡	0.033	0.051	12468
Straight gyrus_L‡	0.033	0.079	3142
Lateral part of anterior temporal lobe _R‡	0.032	0.064	2842
Putamen_R‡	0.032	0.056	4063
Anterior part of cingulate gyrus_L‡	0.032	0.060	7747
Inferior frontal gyrus_R‡	0.032	0.059	15294
Posterior temporal lobe_R‡	0.030	0.044	47598
Whole gray matter	0.030	0.048	**851002**

*Regions within the set of AD-typical regions were highlighted as red. SD: Standard deviation. '_L' and '_R' indicate the left and right hemisphere, respectively. *and † denote AAR was significantly different from (p <0.05, two-tailed paired-sample t-test) that of Whole-GM and AD-typical regions respectively. ‡ denotes AAR was significant different from zero (two-tailed one-sample t-test).*

***Table 23**. Top 23 FARs with a higher AAR than the whole gray matter of Aβ-positive symptomatic MC*

Region	Mean	SD	Volume(mm^3)
Caudate nucleus_L‡	0.058	0.098	3456
Inferiolateral remainder of parietal lobe_R*,‡	0.056	0.074	38214
Lateral orbital gyrus_R‡	0.056	0.096	2967
Lateral remainder of occipital lobe_R*,‡	0.054	0.054	38789
Cuneus_L‡	0.053	0.063	9438
Superior parietal gyrus_R‡	0.053	0.066	37509
Inferiolateral remainder of parietal lobe_L	0.052	0.084	37662
Lateral remainder of occipital lobe_L‡	0.052	0.064	38030
Superior parietal gyrus_L‡	0.050	0.084	38141
Middle and inferior temporal gyrus_L‡	0.049	0.058	13115
Anterior orbital gyrus_R‡	0.048	0.082	4807
Lateral orbital gyrus_L‡	0.048	0.085	3328
Superior frontal gyrus_L‡	0.045	0.061	46866
Posterior part of superior temporal gyrus_L‡	0.044	0.059	12220
Inferior frontal gyrus_R‡	0.044	0.089	15294
Middle frontal gyrus_R‡	0.043	0.084	42929
Anterior part of superior temporal gyrus_L‡	0.043	0.073	4033
AD-typical regions‡	0.043	0.051	**530664**
Posterior temporal lobe_R‡	0.043	0.047	47598
Middle frontal gyrus_L‡	0.043	0.066	44690
Putamen_R‡	0.043	0.072	4063
Cuneus_R‡	0.042	0.054	9224
Putamen_L‡	0.042	0.066	3957
Whole gray matter‡	0.041	0.048	**851002**

*Regions within the set of AD-typical regions were highlighted as red. SD: Standard deviation. '_L' and '_R' indicate the left and right hemisphere, respectively. *and † denote AAR was significantly different from (p <0.05, two-tailed paired-sample t-test) that of Whole-GM and*

AD-typical regions respectively. ‡ denotes AAR was significant different from zero (two-tailed one-sample t-test).

4.2.3. High percentage of mutation APP in amyloid negative MCs

The percentage of APP (61.54%/66.67%) in asymptomatic/all Aβ-negative MCs was significantly higher (Fisher's exact test, p=0.0036/0.0002) than the percentage of other mutation types (7.94%/15.62%) in asymptomatic/all Aβ-negative MCs (table 24), implying that the calculation of EYO of APP carriers may be not as accurate as PSEN1.

Table 24. *The number of different mutation types (PSEN1, PSEN2 and APP) in each group*

All subjects		PSEN1	PSEN2	APP
MC with EYO>= -15 (n=78)		61	2	15
Aβ-positive MC	All (n=62)	54	2	6
	Asymptomatic (n=28)	23	1	4
	Symptomatic (n=34)	31	1	2
Aβ-negative MC	*All (n=16)	7	0	9
	Symptomatic MC (n=3)	2	0	1
	†Asymptomatic MC(n=13)	5	0	8

** The percentage of APP in Aβ-negative MC was significantly higher than other mutation types, p=0.0002, Fisher's exact test.*
† The percentage of APP in Aβ-negative asymptomatic MC was significantly higher than other mutation types, p=0.0036, Fisher's exact test.

Table 25 showed that baseline SUVR and AAR of APP was lower (No significance, Mann Whitney test) than that of PSEN1 in Aβ-negative MC group, although APP had similar EYO as PSEN1. In Aβ-positive MC, APP had higher (No significance, Mann Whitney test) baseline SUVR and AAR than other mutation types.

Table 25. *Comparisons of APP and PSEN and PSEN2*

		EYO	Age	SUVR	AAR
MC with EYO>= -15 (n=78)	PSEN1+2 (n=63)	§-0.10±5.43	42.94±9.69	*1.12±0.32	0.036±0.051
	APP(n=15)	-3.55±5.24	45.47±5.28	0.86±0.31	0.020±0.039
Aβ-positive MC (n=62)	PSEN1+2 (n=56)	0.30±5.38	43.77±9.47	1.17±0.30	0.038±0.053
	APP(n=6)	-3.00±6.29	44.33±5.68	1.20±0.16	0.053±0.036
Aβ-negative MC(n=16)	PSEN1 (n=7)	-3.29±5.04	§36.29±9.48	0.75±0.19	†0.019±0.018
	APP(n=9)	-3.91±4.79	46.22±5.19	0.64±0.06	-0.003±0.021

** Baseline SUVR of PSEN 1+2 was significantly higher than APP, p=0.0067, two sample t-test.*
† denotes significantly higher than APP, p=0.091, Mann Whitney test.
§ denotes significantly higher than APP, p<0.05, Mann Whitney test.

4.2.4. Trajectory of SUVR as a function of EYO

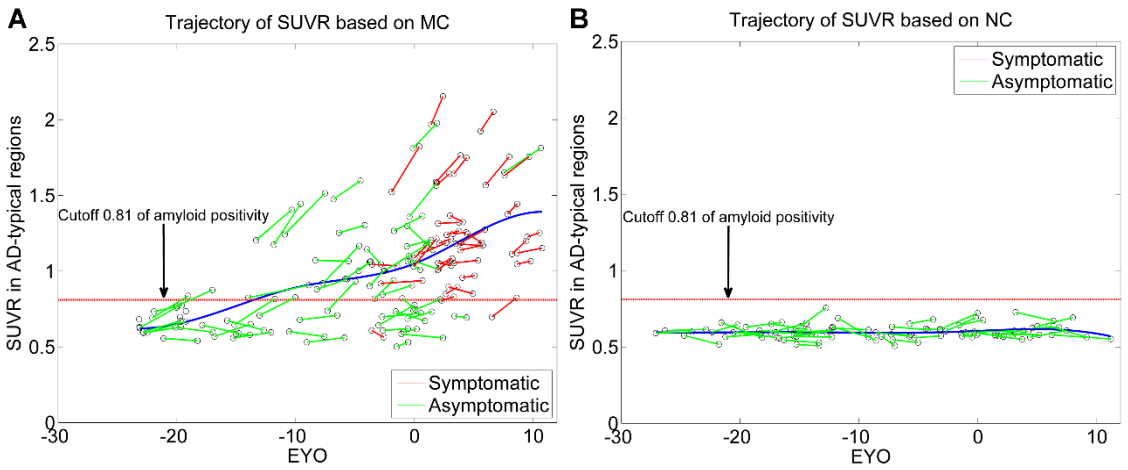

Fig. 19. Trajectory of SUVR in MC accumulators (A) and NC (B) as a function of EYO.

Fig. 19 illustrates the trajectory of SUVR in MC (fig. 19A) and NC (fig. 19B) as a function of EYO. As shown in fig.20A, SUVR of MC increases and reaches amyloid positivity after EYO -15. After reaching amyloid positivity, SUVR increases slightly, but increasing rate of SUVR tends to increase after EYO above zero. In the end, SUVR tends to reach plateau. In contrast, the SUVR of NC didn't show any obvious increase over the whole period.

4.2.5. Fast accumulating regions of Aβ-negative asymptomatic MC with EYO>= -15

Amyloid deposition of Aβ-negative asymptomatic MC with EYO>= -15 was relatively low, although SUVR of them was significantly higher than NC group. It may be more suitable to prevent further SUVR increase rather than reducing baseline SUVR. However, AAR in AD-typical region is not significantly different from zero. In Aβ-negative asymptomatic MC with EYO>= -15, 20 regions had higher AAR than whole-GM. The HCA analysis revealed that the bilateral superior parietal, postcentral and precentral, and left middle frontal and inferiolateral remainder of parietal lobe were the top fast Aβ accumulating regions. Thus, these 8 regions were composed into a set of the fast accumulating regions (FARs). AAR of the composited FAR (0.014±0.019) in Aβ-

negative asymptomatic MC with EYO>= -15 was significantly higher (p=0.021, one-sample t-test) than zero, and 1.75 times significantly (p=0.011, paired-sample t-test) higher than corresponding AAR of AD-typical regions (0.008±0.019).

4.2.6. Implications for DIAN-TU trial

As described above, it may make sense to attenuate a (further) Aβ accumulation rather than reduce baseline Aβ burden for Aβ-negative asymptomatic MC with EYO>= -15. Assuming a linear relationship between Aβ accumulation and time within two years[6, 53] utilization of FARs as target region for those individuals would reduce the sample size to treat by around 67% as compared to AD-typical regions (table 26). Assuming that an anti-amyloid drug attenuates a further SUVR increase by 100% within 24 months, utilization of FARs as target region in trial with Aβ-negative asymptomatic MC would shorten the trial duration by 14 months as compared to AD-typical regions.

Table 26. *Number of subjects per arm needed to detect Aβ-modifying treatment effect in clinical trial with 80% power and two-tailed (α=0.05) using fast accumulating regions (FARs) and AD-typical regions as the target respectively for Aβ-negative asymptomatic MC.*

Sample size needed to detect Aβ-modifying treatment	Aβ-negative asymptomatic MC with EYO>= -15	
	AD-typical	FAR
20% attenuation in further SUVR	2215	724
50% attenuation in further SUVR	356	117
100% attenuation in further SUVR	90	30

Regarding to the Aβ-positive MC, two mechanisms of actions of an anti-amyloid drug could be considered: 1) the drug attenuates a (further) Aβ accumulation, and 2) the drug reduces baseline Aβ burden. The sample size for using MC with EYO >= -15 and Aβ-positive MC as the target to detect SUVR change in AD-typical regions in the anti-amyloid drug trial were calculated in table 27, which may provide the sampe size needed for measurements of amyloid PET imaging in DIAN-TU.

Table 27. *Number of subjects per arm needed to detect Aβ-modifying treatment effect in clinical trial with 80% power and two-tailed (α=0.05) using MC with EYO>=-15 and Aβ-positive MC as the target respectively..*

Sample size needed to detect Aβ-modifying treatment per arm	**AD-typical regions as the target region**	
	MC with EYO >= -15 (n=78)	Aβ-positive MC (n=65)
20% attenuation in further SUVR	867	673
50% attenuation in further SUVR	140	109
10% decrease in SUVR from baseline	151	108
20% decrease in SUVR from baseline	39	28

V. Discussion

Amyloid PET imaging has provided us a very useful tool to *in-vivo* study spatial pattern of Aβ accumulation in AD. It has been suggested that Aβ plaques contribute to cell death by interfering with neuron-to-neuron communication at synapses. More and more anti-amyloid drug trials have included amyloid PET as the primary or secondary measurement to evaluate the treatment effect. In this thesis, spatial and temporal pattern of Aβ accumulation of sAD and ADAD were investigated using amyloid PET imaging.

This thesis produced a series of interesting findings, as in detail discussed below. The results of this thesis proved that regional rate of Aβ accumulation was not constant across the whole process of AD, regardless of sAD and ADAD. Indeed, AAR may vary in distinct region and stage of AD. We should not neglect the influence of this variation during the anti-amyloid drug trial. Spatial pattern of Aβ accumulation at early stage (phase 1 and 2) of pre-dementia sAD was similar as those asymptomatic MC of ADAD, most of Aβ active regions can be tracked well by the most commonly used AD-typical cortical regions, while a few top FARs of either individuals at phase 3 of pre-dementia sAD or symptomatic MC of ADAD were not within the set of AD-typical regions. In other words, some regions who have lower AAR may accumulate Aβ faster in the late stage of amyloidosis, while some FARs of the early stage may slow down at Aβ accumulation at the late stage. My findings support that trajectory of SUVR has a sigmoid shape, namely Aβ accumulation rate increases as SUVR does in the early stage, afterwards, the rate may become the maximal and tend to reduce with an increasing SUVR, and SUVR reaches the plateau in the end. Notably, the knowledge of these patterns may have important implications for design and analyses of anti-amyloid trials.

Predicting spatial pattern of Aβ accumulation by baseline amyloid PET

In first project, I investigated whether baseline PET data can predict spatial pattern of Aβ accumulation over 2 years. In a group of patients with incipient and mild Alzheimer's dementia, pseudo-temporal accumulating rate derived from baseline ^{18}F-florbetapir PET using a pseudo-temporal image analysis explained 87% of the variance in AARs across 62 regions. The correlation was significant throughout the disease

severity (incipient or manifest dementia), age intervals, genders, and the APOE genotypes. This pseudo-temporal image analysis may be applied to examine spatial patterns of Aβ accumulation in other Aβ-associated disorders.

Braak and Braak initially studied the progression of Aβ deposition in cross-sectional data from *post mortem* brain tissue using a pseudo-temporal analysis approach [115]. Recently, Yotter and colleagues conducted a pseudo-temporal analysis of PET images at the voxel level [79]. Assuming that total amyloid burden would be a reasonable approximation of the disease severity, they estimated spatial patterns of the longitudinal Aβ accumulation by using cross-sectional image data, observing that the "pseudo-temporal" pattern of regional Aβ deposition was stronger related to cognitive function of healthy elderly individuals than total amyloid burden [79]. Although their results were plausible, they were not validated against longitudinal data. This chapter adopted the method by Yotter et al. for region-based analyses and verified its efficacy using longitudinal data in clinically manifest AD.

The key finding of this part is the positive correlation between the baseline measurements of Aβ and their longitudinal changes across regions. The results revealed that 55 % of the variance in AARs could be explained by baseline SUVR. In other words, regions with a high/low baseline Aβ load are also those with a high/low AAR at the stage of clinically manifest AD. It is important to distinguish this approach from an "across-subject" paradigm, where baseline measurements of whole brain uptake are correlated with longitudinal measurements of whole brain tracer uptake across subjects, e.g., [6]. This study observed slowing of Aβ accumulation rate at the advanced stage of AD [6]. The findings of this thesis do not oppose those results. Only patients with incipient to mild Alzheimer's dementia were included in the present study. It is possible that some brain regions may continue to accumulate Aβ with a high AAR even though AAR of the whole brain may be slowing at the late stage of AD.

According to the findings of the step-wise linear regression analysis, pseudo-temporal accumulating rate explained significantly more variance (+35%) in AAR than baseline SUVR alone, implying it may be plausible to use total amyloid burden as a estimation for the progression of AD. Remarkably, the pseudo-temporal accumulating rate could identify the same fast and slow accumulating regions as AAR. Both of these two rates proved that the bilateral anterior cingulate, superior and middle frontal gyri, left superior parietal, anterior orbital, posterior cingulate, and inferiolateral remainder of the parietal lobe were FARs. By contrast, the bilateral hippocampus, caudate nucleus,

thalamus, amygdala and parahippocampal gyri were SARs. These results are well consistent with one previous PiB-PET study [74]. They examined regional progression of Aβ in Alzheimer's dementia, and observed that regions of the frontal lobe followed by those of the parietal lobe showed the highest accumulation rate, while temporal lobe appeared to have the lowest rate across the neocortex, which was in line with the findings in this thesis. Further, most of the FARs accumulated Aβ faster in the left hemisphere [74]. In accordance with the present study, Rinne et al. also found the same order of accumulation rate (frontal->parietal->occipital->temporal) [71]. However, the lateral temporal cortex was found to be FAR by other groups found [26, 27]. Surprisingly, the posterior cingulate region was observed to accumulate Aβ slower than the anterior cingulate region, while a few studies reported the posterior cingulate cortex to be one of the most active Aβ accumulating regions [71, 72]. The discrepancy may be explained by methodological factors such as lack of PVC [71, 72] and different reference region [26, 71, 72]. To note is, that most longitudinal studies with amyloid PET measured SUVR either in the whole brain or in AD-typical regions, without a detailed regional analysis. Regarding to the slow accumulating regions, only Grimmer et al. (2010) conducted a similarly detailed analysis including 90 volumes of interests. In line with the findings in current study, they reported low or no increases in Aβ accumulation in the archipallium, thalamus, and the caudate nucleus [74].

So far, no longitudinal amyloid PET study has been reported for atypical AD, Lewy body disease or mixed (AD and vascular) diseases. This pseudo-temporal analysis approach used in present study may be utilized to predict spatial patterns of Aβ accumulation in these clinical entities. Particularly, brain regions with the highest Aβ accumulations rate may be predicted by using the proposed pseudo-temporal analysis method, and those regions may be used as the target regions for anti-amyloid clinical trials. The results in present study demonstrated that AAR in the set of AD-typical regions was significantly higher than that in whole-GM, confirming the relevance of these regions in AD. However, the pseudo-temporal analysis revealed a set of regions with a significantly higher AAR than AD-typical regions. Consequently, using FAR as the target region in an anti-amyloid drug trial could reduce the duration and sample size by approximately 19 % and 9% respectively, as compared to AD-typical regions.

Note that only Aβ-positive patients due to AD were used to summarize the relationship between longitudinal measurements and cross-sectional measurements in this thesis, which will ensure the presence of the AD pathology as origin of the clinical

phenotype. Asymptomatic individuals were excluded from the present study due to their unclear clinical fate. Indeed, presence of a significant Aβ load cannot confirm a future development of (typical) clinical AD. Instead, the subject may have a mixed dementing disorder, Lewy body disease, or an atypical AD. Thus, if such subjects were included in the present study, it might have a heterogeneous sample of patients with unclear clinical phenotype, as well as with distinct spatial patterns of Aβ accumulation.

Yet, according to the additional analysis without considering amyloid status or the presence of AD pathology for 417 subjects, there is still a strong correlation between pseudo-temporal accumulating rate of Aβ and AARs across 62 regions (R^2 =0.84, $p<0.001$). In addition, Yotter and colleagues also reported the utilization of pseudo-temporal image analysis in amyloid negative subjects [79]. Therefore, the proposed method can be effective in amyloid-negative subjects, too. Such an approach would allow capturing the whole trajectory of Aβ accumulation, including a long preclinical phase. Given uncertainty about both pathological and clinical pathways, however, interpretation of results would be problematic.

One limitation of the part was that the follow up duration were only 2 years, which were very short as compared to the two decades' interval of the whole period amyloid progression of AD. The correspondence at the level of individual regions was far from perfect, especially beyond top 10 FARs and slow accumulating regions, which may be explained by the short FU duration. Since the pseudo-temporal rate is trying to capture the whole disease duration, thus, one would expect a larger correspondence between the measurements when a longer FU is available. This issue should be addressed by future studies.

Rate of beta-amyloid accumulation varies with baseline amyloid burden in pre-dementia stage of sporadic Alzheimer's disease

In the second project, I applied the pseudo-temporal analysis to explore the longitudinal trajectory of Aβ accumulation at the pre-dementia stage of AD in the context of clinical trials. In line with previous studies, the trajectory follows an inverted U-shape [27, 43, 90, 107] that continued into a "tail" at a late stage [27]. Thus, three phases of longitudinal Aβ accumulation could be defined: acceleration, deceleration and a stable phase. One major finding is that the established set of AD-typical regions did not adequately track most active Aβ accumulating regions in the third phase of the

trajectory. Furthermore, according to baseline $SUVR_{GM}$ the whole dataset could be divided into two main categories: 1) fast accumulators (54% of the whole cohort): subjects with the above-average AAR in whole-GM, 2) and slow accumulators: those with a below-average AAR. Inclusion of fast accumulators instead of an unselected cohort in an anti-amyloid trial would allow a substantial reduction of a sample size to treat.

Previous studies reported a bimodal distribution of Aβ accumulation rate, and they classified individuals as accumulators and non-accumulators accordingly [27, 90]. In present study, however, individual AARs were distributed normally. The inconsistency may be due to the fact that in line with typical anti-amyloid trial inclusion criteria only Aβ-positive subjects were included in the present study. Here, fast and slow accumulators were classified according to the mean AAR in whole-GM. To be more specific, subjects who accumulate Aβ faster *at this time* than an average Aβ-positive subject over the period of his/her "Aβ-positive life" (around 36 years in present study) were regarded as fast accumulators. The robustness of this intuitive cut-off was testified by a cross-validation test. Using fast accumulators as the target subject in a clinical trial would allow reaching PET-based endpoints faster as compared to an unselected cohort of subjects. The same size needed to detect significant treatment effect could be reduced as well. Concerning a clinical anti-amyloid drug trial aiming to attenuate further Aβ accumulation, inclusion of fast accumulators only would reduce the sample size by around 24 %. In a trial aiming to reduce baseline Aβ burden, a reduction by 61 to 70% can be reached. Furthermore, data on fast accumulators can be potentially utilized to obtain an earlier, preliminary estimation of a drug effect.

Regional analyses revealed that most AD-typical regions showed a higher AAR than whole-GM in the phases 1 and 2, supporting AD-typical regions as a suitable target region in anti-amyloid drug trials. In the phase 3, however, the bilateral cuneus and lateral remainder of occipital lobe, the left precentral and postcentral regions were among top 10 FARs, but not within the set of AD-typical regions. Consequently, it is very likely that AAR in AD-typical regions tends to become slower after Aβ load reaching a certain level, while the phylogenetically older primary visual and sensorimotor cortices become progressively affected by Aβ. A cluster analysis revealed the left middle frontal, superior frontal, postcentral, lateral anterior temporal lobe, bilateral lateral remainder of occipital lobe, and right cuneus to be within the same cluster as most active Aβ accumulating regions in the phase 3. Thus, this set of FARs

were further compared with the established set of AD-typical regions as target in a putative anti-amyloid trial. The results appeared to be dependent on the mechanism of drug action. Specifically, the utilization of the above FARs would enable reducing the sample size to treat by roughly one third for trial aiming to attenuate further Aβ accumulation. However, the sample size would marginally increase in the drug trial aiming to reduce a baseline Aβ burden. This may be explained by that the mean baseline SUVR in FARs was lower than that in AD-typical regions.

According to the trajectory of AAR as a function of baseline $SUVR_{GM}$, the control and experimental groups should be matched at baseline $SUVR_{GM}$. As shown in the simulation of drug trial (Fig. 15), a difference of 0.25 baseline $SUVR_{GM}$ in one extreme case can produce extremely larger treatment effect than the expected drug effects. But even with a difference of 0.10 baseline $SUVR_{GM}$, the drug effect can be greatly overestimated or underestimated by 75 and 90 %, respectively. Moreover, this treatment effect bias may occur not only when average AARs of two groups are located on the same accelerating or decelerating phase of the trajectory, but also appears when average AARs of two groups belong to different phases (Fig. 19). For example, if the proportion of phase 1 subjects is substantially larger in the treated group, their on average higher AAR would cause an underestimation of a drug effect. This effect is aggravated by a (consequently) higher proportion of phase 2 subjects in the control group. If the proportion of phase 1 subjects is higher in the control group, an overestimation of a drug effect is produced.

This part has several limitations. First, although the cut-offs appeared to be robust according to the cross-validation test, they should be verified prospectively using multi-centers' data. Second, as it is true for all semi-quantitative PET studies with SUVR as outcome measure, this study assumes that a hypothetical drug does not influence cerebral blood flow. Third, current evidence from both genetic at-risk and older cohort studies indicate that Aβ accumulation is one of the earliest measurable stages of AD, but the presence of one or more additional biomarker abnormalities or subtle cognitive symptoms may increase the likelihood of rapid emergence of cognitive symptomatology and clinical decline. However, this study didn't add other biomarkers into the criteria of selecting subjects in order to keep a large sample size to model the trajectory of AAR, which may bring some atypical dementia into the dataset. Still all the subjects analyzed in this study had great risk to be AD in future, and several current on-going anti-amyloid drug trials select this population as the target subject [58, 60, 62]. Furthermore, it may

be plausible to use total amyloid burden as an alternative estimate for the progression of AD at this moment, but note that the trajectory of AAR as a function of real time may be different. The 2-year FU time was rather short as compared to the several decades' period of Aβ accumulation, thus it may need longitudinal data with a longer period to validate the findings in this study in future. Furthermore, it may get more accurate AAR using more PET scans, however, only the first two PET scans with approximately 2 years FU were used to estimate the rate of Aβ accumulation in this study, by considering that the most commonly used period of anti-amyloid drug trials is 2 years and only around a few subjects had more than 2 PET scans when I collected data from ADNI.

Spatial and temporal pattern of Aβ accumulation in autosomal dominant Alzheimer's disease

In the third project, I explored the spatial pattern of Aß deposition and accumulation in ADAD based on DIAN database. The set of AD-typical regions derived from sAD could efficiently track the amyloid deposition and accumulation in asymptomatic MC. In Aβ-positive symptomatic MC, several top FARs left cuneus, and bilateral lateral remainder of occipital lobe were out of the set of AD-typical regions, which was consitent with those findings of phase 3 of pre-dementia sAD (table 13). These findings suggest that the spatial and temporal pattern of Aβ accumulation in Aβ-positive MCs was similar to Aβ-positive subjects at the pre-dementia stage of sAD. The simmilar patterns of amyloid deposition and accumulation in ADAD supports translation of findings in ADAD to sAD.

The main inclusion criteria of ongoing DIAN-TU trial are as follows: 1) asymptomatic MCs are within -15 to +10 years of EYO; 2) symptomatic MCs are within 10 years of their age at symptom onset [59]. The trajectories of SUVR revealed that SUVR in MC increases as EYO becomes larger, while SUVR in NC shows no obvious increase over the whole period. According to the trajectory, SUVR starts to increase when EYO is still below -20. Consistent with the trajectory published by Bateman and colleagues [44], the trajectory of SUVR in MC tends to reach plateau in the end. To note is, the dataset in present study has no individuals with EYO > 10, therefore the trajectory may be different if more individuals in the late stage (EYO>10) were added. According to the trajectory, several MCs with EYO > -15 were Aβ-negative, and most of them had a negative AAR, although they meet the criteria of inclusion in DIAN-TU. Out of 78

MCs with -15 ≤ EYO ≤ 10, 16 were Aβ-negative. Combining those Aβ-negative MC with Aβ-positive MC would reduce the effect size of Aβ-positive MC by 24%. Interestingly, the percentage of APP (66.67%) in Aβ-negative MCs was significantly (Fisher's exact test, p=0.0002) higher than the percentage of other mutation types (15.62%) in Aβ-negative MCs, implying the cutoff EYO -15 may be not accurate to identify MC of APP with substantial Aβ deposition. Consequently, we may need to consider amyloid positivity status when we recruit APP for DIAN-TU trial or conclude one more accurate mean mutation age for APP in future.

Regarding to those Aβ-negative asymptomatic MCs recruited into current DIAN-TU, their baseline SUVR in AD-typical regions was slightly higher than Aβ-negative NC, but was still extremely lower than Aβ-positive MC. The effect size of baseline SUVR in those Aβ-negative asymptomatic MC was only one fourth of Aβ-positive MCs. Consequently, it may be more reasonable to conduct drug trial aiming to attenuate further SUVR increase for them rather than one trial aiming to reduce baseline SUVR. However, they had no significant longitudinal Aβ accumulation in AD-typical regions over two years' follow-up regardless of EYO >= -15 or not. DIAN-TU trial may need to exclude those Aβ-negative MCs, or find out a new target region with higher AAR than AD-typical regions to detect longitudinal change of SUVR in a trial aiming to attenuate further SUVR increase. In Aβ-negative asymptomatic MCs and NCs, none of 62 regions had significant increase in SUVR from baseline to FU for Aβ-negative asymptomatic NC and Aβ-negative asymptomatic MC with EYO < -15. However, bilateral superior parietal gyrus, postcentral gyrus and precentral gyrus, and right posterior cingulate gyrus had significant increase from baseline to FU in Aβ-negative asymptomatic MC with EYO >= -15. Moreover, the HCA analysis revealed that the bilateral superior parietal, postcentral and precentral, and left middle frontal and inferiolateral remainder of parietal lobe were the top fast Aβ accumulating regions for Aβ-negative asymptomatic MC with EYO >= -15. As a result, bilateral superior parietal, postcentral and precentral, and left middle frontal and inferiolateral remainder of parietal lobe were combined as one composited FAR. Significant positive AAR of the composited FAR (0.014±0.019) was 1.75 times (p=0.011, paired-sample t-test) higher than corresponding AAR of AD-typical regions (0.008±0.019). Using the composited FAR as the target region to detect further SUVR change could reduce sample size and shorten trial duration by 67% and 43% respectively as compared to the set of AD-typical region.

In Aβ-positive MC group, all the 62 regions had significantly higher SUVR than that in corresponding region of Aβ-negative asymptomatic NC at both baseline and FU, twenty eight regions had higher SUVR than whole-GM at baseline, and out of them only bilateral putamen and caudate nucleus were not within the set of AD-typical regions, which was consistent with previous studies [96]. There was no obvious difference in spatial pattern of baseline SUVR for Aβ-positive asymptomatic and symptomatic MC, both of which could be well tracked by the set of AD-typical regions. Therefore, the set of AD-typical regions could be utilized as the target region to detect SUVR change from baseline in anti-amyloid drug trial for Aβ-positive MC. To note is, those top regions with high SUVR of Aβ-positive asymptomatic MCs had significantly lower baseline SUVR than symptomatic individuals, implying Aβ-positive asymptomatic MCs still have potential to keep amyloid accumulating. It may take around 6 years (EYO = -5.97) for those asymptomatic MCs to be symptomatic. Considering temporal change of Aβ, 56 regions had significant increase in SUVR from baseline to FU in Aβ-positive MCs, and out of 27 regions with higher AAR than whole-GM, only bilateral putamen, left caudate nucleus and right lateral remainder of occipital lobe were not within the set of AD-typical regions. The spatial patterns of baseline SUVR and AAR in Aβ-positive MC confirm the relevance of AD-typical regions for ADAD. Regarding to the spatial pattern of AAR, Aβ-positive asymptomatic MC (table 22) had higher AAR than whole-GM in 33 regions, out of which, only bilateral putamen were not within the set of AD-typical regions. However, out of only 23 regions had higher AAR than whole-GM in Aβ-positive symptomatic MC (table 23), 7 regions were not within the set of AD-typical regions. These findings were in accordance with those results of pre-dementia stage of sAD. Most of the top FARs of Aβ-positive asymptomatic MCs collected from DIAN databse (table 22) were also with those of Aβ-positive CN subjects collected from ADNI database (table 8). Those regions out of the set of AD-typical regions (left cuneus, and bilateral lateral remainder of occipital lobe) in Aβ-positive symptomatic MC were also within those top FARs of phase 3 at pre-dementia sAD (table 13). Previous study reported that those regions may be late-affected regions of amyloid deposition in ADAD [93]. Therefore they should be added into the target region to detect the amyloid accumulation in a given study or drug trial if symptomatic MC or individuals in phase 3 of pre-dementia sAD were used as the target.

It has been observed that there was significant correlation between baseline SUVR and AAR, CDR-SB, MMSE and cognitive-composite for the whole MC cohort, however

the association varied after controlling amyloid positivity and symptomatic status. No correlation was observed for any two parameters in Aβ-negative MC, implying that those Aβ-negative MC may have not deposited substantial Aβ in brain yet. As Aβ-negative MC developed to Aβ-positive asymptomatic MC, significant correlation ($R = 0.37$, $p=0.0433$) was observed between AAR and cognitive-composite but not in CDR-SB and MMSE, which may be because cognitive-composite is more sensitive to detect early cognitive decline than other two according to its definition [92]. However, there was no association between baseline SUVR/AAR and cognitive parameters at all in Aβ-positive symptomatic MC. These results imply that the further Aβ accumulation in MC with substantial amyloidosis may contribute to the early cognitive decline before reaching symptomatic, the cognitive change of symptomatic stage may be more related to other physiological parameters, such as hippocampal atrophy, glucose metabolism and cortical thickness.

This part has two limitations. First, the number of Aβ-negative asymptomatic MCs with EYO >= -15 was very small, thus the proposed FAR may need to be validated in a dataset with a larger sample size in future. Second, the percentage of APP and PSEN2 was relatively low as compared to PSEN1, which may affect the finding of a higher percentage of APP in Aβ-negative MCs than other mutation types in future.

VI. Conclusions and Outlook

Understanding the natural course of Aβ accumulation over time is important for tracking disease progression, prediction of outcomes as well as designing stage-specific clinical anti-amyloid drug trials. In this thesis, I investigated the spatial and temporal pattern of Aβ accumulation in subjects with preclinical and manifest sAD and ADAD. Overall, these results provide meaningful references for planning and analyses of anti-amyloid clinical trials with PET as biomarker.

In the first project, the spatial pattern of AAR in Aβ-positive patients with sAD was studied, one pseudo-temporal method proved that longitudinal Aβ accumulation could be predicted by baseline PET in individuals with dementia due to AD. This approach may be used to search for preliminary top FARs in the beginning of anti-amyloid drug trial, which will enable us to find out the regions those could be used as the target region to detect longitudinal change of Aβ during FU, thereby shorten the trial duration and sample size. This pseudo-temporal analysis may be applied to explore spatial patterns of Aβ in other Aβ-related diseases, as those diseases usually have rare longitudinal data available.

In the second project, the trajectory of AAR as a function of baseline SUVR was explored using Aβ-positive CN and MCI subjects. It has been demonstrated that there are significant variations in Aβ accumulation across subjects and regions at the pre-dementia stage of sAD. They should be taken into account when designing and analyzing anti-amyloid drug trials. Three different phases were defined based on this pseudo-temporal trajectory of AAR at the pre-dementia stage of sAD. Fast accumulators were identified by baseline SUVR out of the whole cohort. Furthermore, treated and placebo groups should be matched for baseline $SUVR_{GM}$, otherwise one overestimation or underestimation of treatment effect may be obtained.

In the third project, the spatial pattern of basesline SUVR and AAR was invetigated in ADAD based on DIAN database. The spatial patterns of baseline SUVR and AAR of Aβ accumulation in ADAD were similar as sAD except for some subcortical region. To be more specific, the set of AD-typical regions could capture most of the cortical FARs in Aβ-positive asymptomatic MCs. However, several FARs were out of the set of AD-typical regions in Aβ-positive symptomatic MCs, which were within those regions found

at phase 3 of pre-dementia stage of sAD. A higher percentage (66.67%) of APP in Aβ-negative MCs was observed than other mutations (15.62%), implying that mean mutation age of APP may be not as accurate as PSEN1 or PSEN2.

Nowadays, there are overwhelming and unpredictable challenges for researchers to fully understand the mechanisms of AD and find out the efficient way to remove those pathological factors that resulting in the cognitive decline and bringing fatal damage to brain. PET imaging with amyloid PET provides one excellent method to assist the diagnosis of AD at a very early stage. After failure in a lot of drug trials, more and more researchers suggest that it may be necessary to conduct the drug trial for such a disease at an early stage, such as CN or MCI of sAD, or asymptomatic MC of ADAD. Amyloid PET has been commonly used the primary or secondary measurement in the anti-amyloid drug trial. Those regions (FARs) with high AAR may be used as the target region for the trials aiming to attenuate further SUVR increase, since they have fast amyloid accumulating rate. A higher AAR could reduce the sample size and shorten the trial duration, which will thereby reduce the cost of the drug trial. More importantly, those individuals involved in the trials are probably at preclinical stage of AD, in other words, they are still health. The less individuals an anti-amyloid trial needs, the less healthy people are involved. The findings in this thesis could provide meaningful reference for the drug trial using individuals with pre-dementia sAD or ADAD as the target. It turns out that sAD and ADAD have similar spatial pattern of Aβ accumulation, which may support the transformation of those findings of ADAD to sAD in future.

In future, there are still many interesting topics remaining to be investigated. Firstly, it has been suggested that using more biomarkers in the preclinical stage of AD may gain more accurate assessment for this disease regardless of diagnosis or assessment for a drug trial, but it is unclear whether those FARs of Aβ accumulation in one specific stage of AD also work for other biomarkers, or if those FARs derived from amyloid PET imaging correlate with the activities of other biomarkers. Secondly, there are still follow-up studies in ADNI for those CN participants at preclinical AD and individuals with MCI. Using as many PET scans as possible will enable us to obtain a more accurate AAR, thereby we may establish a more reliable trajectory of AAR. With the help of this new trajectory, more reliable cutoffs of different phases and fast/slow accumulators may be obtained. In addition, those Aβ-negative asymptomatic MC with EYO < -15 will probably have follow-up assessment. Thus they could be used to validate the proposed

set of FARs based on Aβ-negative asymptomatic MC with EYO >= -15. The last but not the least, it has been suggested that more additional biomarker abnormalities, APOE 4 status or subtle cognitive symptoms may increase the likelihood of rapid emergence of cognitive symptomatology and clinical decline. Consequently, we should combine multiple medical images and other related genetic factor or cognitive parameters to identify people without dementia but have a great risk to be AD for the target subjects in the anti-amyloid drug trial in future.

More and more institutes and medical centers have joined into the fighting with AD. Different databases related to AD have been established in America, Europe, Australia and other countries, such as ADNI, DIAN, and AIBL (The Australian Imaging, Biomarker & Lifestyle Flagship Study of Ageing) etc, which provide the opportunity for researcher all over the world to investigate the progression of AD and learn how to treat such a neurodegenerative disease. As far as I know, a big database (The Chinese Familial Alzheimer's Disease Network, CFAN)[116] related to ADAD is under recruitment in China. It is very likely that other countries in the world are also establishing their own database for AD. Although there are unpredictable challenges for us to fully understand the mechanism of AD and find out efficient approach to treat this disease, we still believe that we can defeat it one day by collaborating with researcher all over the world.

References

[1] World_Alzheimer_Report. Improving healthcare for people living with dementia. 2016.

[2] Wilson RS, Segawa E, Boyle PA, Anagnos SE, Hizel LP, Bennett DA. The natural history of cognitive decline in Alzheimer's disease. Psychology and aging. 2012;27:1008-1017.

[3] Barker WW, Luis CA, Kashuba A, Luis M, Harwood DG, Loewenstein D, et al. Relative frequencies of Alzheimer disease, Lewy body, vascular and frontotemporal dementia, and hippocampal sclerosis in the State of Florida Brain Bank. Alzheimer Disease & Associated Disorders. 2002;16:203-212.

[4] Selkoe DJ. Alzheimer's disease: genes, proteins, and therapy. Physiological reviews. 2001;81:741-766.

[5] Hardy J, Selkoe DJ. The amyloid hypothesis of Alzheimer's disease: progress and problems on the road to therapeutics. Science. 2002;297:353-356.

[6] Villemagne VL, Burnham S, Bourgeat P, Brown B, Ellis KA, Salvado O, et al. Amyloid β deposition, neurodegeneration, and cognitive decline in sporadic Alzheimer's disease: a prospective cohort study. Lancet Neurol. 2013;12:357-367.

[7] Reiman EM, Quiroz YT, Fleisher AS, Chen K, Velez-Pardo C, Jimenez-Del-Rio M, et al. Brain imaging and fluid biomarker analysis in young adults at genetic risk for autosomal dominant Alzheimer's disease in the presenilin 1 E280A kindred: a case-control study. The Lancet Neurology. 2012;11:1048-1056.

[8] Bateman RJ, Xiong C, Benzinger TL, Fagan AM, Goate A, Fox NC, et al. Clinical and biomarker changes in dominantly inherited Alzheimer's disease. The New England journal of medicine. 2012;367:795-804.

[9] McKhann G, Drachman D, Folstein M, Katzman R, Price D, Stadlan EM. Clinical diagnosis of Alzheimer's disease Report of the NINCDS-ADRDA Work Group* under the auspices of Department of Health and Human Services Task Force on Alzheimer's Disease. Neurology. 1984;34:939-944

[10] Association As. 2017 Alzheimer's disease facts and figures. Alzheimer's & dementia. 2017;13:325-373.

[11] Goate A, Chartier-Harlin M-C. Segregation of a missense mutation in the amyloid precursor protein gene with familial Alzheimer's disease. Nature. 1991;349:704.

[12] Sherrington R, Rogaev EI, Liang Ya, Rogaeva EA, Levesque G, Ikeda M, et al. Cloning of a gene bearing missense mutations in early-onset familial Alzheimer's disease. Nature. 1995;375:754-760.
[13] Levy-Lahad E, Wasco W, Poorkaj P, Romano DM, Oshima J, Pettingell WH, et al. Candidate gene for the chromosome 1 familial Alzheimer's disease locus. Science. 1995:973-977.
[14] Goldman JS, Hahn SE, Catania JW, LaRusse-Eckert S, Butson MB, Rumbaugh M, et al. Genetic counseling and testing for Alzheimer disease: joint practice guidelines of the American College of Medical Genetics and the National Society of Genetic Counselors. Genetics in medicine : official journal of the American College of Medical Genetics. 2011;13:597-605.
[15] Sperling RA, Aisen PS, Beckett LA, Bennett DA, Craft S, Fagan AM, et al. Toward defining the preclinical stages of Alzheimer's disease: recommendations from the National Institute on Aging-Alzheimer's Association workgroups on diagnostic guidelines for Alzheimer's disease. Alzheimer's & dementia : the journal of the Alzheimer's Association. 2011;7:280-292.
[16] Albert MS, DeKosky ST, Dickson D, Dubois B, Feldman HH, Fox NC, et al. The diagnosis of mild cognitive impairment due to Alzheimer's disease: recommendations from the National Institute on Aging-Alzheimer's Association workgroups on diagnostic guidelines for Alzheimer's disease. Alzheimer's & dementia : the journal of the Alzheimer's Association. 2011;7:270-279.
[17] McKhann GM, Knopman DS, Chertkow H, Hyman BT, Jack CR, Jr., Kawas CH, et al. The diagnosis of dementia due to Alzheimer's disease: recommendations from the National Institute on Aging-Alzheimer's Association workgroups on diagnostic guidelines for Alzheimer's disease. Alzheimer's & dementia : the journal of the Alzheimer's Association. 2011;7:263-269.
[18] Jack CR, Knopman DS, Jagust WJ, Petersen RC, Weiner MW, Aisen PS, et al. Tracking pathophysiological processes in Alzheimer's disease: an updated hypothetical model of dynamic biomarkers. Lancet Neurol. 2013;12:207-216.
[19] Fagan AM, Roe CM, Xiong C, Mintun MA, Morris JC, Holtzman DM. Cerebrospinal fluid tau/β-amyloid42 ratio as a prediction of cognitive decline in nondemented older adults. Archives of neurology. 2007;64:343-349.

[20] Shaw LM, Vanderstichele H, Knapik-Czajka M, Clark CM, Aisen PS, Petersen RC, et al. Cerebrospinal fluid biomarker signature in Alzheimer's disease neuroimaging initiative subjects. Ann Neurol. 2009;65:403-413.
[21] Mattsson N, Zetterberg H, Hansson O, Andreasen N, Parnetti L, Jonsson M, et al. CSF biomarkers and incipient Alzheimer disease in patients with mild cognitive impairment. JAMA. 2009;302:385-393.
[22] Visser PJ, Verhey F, Knol DL, Scheltens P, Wahlund L-O, Freund-Levi Y, et al. Prevalence and prognostic value of CSF markers of Alzheimer's disease pathology in patients with subjective cognitive impairment or mild cognitive impairment in the DESCRIPA study: a prospective cohort study. The Lancet Neurology. 2009;8:619-627.
[23] Mattsson N, Insel PS, Donohue M, Jagust W, Sperling R, Aisen P, et al. Predicting Reduction of Cerebrospinal Fluid β-Amyloid 42 in Cognitively Healthy Controls. JAMA neurology. 2015;72:554-560.
[24] Klunk WE, Engler H, Nordberg A, Wang Y, Blomqvist G, Holt DP, et al. Imaging brain amyloid in Alzheimer's disease with Pittsburgh Compound-B. Annals of neurology. 2004;55:306-319.
[25] Rowe CC, Ellis KA, Rimajova M, Bourgeat P, Pike KE, Jones G, et al. Amyloid imaging results from the Australian Imaging, Biomarkers and Lifestyle (AIBL) study of aging. Neurobiology of aging. 2010;31:1275-1283.
[26] Villemagne VL, Pike KE, Chetelat G, Ellis KA, Mulligan RS, Bourgeat P, et al. Longitudinal assessment of Abeta and cognition in aging and Alzheimer disease. Ann Neurol. 2011;69:181-192.
[27] Villain N, Chetelat G, Grassiot B, Bourgeat P, Jones G, Ellis KA, et al. Regional dynamics of amyloid-beta deposition in healthy elderly, mild cognitive impairment and Alzheimer's disease: a voxelwise PiB-PET longitudinal study. Brain : a journal of neurology. 2012;135:2126-2139.
[28] Landau SM, Mintun MA, Joshi AD, Koeppe RA, Petersen RC, Aisen PS, et al. Amyloid deposition, hypometabolism, and longitudinal cognitive decline. Ann Neurol. 2012;72:578-586.
[29] Landau SM, Fero A, Baker SL, Koeppe R, Mintun M, Chen K, et al. Measurement of longitudinal beta-amyloid change with 18F-florbetapir PET and standardized uptake value ratios. Journal of nuclear medicine : official publication, Society of Nuclear Medicine. 2015;56:567-574.

[30] Landau SM, Thomas BA, Thurfjell L, Schmidt M, Margolin R, Mintun M, et al. Amyloid PET imaging in Alzheimer's disease: a comparison of three radiotracers. European journal of nuclear medicine and molecular imaging. 2014;41:1398-1407.
[31] Clark CM, Pontecorvo MJ, Beach TG, Bedell BJ, Coleman RE, Doraiswamy PM, et al. Cerebral PET with florbetapir compared with neuropathology at autopsy for detection of neuritic amyloid-β plaques: a prospective cohort study. Lancet Neurology. 2012;11:669-678.
[32] Buerger K, Ewers M, Pirttila T, Zinkowski R, Alafuzoff I, Teipel SJ, et al. CSF phosphorylated tau protein correlates with neocortical neurofibrillary pathology in Alzheimer's disease. Brain : a journal of neurology. 2006;129:3035-3041.
[33] Blennow K, Hampel H. CSF markers for incipient Alzheimer's disease. The Lancet Neurology. 2003;2:605-613.
[34] Fagan AM, Head D, Shah AR, Marcus D, Mintun M, Morris JC, et al. Decreased cerebrospinal fluid Abeta(42) correlates with brain atrophy in cognitively normal elderly. Ann Neurol. 2009;65:176-183.
[35] Fagan AM, Xiong C, Jasielec MS, Bateman RJ, Goate AM, Benzinger TL, et al. Longitudinal change in CSF biomarkers in autosomal-dominant Alzheimer's disease. Science translational medicine. 2014;6:226ra230.
[36] Jagust WJ, Bandy D, Chen K, Foster NL, Landau SM, Mathis CA, et al. The Alzheimer's Disease Neuroimaging Initiative positron emission tomography core. Alzheimers Dement. 2010;6:221-229.
[37] Jack CR, Jr., Wiste HJ, Weigand SD, Knopman DS, Mielke MM, Vemuri P, et al. Different definitions of neurodegeneration produce similar amyloid/neurodegeneration biomarker group findings. Brain : a journal of neurology. 2015;138:3747-3759.
[38] Li Y, Rinne JO, Mosconi L, Pirraglia E, Rusinek H, DeSanti S, et al. Regional analysis of FDG and PIB-PET images in normal aging, mild cognitive impairment, and Alzheimer's disease. European journal of nuclear medicine and molecular imaging. 2008;35:2169-2181.
[39] Dickerson BC, Wolk DA, Alzheimer's Disease Neuroimaging I. MRI cortical thickness biomarker predicts AD-like CSF and cognitive decline in normal adults. Neurology. 2012;78:84-90.
[40] Vemuri P, Wiste HJ, Weigand SD, Shaw LM, Trojanowski JQ, Weiner MW, et al. MRI and CSF biomarkers in normal, MCI, and AD subjects Diagnostic discrimination and cognitive correlations. Neurology. 2009;73:287-293.

[41] Jack CR, Jr., Wiste HJ, Vemuri P, Weigand SD, Senjem ML, Zeng G, et al. Brain beta-amyloid measures and magnetic resonance imaging atrophy both predict time-to-progression from mild cognitive impairment to Alzheimer's disease. Brain. 2010;133:3336-3348.
[42] Jack CR, Jr., Lowe VJ, Weigand SD, Wiste HJ, Senjem ML, Knopman DS, et al. Serial PIB and MRI in normal, mild cognitive impairment and Alzheimer's disease: implications for sequence of pathological events in Alzheimer's disease. Brain : a journal of neurology. 2009;132:1355-1365.
[43] Jack CR, Wiste HJ, Lesnick TG, Weigand SD, Knopman DS, Vemuri P, et al. Brain β-amyloid load approaches a plateau. Neurology. 2013;80:890-896.
[44] Bateman RJ, Xiong C, Benzinger TLS, Fagan AM, Goate A, Fox NC, et al. Clinical and Biomarker Changes in Dominantly Inherited Alzheimer's Disease. N Engl J Med. 2012;367:795-804.
[45] Fleisher AS, Chen K, Quiroz YT, Jakimovich LJ, Gutierrez Gomez M, Langois CM, et al. Associations between biomarkers and age in the presenilin 1 E280A autosomal dominant Alzheimer disease kindred: a cross-sectional study. JAMA neurology. 2015;72:316-324.
[46] Fleisher AS, Chen K, Quiroz YT, Jakimovich LJ, Gomez MG, Langois CM, et al. Florbetapir PET analysis of amyloid-β deposition in the presenilin 1 E280A autosomal dominant Alzheimer's disease kindred: a cross-sectional study. Lancet Neurology. 2012;11:1057-1065.
[47] Roberts R, Knopman DS. Classification and epidemiology of MCI. Clinics in geriatric medicine. 2013;29:753-772.
[48] Salloway S, Sperling R, Fox NC, Blennow K, Klunk W, Raskind M, et al. Two phase 3 trials of bapineuzumab in mild-to-moderate Alzheimer's disease. The New England journal of medicine. 2014;370:322-333.
[49] Doody RS, Thomas RG, Farlow M, Iwatsubo T, Vellas B, Joffe S, et al. Phase 3 trials of solanezumab for mild-to-moderate Alzheimer's disease. N Engl J Med. 2014;370:311-321.
[50] Gilman S, Koller M, Black RS, Jenkins L, Griffith SG, Fox NC, et al. Clinical effects of Abeta immunization (AN1792) in patients with AD in an interrupted trial. Neurology. 2005;64:1553-1562.

[51] Salloway S, Sperling R, Keren R, Porsteinsson AP, Van Dyck CH, Tariot PN, et al. A phase 2 randomized trial of ELND005, scyllo-inositol, in mild to moderate Alzheimer disease. Neurology. 2011;77:1253-1262.
[52] Doody RS, Raman R, Farlow M, Iwatsubo T, Vellas B, Joffe S, et al. A phase 3 trial of semagacestat for treatment of Alzheimer's disease. The New England journal of medicine. 2013;369:341-350.
[53] Salloway S, Sperling R, Gilman S, Fox NC, Blennow K, Raskind M, et al. A phase 2 multiple ascending dose trial of bapineuzumab in mild to moderate Alzheimer disease. Neurology. 2009;73:2061-2070.
[54] Liu E, Schmidt ME, Margolin R, Sperling R, Koeppe R, Mason NS, et al. Amyloid-β 11C-PiB-PET imaging results from 2 randomized bapineuzumab phase 3 AD trials. Neurology. 2015;85:692-700.
[55] Lenz RA, Pritchett YL, Berry SM, Llano DA, Han S, Berry DA, et al. Adaptive, dose-finding phase 2 trial evaluating the safety and efficacy of ABT-089 in mild to moderate Alzheimer disease. Alzheimer Disease & Associated Disorders. 2015;29:192-199.
[56] Holmes C, Boche D, Wilkinson D, Yadegarfar G, Hopkins V, Bayer A, et al. Long-term effects of Aβ42 immunisation in Alzheimer's disease: follow-up of a randomised, placebo-controlled phase I trial. The Lancet. 2008;372:216-223.
[57] Siemers ER, Sundell KL, Carlson C, Case M, Sethuraman G, Liu-Seifert H, et al. Phase 3 solanezumab trials: Secondary outcomes in mild Alzheimer's disease patients. Alzheimers Dement. 2015;12:110-120.
[58] API. p. https://www.clinicaltrials.gov/ct2/show/NCT02565511.
[59] DIAN T. p. https://clinicaltrials.gov/ct2/show/NCT01760005.
[60] A4-Study. p. https://clinicaltrials.gov/ct2/show/NCT02008357.
[61] MK-8931 T. p. https://clinicaltrials.gov/ct2/show/NCT01953601.
[62] JNJ-54861911. p. https://clinicaltrials.gov/ct2/show/NCT02569398.
[63] LY3314814 T. p. https://clinicaltrials.gov/ct2/show/NCT02245737.
[64] Perrin RJ, Fagan AM, Holtzman DM. Multimodal techniques for diagnosis and prognosis of Alzheimer's disease. Nature. 2009;461:916-922.
[65] Aisen PS, Petersen RC, Donohue MC, Gamst A, Raman R, Thomas RG, et al. Clinical core of the Alzheimer's disease neuroimaging initiative: Progress and plans. Alzheimers Dement. 2010;6:239-246.

[66] Frisoni GB, Fox NC, Jack CR, Jr., Scheltens P, Thompson PM. The clinical use of structural MRI in Alzheimer disease. Nat Rev Neurol. 2010;6:67-77.
[67] Jack CR, Knopman DS, Jagust WJ, Shaw LM, Aisen PS, Weiner MW, et al. Hypothetical model of dynamic biomarkers of the Alzheimer's pathological cascade. Lancet Neurol. 2010;9:119-128.
[68] Petersen RC. Alzheimer's disease: progress in prediction. Lancet Neurol. 2010;9:4-5.
[69] Weiner MW, Aisen PS, Jack CR, Jr., Jagust WJ, Trojanowski JQ, Shaw L, et al. The Alzheimer's disease neuroimaging initiative: progress report and future plans. Alzheimers Dement. 2010;6:202-211.
[70] Ewers M, Sperling RA, Klunk WE, Weiner MW, Hampel H. Neuroimaging markers for the prediction and early diagnosis of Alzheimer's disease dementia. Trends Neurosci. 2011;34:430-442.
[71] Rinne JO, Brooks DJ, Rossor MN, Fox NC, Bullock R, Klunk WE, et al. 11 C-PiB PET assessment of change in fibrillar amyloid-β load in patients with Alzheimer's disease treated with bapineuzumab: a phase 2, double-blind, placebo-controlled, ascending-dose study. Lancet Neurology. 2010;9:363-372.
[72] Engler H, Forsberg A, Almkvist O, Blomquist G, Larsson E, Savitcheva I, et al. Two-year follow-up of amyloid deposition in patients with Alzheimer's disease. Brain : a journal of neurology. 2006;129:2856-2866.
[73] Scheinin NM, Aalto S, Koikkalainen J, Lotjonen J, Karrasch M, Kemppainen N, et al. Follow-up of [11C]PIB uptake and brain volume in patients with Alzheimer disease and controls. Neurology. 2009;73:1186-1192.
[74] Grimmer T, Tholen S, Yousefi BH, Alexopoulos P, Forschler A, Forstl H, et al. Progression of cerebral amyloid load is associated with the apolipoprotein E epsilon4 genotype in Alzheimer's disease. Biol Psychiatry. 2010;68:879-884.
[75] Brendel M, Hogenauer M, Delker A, Sauerbeck J, Bartenstein P, Seibyl J, et al. Improved longitudinal [(18)F]-AV45 amyloid PET by white matter reference and VOI-based partial volume effect correction. NeuroImage. 2015;108:450-459.
[76] Chen K, Roontiva A, Thiyyagura P, Lee W, Liu X, Ayutyanont N, et al. Improved Power for Characterizing Longitudinal Amyloid- PET Changes and Evaluating Amyloid-Modifying Treatments with a Cerebral White Matter Reference Region. Journal of Nuclear Medicine. 2015;56:560-566.

[77] Gomperts SN, Locascio JJ, Marquie M, Santarlasci AL, Rentz DM, Maye J, et al. Brain amyloid and cognition in Lewy body diseases. Mov Disord. 2012;27:965-973.
[78] Lee JH, Kim SH, Kim GH, Seo SW, Park HK, Oh SJ, et al. Identification of pure subcortical vascular dementia using 11C-Pittsburgh compound B. Neurology. 2011;77:18-25.
[79] Yotter RA, Doshi J, Clark V, Sojkova J, Zhou Y, Wong DF, et al. Memory decline shows stronger associations with estimated spatial patterns of amyloid deposition progression than total amyloid burden. Neurobiol Aging. 2013;34:2835-2842.
[80] Lovestone S, Boada M, Dubois B, Hüll M, Rinne JO, Huppertz H-J, et al. A Phase II Trial of Tideglusib in Alzheimer's Disease. Journal of Alzheimer's disease : JAD. 2015;45:75-88.
[81] Godyn J, Jonczyk J, Panek D, Malawska B. Therapeutic strategies for Alzheimer's disease in clinical trials. Pharmacological reports : PR. 2016;68:127-138.
[82] Sevigny J, Chiao P, Bussière T, Weinreb PH, Williams L, Maier M, et al. The antibody aducanumab reduces Aβ plaques in Alzheimer's disease. Nature. 2016;537:50-56.
[83] Hampel H, Schneider LS, Giacobini E, Kivipelto M, Sindi S, Dubois B, et al. Advances in the therapy of Alzheimer's disease: targeting amyloid beta and tau and perspectives for the future. Expert review of neurotherapeutics. 2015;15:83-105.
[84] Huang Y, Mucke L. Alzheimer mechanisms and therapeutic strategies. Cell. 2012;148:1204-1222.
[85] Cummings JL, Doody R, Clark C. Disease-modifying therapies for Alzheimer disease challenges to early intervention. Neurology. 2007;69:1622-1634.
[86] Sperling RA, Rentz DM, Johnson KA, Karlawish J, Donohue M, Salmon DP, et al. The A4 study: stopping AD before symptoms begin? Science translational medicine. 2014;6:228fs213.
[87] Sojkova J, Zhou Y, An Y, Kraut MA, Ferrucci L, Wong DF, et al. Longitudinal patterns of β-amyloid deposition in nondemented older adults. Archives of neurology. 2011;68:644-649.
[88] Koivunen J, Scheinin N, Virta JR, Aalto S, Vahlberg T, Någren K, et al. Amyloid PET imaging in patients with mild cognitive impairment A 2-year follow-up study. Neurology. 2011;76:1085-1090.

[89] Villemagne VL, Ong K, Mulligan RS, Holl G, Pejoska S, Jones G, et al. Amyloid imaging with (18)F-florbetaben in Alzheimer disease and other dementias. J Nucl Med. 2011;52:1210-1217.
[90] Villemagne VL, Burnham S, Bourgeat P, Brown B, Ellis KA, Salvado O, et al. Amyloid β deposition, neurodegeneration, and cognitive decline in sporadic Alzheimer's disease: a prospective cohort study. The Lancet Neurology. 2013;12:357-367.
[91] Hampel H, Lista S. Alzheimer disease: from inherited to sporadic AD-crossing the biomarker bridge. Nature reviews Neurology. 2012;8:598-600.
[92] Bateman RJ, Benzinger TL, Berry S, Clifford DB, Duggan C, Fagan AM, et al. The DIAN-TU Next Generation Alzheimer's prevention trial: Adaptive design and disease progression model. Alzheimer's & dementia : the journal of the Alzheimer's Association. 2017;13:8-19.
[93] Benzinger TLS, Blazey T, Jack CR, Koeppe RA, Su Y, Xiong C, et al. Regional variability of imaging biomarkers in autosomal dominant Alzheimer's disease. Proceedings of the National Academy of Sciences. 2013;110:E4502-E4509.
[94] Klunk WE, Price JC, Mathis CA, Tsopelas ND, Lopresti BJ, Ziolko SK, et al. Amyloid deposition begins in the striatum of presenilin-1 mutation carriers from two unrelated pedigrees. The Journal of neuroscience : the official journal of the Society for Neuroscience. 2007;27:6174-6184.
[95] Knight WD, Okello AA, Ryan NS, Turkheimer FE, Rodriguez Martinez de Llano S, Edison P, et al. Carbon-11-Pittsburgh compound B positron emission tomography imaging of amyloid deposition in presenilin 1 mutation carriers. Brain : a journal of neurology. 2011;134:293-300.
[96] Villemagne VL, Ataka S, Mizuno T, Brooks WS, Wada Y, Kondo M, et al. High striatal amyloid β-peptide deposition across different autosomal Alzheimer disease mutation types. Archives of neurology. 2009;66:1537-1544.
[97] Su Y, Blazey TM, Owen CJ, Christensen JJ, Friedrichsen K, Joseph-Mathurin N, et al. Quantitative Amyloid Imaging in Autosomal Dominant Alzheimer's Disease: Results from the DIAN Study Group. PloS one. 2016;11:e0152082.
[98] Grubbs FE. Procedures for detecting outlying observations in samples. Technometrics. 1969;11:1-21.

[99] Saunders AM, Strittmatter WJ, Schmechel D, George-Hyslop PHS, Pericak-Vance MA, Joo SH, et al. Association of apolipoprotein E allele ϵ4 with late-onset familial and sporadic Alzheimer's disease. Neurology. 1993;43:1467-1467.
[100] Ashburner J, Friston KJ. Unified segmentation. Neuroimage. 2005;26:839-851.
[101] Hammers A, Allom R, Koepp MJ, Free SL, Myers R, Lemieux L, et al. Three-dimensional maximum probability atlas of the human brain, with particular reference to the temporal lobe. Hum Brain Mapp. 2003;19:224-247.
[102] Rousset OG, Collins DL, Rahmim A, Wong DF. Design and implementation of an automated partial volume correction in PET: application to dopamine receptor quantification in the normal human striatum. J Nucl Med. 2008;49:1097-1106.
[103] Fleisher AS, Chen K, Liu X, Ayutyanont N, Roontiva A, Thiyyagura P, et al. Apolipoprotein E epsilon4 and age effects on florbetapir positron emission tomography in healthy aging and Alzheimer disease. Neurobiology of aging. 2013;34:1-12.
[104] Guo T, Brendel M, Grimmer T, Rominger A, Yakushev I, Alzheimer's Disease Neuroimaging I. Predicting Regional Pattern of Longitudinal beta-Amyloid Accumulation by Baseline PET. Journal of nuclear medicine : official publication, Society of Nuclear Medicine. 2017;58:639-645.
[105] Thomas BA, Cuplov V, Bousse A, Mendes A, Thielemans K, Hutton BF, et al. PETPVC: a toolbox for performing partial volume correction techniques in positron emission tomography. Physics in medicine and biology. 2016;61:7975-7993.
[106] Fleisher AS, Joshi AD, Sundell KL, Chen YF, Kollack-Walker S, Lu M, et al. Use of white matter reference regions for detection of change in florbetapir positron emission tomography from completed phase 3 solanezumab trials. Alzheimer's & dementia : the journal of the Alzheimer's Association. 2017.
[107] Blautzik J, Brendel M, Sauerbeck J, Kotz S, Scheiwein F, Bartenstein P, et al. Reference region selection and the association between the rate of amyloid accumulation over time and the baseline amyloid burden. European journal of nuclear medicine and molecular imaging. 2017.
[108] Johnson SC. Hierarchical clustering schemes. Psychometrika. 1967;32:241-254.
[109] Rice J. Mathematical statistics and data analysis: Nelson Education; 2006.
[110] Cohen J. Statistical power analysis for the behavioral sciences (2nd ed.) ed. New York: Psychology Press; 1988.

[111] Rosnow RL, Rosenthal R. Computing contrasts, effect sizes, and counternulls on other people's published data: General procedures for research consumers. Psychological Methods. 1996;1:331.
[112] Faul F, Erdfelder E, Lang A-G, Buchner A. G* Power 3: A flexible statistical power analysis program for the social, behavioral, and biomedical sciences. Behav Res Methods. 2007;39:175-191.
[113] Morris JC, Aisen PS, Bateman RJ, Benzinger TLS, Cairns NJ, Fagan AM, et al. Developing an international network for Alzheimer's research: the Dominantly Inherited Alzheimer Network. Clin Investig (Lond). 2012;2:975-984.
[114] Su Y, D'Angelo GM, Vlassenko AG, Zhou G, Snyder AZ, Marcus DS, et al. Quantitative analysis of PiB-PET with FreeSurfer ROIs. PLoS One. 2013;8:e73377.
[115] Braak H, Braak E. Staging of Alzheimer-related cortical destruction. Int Psychogeriatr. 1997;9:257-261.
[116] CFAN. The Chinese Familial Alzheimer's Disease Network. p. http://www.chinacfan.org/FrontPage/Index_En.aspx.

List of Publications within the scope of the thesis

[1]. Guo T, et al., Voraussage der regionalen Amyloid‐Akkumulation mittels Baseline‐Amyloid PET bei Alzheimer Krankheit. The 54th Annual Meeting of the German Society of Nuclear Medicine, April 20-23, 2016, in Dresden, Germany (Oral presentation).

[2]. Guo T, et al. Baseline amyloid PET predicts spatial pattern of beta-amyloid accumulation over time [J]. The Society of Nuclear Medicine & Molecular Imaging (SNMMI) 2016 Annual Meeting, June 11-15, 2016 in San Diego, CA, (Oral presentation). Journal of Nuclear Medicine, 2016, 57(supplement 2): 510-510.

[3]. Guo T, et al. Predicting Regional Pattern of Longitudinal β-Amyloid Accumulation by Baseline PET [J]. Journal of Nuclear Medicine, 2017, 58(4): 639-645.

[4]. Guo T, et al. Rate of beta-amyloid accumulation varies with baseline amyloid burden: implications for anti-amyloid drug trials [J]. Alzheimer's & Dementia, 2017 (Revision).

Acknowledgements

Data used in preparation of chapter 2 and 3 of this thesis were obtained from the Alzheimer's Disease Neuroimaging Initiative (ADNI) database (adni.loni.usc.edu). As such, the investigators within the ADNI contributed to the design and implementation of ADNI and/or provided data but did not participate in analysis or writing of this report. A complete listing of ADNI investigators can be found at: http://adni.loni.usc.edu/wp-content/uploads/how_to_apply/ADNI_Acknowledgement_List.pdf. The chapter 2 and 3 of this study was supported by the German Alzheimer Forschung Initiative e.V. (AFI).

Data collection and sharing for chapter 4 of this thesis was supported by The Dominantly Inherited Alzheimer's Network (DIAN, UF1 AG032438) funded by the National Institute on Aging (NIA) and the German Center for Neurodegenerative Diseases (DZNE). I acknowledge the altruism of the participants and their families and contributions of the DIAN research and support staff at each of the participating sites for their contributions to this study. The chapter 4 of this study was supported by the German Center for Neurodegenerative Diseases (DZNE).

I would like to thank all who have given support and encouragement enthusiastically to this work. Here I would give my special thanks to:

- Prof. Markus Schwaiger for the opportunity to work in department of nuclear medicine, and very helpful discussion on my project.
- Dr. Stephan Nekolla and Dr. Timo Grimmer for the assistance and very useful discussion on my project.
- Dr. Igor Yakushev for the guidance and support on every detail about this work, and the careful proofreading of the thesis.
- The whole colleagues in nuclear medicine for the harmonious atmosphere.
- My wife Dai Shi, my parents, my young sister and all my friends for the care and backup on my daily life.

And there are some to which I would like to express my gratitude in my native language.

感谢我的家人，感谢你们给予的关怀和无私的爱！你们的支持是我完成博士学习最坚强的后盾！

最后用一句先哲的话勉励自己：见贤思齐，见不贤而内自省也！